ISTANBUL TECHNICAL UNIVERSITY ★ GRADUATE SCHOOL

# EARTHQUAKE DAMAGE DETECTION WITH SATELLITE IMAGERY AND DEEP LEARNING APPROACHES: A CASE STUDY OF THE FEBRUARY 2023, KAHRAMANMARAŞ, TURKEY EARTHQUAKE SEQUENCE

**M.Sc. THESIS**

**Fatma ELİK**

**Department of Communication Systems**

**Satellite Communication and Remote Sensing Programme**

**Thesis Advisor: Prof. Dr. Elif SERTEL**

**Istanbul Technical University**

**JULY 2023**

ISTANBUL TECHNICAL UNIVERSITY ★ GRADUATE SCHOOL

# EARTHQUAKE DAMAGE DETECTION WITH SATELLITE IMAGERY AND DEEP LEARNING APPROACHES: A CASE STUDY OF THE FEBRUARY 2023, KAHRAMANMARAŞ, TURKEY EARTHQUAKE SEQUENCE

**M.Sc. THESIS**

**Fatma ELİK**

**(705201004)**

**Department of Communication Systems**

**Satellite Communication and Remote Sensing Programme**

**Thesis Advisor: Prof. Dr. Elif SERTEL**

**Istanbul Technical University**

**JULY 2023**

İSTANBUL TEKNİK ÜNİVERSİTESİ ★ LİSANSÜSTÜ EĞİTİM ENSTİTÜSÜ

# UYDU GÖRÜNTÜLERİ VE DERİN ÖĞRENME YAKLAŞIMLARI İLE HASAR TESPİTİ: 2023 ŞUBAT KAHRAMANMARAŞ, TÜRKİYE DEPREM DİZİSİNDEN BİR VAKA ÇALIŞMASI

**YÜKSEK LİSANS TEZİ**

**Fatma ELİK**

**(705201004)**

**Tez Danışmanı: Prof. Dr. Elif SERTEL**

**İstanbul Teknik Üniversitesi**

**TEMMUZ 2023**

Fatma ELİK, a M.Sc. student of ITU Graduate School student ID 705201004 successfully defended the thesis entitled "EARTHQUAKE DAMAGE DETECTION WITH SATELLITE IMAGERY AND DEEP LEARNING APPROACHES: A CASE STUDY OF THE FEBRUARY 2023 KAHRAMANMARAŞ, TURKEY, EARTHQUAKE SEQUENCE", which she prepared after fulfilling the requirements specified in the associated legislations, before the jury whose signatures are below.

**Thesis Advisor : Prof. Dr. Elif SERTEL** ..............................

Istanbul Technical University

**Jury Members : Prof. Dr. Tuncay TAYMAZ** .............................

Istanbul Technical University

**Jury Members: Dr. Tolga BAKIRMAN** ..............................

Yıldız Technical University

**Date of Submission : 26 July 2023**

**Date of Defense : 14 August 2023**

vi

*Hayatımdaki en büyük desteğim olan aileme ithaf ediyorum.*

## FOREWORD

Firstly, I would like to extend my sincere gratitude to my supervisor Prof. Dr. Elif SERTEL and Esra AYDIN, for their unwavering support and guidance throughout my research. Their expertise and encouragement have been invaluable to the completion of this thesis.

I am also deeply grateful to my family for their constant presence and unwavering support throughout my higher education journey. Their love and encouragement have been instrumental in my academic pursuits.

I would like to express my thanks to Can Ünen for his essential guidance and assistance during this research journey. Additionally, I am indebted to Yer Çizenler NGO for their invaluable contribution in providing the data points used in this study.

It is important to acknowledge that this thesis has been made possible through the financial support of The Scientific and Technological Research Council of Turkey (TUBITAK) under the 2210-D National Industrial MSc/MA Scholarship Program.

July 2023

Fatma ELİK

Geophysical Engineer

**Contents** **Page**


**FOREWORD** .......... **ix**
**LIST OF FIGURES** .......... **xv**
**TABLE OF LISTS** .......... **xix**
**EARTHQUAKE DAMAGE DETECTION WITH SATELLITE IMAGERY AND DEEP LEARNING APPROACHES: A CASE STUDY OF THE FEBRUARY 2023 KAHRAMANMARAŞ, TURKEY, EARTHQUAKE SEQUENCE** .......... **xxi**
**UYDU GÖRÜNTÜLERİ VE DERİN ÖĞRENME YAKLAŞIMLARI İLE DEPREM HASAR TESPİTİ: 2023 ŞUBAT, KAHRAMANMARAŞ, TÜRKİYE DEPREM DİZİSİNDEN BİR VAKA ÇALIŞMASI** .......... **xxiii**
**1. INTRODUCTION** .......... **1**
1.1 Purpose of Thesis .......... 1
1.2 Literature Review .......... 3
**2. STUDY AREA AND DATA** .......... **9**
2.1 Şehitkamil District, Gaziantep Province .......... 15
2.2 Ekinözü District, Kahramanmaraş Province .......... 20
2.3 Antakya District, Hatay Province .......... 25
2.4 Data .......... 29
2.4.1 Satellite images .......... 29
2.4.2 Damage points .......... 30
2.4.3 Building footprints .......... 33
**3. METHODOLOGY** .......... **41**
3.1 Deep Neural Networks (DNN) .......... 41
3.1.1 Unet .......... 41
3.1.2 DeepLabV3 .......... 42
3.1.3 Pyramid Scene Parsing Network (PSNET) .......... 44
3.2 Software .......... 46
3.2.1 Arcgis Pro and software libraries .......... 46
3.2.2 Preparation of the training data .......... 47
3.2.3 Export training data .......... 68
3.2.4 Training .......... 72
**4. RESULTS AND DISCUSSION** .......... **77**
4.1 Inference .......... 77
4.2 Implementation details .......... 80
4.3 Evaluation Metrics .......... 80
4.3.1 Precision and recall .......... 81
4.3.2 F1 score .......... 81
4.3.3 Mean Intersection over union .......... 82
4.4 Results .......... 82
4.4.1 Experiment-1: Unet architecture for Kahramanmaraş province 83
4.4.2 Experiment-2: DeepLabV3 architecture for Kahramanmaraş province .......... 86
4.4.3 Experiment-3: PSPNet architecture for Kahramanmaraş province .......... 95

4.4.4 Experiment-4: Kahramanmaraş experiment for 128x128 chip size 99
4.4.5 Experiment-5: Hatay experiment for 256x256 chip size.......... 101
4.5 Discussion ........................................................................ 104
**5. CONCLUSION..................................................................... 107**
**REFERENCES ....................................................................... 109**
**APPENDIX ............................................................................ 117**
**CURRICULUM VITAE ............................................................ 135**

**ABBREVIATIONS**

**ANN : Artificial Neural Network**
**AFAD: the Disaster and Emergency Management Presidency**
**ASPP : Atrous Spatial Pyramid Pooling**
**CNN : Convolutional Neural Network**
**CV: Computer Vision**
**DL:Deep Learning**
**DMS: Disaster Management Systems**
**DNN : Deep Neural Network**
**DRP: Disaster Response Program**
**EAF: East Anatolian Fault**
**EO : Earth Observation**
**FCN : Fully Convolutional Network**
**HOTOSM: Humanitarian OpenStreetMap Team**
**IoU : Intersection over Union**
**KOERI :Kandilli Observatory And Earthquake Research Institute**
**mIoU:Mean Intersection of Union**
**ML : Machine Learning**
**MLP :Multi-Layer Perceptron**
**NGO: Non-Governmental Organizations**
**PGA :Peak Ground Acceleration**
**PSPNet: Pyramid Scene Parsing Network**
**RF: Random Forest**
**ReLU : Rectified Linear Unit**
**RGB : Red Green Blue**
**RS : Remote Sensing**
**SAR: Synthetic Aperture Rad**
**SVM: Support Vector Machine**
**VHR: Very High-Resolution**
**VS30: The time-averaged shear-wave velocity (VS) to a depth of 30 meters**
**UAV: Unmanned aerial vehicle**

## LIST OF FIGURES

**Figure 2. 1.** Kahramanmaraş epicentered earthquakes (Kandilli Observatory and Earthquake Research Institute, 2023). ........ 10

**Figure 2. 2.** The research area is depicted on a map (Goldberg et al., 2023a). ........ 10

**Figure 2. 3.** The research area is depicted on a map (Goldberg et al., 2023a). ........ 12

**Figure 2. 4.** Location map of Sofalaca neighborhood-Şehitkamil district -Gaziantep province (Mw=7.7) earthquake (Kandilli Observatory and Earthquake Research Institute, 2023). ........ 16

**Figure 2. 5.** February 6 2023, 04:17 Location map of Şehitkamil-Gaziantep earthquake given by different centers (KRDAE, 2023). ........ 17

**Figure 2. 6.** Gaziantep assessed damaged points on Maxar images. ........ 18

**Figure 2. 7.** Şehitkamil District, Gaziantep Province. ........ 19

**Figure 2. 8.** Location Map of the Ekinözü-Kahramanmaraş (Mw=7.6) Earthquake (Kandilli Observatory and Earthquake Research Institute, 2023). ........ 20

**Figure 2. 9.** February 6 2023, 13:24 Location information of Ekinözü-Kahramanmaraş earthquake given by different seismology centers (KRDAE, 2023). ........ 21

**Figure 2. 10.** Kahramanmaraş assessed damaged points over Maxar imagery. ........ 22

**Figure 2. 11.** Pazarcık District, Kahramanmaraş Province ........ 23

**Figure 2. 12.** Kahramanmaraş with Area of Interest. ........ 24

**Figure 2. 13.** Primal solution location of the Büyükçat-Samandağ-Hatay (Ml=6.4) earthquake Earthquake (Kandilli Observatory and Earthquake Research Institute, 2023). ........ 25

**Figure 2. 14.** Büyükçat-Samandağ-Hatay (ML=6.4) location information given by different seismology centers Earthquake (Kandilli Observatory and Earthquake Research Institute, 2023). ........ 26

**Figure 2. 15.** Hatay, Antakya city centre with assessed damage points. ........ 27

**Figure 2. 16.** Antakya District, Hatay Province. ........ 28

**Figure 2. 17.** Before and after the Kahramanmaraş earthquake (Stadiums Become Shelters: Satellite Pics Show Turkey Earthquake Damage, 2023). ........ 29

**Figure 2. 18.** Assessed four scaled damage points for Kahramanmaraş earthquakes (Url-25). ........ 31

**Figure 2. 19.** Four scaled damaged points. ........ 32

**Figure 2. 20.** Damage point taken from (Url-25). ........ 32

**Figure 2. 21.** Recent info building intensity of HOTOSM (HOT Export Tool, 2023). ........ 33

**Figure 2. 22.** The custom area we extracted building shapefiles from (HOT Export Tool, 2023). ........ 33

**Figure 2. 23.** All building polygons and buildings with damage assessment overlaid on the satellite image. ........ 34

**Figure 2. 24.** Buildings with damage assessment based on post-earthquake images do not match here. .......... 35

**Figure 2. 25.** Building footprints and damage data points close up. .......... 36

**Figure 2. 26**. Results of intersection match option. .......... 36

**Figure 2. 27.** Building footprints (green polygons) and damage data points (red points). .......... 38

**Figure 2. 28.** Antakya City Center building footprints, damage points and, close up demonstration. .......... 39

**Figure 3. 1.** Deep Learning approach in ArcGIS Pro ("How U-Net Works," n.d.). .......... 41

**Figure 3. 2.** Unet Architecture ("How U-Net Works," n.d.). .......... 42

**Figure 3. 3.** DeepLabV3 Model ("How DeepLabV3 Works," n.d.). .......... 43

**Figure 3. 4.** DCNN without Atrous Convolution & with Atrous Convolution ("How PSPNet Works," n.d.). .......... 43

**Figure 3. 5.** PSPNet Architecture ("How PSPNet Works," n.d.). .......... 45

**Figure 3. 6.** Skip connections from encoder to U-Net like decoder ("How PSPNet Works," n.d.). .......... 45

**Figure 3. 7.** Arcgis Pro Python API ("Overview of the ArcGIS API for Python," n.d.). .......... 46

**Figure 3. 8.** Deep Learning Approach in ArcGIS Pro. .......... 47

**Figure 3. 9.** Merge explanation in attributes ("An Overview of Attribute Domains", n.d.). .......... 48

**Figure 3. 10.** Coded Value Domains ("Add Coded Value To Domain", n.d.). .......... 49

**Figure 3. 11.** SQL query for attribute management ("Add Coded Value To Domain", n.d.). .......... 49

**Figure 3. 12.** Results of attribute calculations. .......... 51

**Figure 3. 13.** Damaged data points received from Yer Çizenler NGO. .......... 52

**Figure 3. 14.** Heavily Damaged data points received from Yer Çizenler NGO. .......... 52

**Figure 3. 15.** Slightly Damaged data points received from Yer Çizenler NGO. .......... 53

**Figure 3. 16.** Demolished data points received from Yer Çizenler NGO. .......... 53

**Figure 3. 17.** Four scales of damage points are merged. .......... 54

**Figure 3. 18.** Damage points and building footprints in Hatay, Antakya district. .......... 55

**Figure 3. 19.** Choosing the optimum imagery out of the options was crucial. .......... 56

**Figure 3. 20.** Intersect option causes information loss. .......... 57

**Figure 3. 21.** Data loss due to intersection match (before and after selection). .......... 58

**Figure 3. 22.** An example of the best match of the building footprints in Hatay. .......... 59

**Figure 3. 23.** Kahramanmaraş and Gaziantep province footprint match demonstration, respectively. .......... 60

**Figure 3. 24.** Blue polygons are chosen to move and displaced. ................................ 61
**Figure 3. 25.** Damage level Distribution by earthquake affected cities. ..................... 62
**Figure 3. 26.** Number of damaged buildings per city. ................................................ 63
**Figure 3. 27.** Damage Distribution in total. ................................................................ 64
**Figure 3. 28.** Green: all the footprints, orange: within 10m and yellow: within 5m distance. ................................................................................................................ 64
**Figure 3. 29.** Demonstration of the building footprints in detail (all of them, within 10m and 5m respectively). ..................................................................................... 65
**Figure 3. 30.** Area of Interest (AOI) for Hatay Province. ............................................ 66
**Figure 3. 31.** Area of Interest (AOI) for Kahramanmaraş Province. ........................... 66
**Figure 3. 32.** Area of Interest (AOI) for Gaziantep Province. .................................... 67
**Figure 3. 33.** Before and after clipping the raster. ....................................................... 68
**Figure 3. 34.** Export Training Data for Deep LearningTool (Abd-Elrahman,et.al., 2021). ................................................................................................................ 68
**Figure 3. 35.** Image and masks tiles created in training dataset. ................................ 69
**Figure 3. 36.** Training data statistics after exporting. .................................................. 69
**Figure 3. 37.** 256x256 tile sized image batches after all augmentations labeling for Kahramaraş satellite image. .......................................................................... 70
**Figure 3. 38.** Outputs of the Export Training Data tool (Abd-Elrahman,et.al., 2021). 71
**Figure 3. 39.** arcgis.learn is a powerful module (Singh, 2021). .................................. 74
**Figure 3. 40.** arcgis.learn module methods and models. .............................................. 74
**Figure 3. 41**. Outputs of the Train Deep Learming model Tool. ................................. 75
**Figure 3. 42.** Results of Classify Pixels Using Deep Learning Tool in Antakya District. ................................................................................................................ 78
**Figure 3. 43. a)** Red areas: predicted damaged areas, orange: heavily damaged, yellow: slightly damaged areas. ........................................................................... 79

**Figure 4. 1.** Loss functions of the Unet ResNet-34 Architecture. ............................... 84
**Figure 4. 2.** Experiment of Unet ResNet-34 Architecture for Pixel based classsification ................................................................................................................ 85
**Figure 4. 3.** Experiment of DeepLabV3 ResNet 34 Architecture for Pixel based classsification. ........................................................................................... 89
**Figure 4. 4.** Experiment of DeepLabV3 ResNet50 Architecture for Pixel based classsification. ........................................................................................... 90
**Figure 4. 5.** Experiment of DeepLabV3 RexNet50 Architecture for Pixel based classsification. ........................................................................................... 91
**Figure 4. 6.** Experiment of DeepLabV3 DenseNet121 Architecture for Pixel based classsification. ........................................................................................... 92

**Figure 4. 7.** Loss functions of the DeepLabV3. .......................................................... 93

**Figure 4. 8.** Experimental results of the DeepLabV3 architecture. ............................. 94

**Figure 4. 9.** Experiment of PSPNet ResNet34 Architecture for Pixel based classsification.......................................................................................................... 97

**Figure 4. 10.** Experiment of PSPNet ResNet50 Architecture for Pixel based classsification.......................................................................................................... 98

**Figure 4. 11.** 128x128 image size with 64 stride image chips and statistics of the training dataset. .......................................................................................................... 99

**Figure 4. 12.** Ground truth and predictions for Unet ResNet34 Architecture............ 100

**Figure 4. 13.** Statistics of the Hatay dataset. ............................................................ 101

**Figure 4. 14.** Unet Resnet34 Architecture for Hatay dataset. ................................... 102

**Figure 4. 15.** DeepLabV3 ResNet34 Architecture for Hatay dataset. ....................... 103

**Figure 4. 16.** Kahramanmaraş Earthquake Damage Assessment Map with QR of the multiple linked dashboard. ......................................................................... 106

## TABLE OF LISTS

**Table 2. 1.** Kinematics of the Kahramanmaraş Earthquakes (Url-22)........................ 11

**Table 2. 2.** Number of Total Buildings in Earthquake-Affected Provinces (Presidency of The Republic of Turkey Presidency of Strategy and Budget, 2023). ...................... 13

**Table 2. 3.** The number of structures included in the structural damage estimation (March 6, 2023) (Presidency of The Republic of Turkey Presidency of Strategy and Budget, 2023). ........................................................................................................... 14

**Table 2. 4.** Location and magnitude information of Sofalaca-Şehitkamil -Gaziantep (Mw=7.7) earthquake given by different centers. ....................................................... 17

**Table 2. 5.** 06.02.2023 13:24 Location and magnitude information of Ekinözü-Kahramanmaraş earthquake given by different centers. ............................................. 21

**Table 2. 6.** Location and magnitude information of 20.02.2023 20:04 Samandağ-Hatay earthquake given by different centers.......................................................................... 26

**Table 2. 7.** The parameters of the satellite images received from Maxar Technologies for the study areas.......................................................................................................... 30

**Table 3. 1.** Parameters of the Export Training Data for Deep Learning Tool. ............ 73

**Table 3. 2.** Outputs after using of the Train Deep Learming model Tool. .................. 75

**Table 3. 3.** Parameters we used in our custom model................................................. 76

**Table 4. 1.** Experiment of Unet ResNet-34 Architecture for 256x256 sized image. ... 83

**Table 4. 2.** Experiment of Unet ResNet-34 Architecture for 256x256 sized image. ... 83

**Table 4. 3**. Metrics results for the DeepLabV3 architecture with ResNet34 encoder. 86

**Table 4. 4.** Metrics results for the DeepLabV3 architecture with ResNet50 encoder. 86

**Table 4. 5.** Metrics results for the DeepLabV3 architecture with ResNext50 encoder. ........................................................................................................................... 87

**Table 4. 6.** Metrics results for the DeepLabV3 architecture with DenseNet121 encoder. ........................................................................................................................... 87

**Table 4. 7.** Hyperparameters of the DeepLabV3 architecture. ................................... 88

**Table 4. 8.** Metrics results for the PSPNet architecture with ResNet34 encoder. ....... 95

**Table 4. 9.** Metrics results for the PSPNet architecture with ResNet50 encoder. ....... 95

**Table 4. 10.** Hyperparameters of the PSPNet architecture. ........................................ 96

**EARTHQUAKE DAMAGE DETECTION WITH SATELLITE IMAGERY AND DEEP LEARNING APPROACHES: A CASE STUDY OF THE FEBRUARY 2023 KAHRAMANMARAŞ, TURKEY, EARTHQUAKE SEQUENCE**

## SUMMARY


In recent years, the fusion of deep learning techniques, remote sensing technology, and artificial intelligence (AI) has profoundly transformed the field of disaster management and damage assessment. The increased availability of high-resolution satellite imagery and advanced computer vision techniques now makes it possible to analyze Earth observation data at a large scale and with unparalleled precision. This thesis investigates the application of remote sensing and deep learning techniques to perform post-earthquake damage classification using computer vision and focuses specifically on the earthquakes that occurred on February 6th, with an emphasis on Kahramanmaraş province.

The objective of this thesis is to investigate the potential of a variety of deep learning techniques, evaluate their accuracy in recognizing structurally compromised buildings, and utilize satellite imagery in conjunction with diverse open-source spatial data to enhance research on earthquakes. This master's thesis specifically delves into the integration of remote sensing, computer vision, and earth observation methods within the field of geophysics and earthquake studies. Thus, in this study it is aimed to showcase the application of computer vision in the analysis of post-earthquake damage and underscore the importance of rapid intervention in such critical situations. The thesis places significant emphasis on the use of satellite imagery and pixel-based classification for the classification of images in earthquake damage assessment.

The UNet, DeepLabV3, and PSPNet architectures are implemented using the ArcGIS Pro API for Python, an innovative and supportive tool for scientific research. The primary data source for the investigation is RGB images from Maxar Technologies. The research examines three cities that were affected by the February 6, 2023, Kahramanmaraş earthquake sequences: Kahramanmaraş, Hatay, and Gaziantep.

Damage-assessed data points are received thanks to Yer Çizenler Non-Governmental Organization (NGO), and recently modified building footprints are taken from Humanitarian OpenStreetMap (HOTOSM), and they are all used to analyze the damage. Labeled polygons are generated within a 5-meter distance of the damage points. However, assigning values for further and closer distances has a negative impact on the model accuracy. The training data, exported based on the satellite imagery and damage level assigned data points, provides a balanced dataset for Kahramanmaraş, where the building footprints match the images most effectively. In Hatay, the damage level assigned data distribution is the most balanced, but the building footprints do not align

well with the images. Gaziantep presents a good match between the building footprints and images, but the distribution of the damaged data classes is highly imbalanced. Consequently, the decision is made to focus on training the model for Kahramanmaraş province due to the similarity in roof and building types, which has the potential to adapt the approach to other cities in the region as well as the earthquake-affected region under investigation. Image sizes of 256x256 pixels with 128 strides and 4 batches gave us the optimum model results among other options in the DeepLabV3 ResNet50 encoder.

In conclusion, this master's thesis demonstrates the potential of combining remote sensing, computer vision, and earth observation techniques for geophysics and earthquake studies. Also, it is aimed to use different data types from open sources and use these different data types to make damage detection after earthquakes. The utilization of the ArcGIS Pro Python API, satellite imagery, pixel based classsification, and labeled training data provides insights into damage assessment after earthquakes, with Kahramanmaraş Province serving as the focal point for model training. The findings contribute to the development of efficient and accurate disaster management strategies and lay the foundation for further research in this field.

**UYDU GÖRÜNTÜLERİ VE DERİN ÖĞRENME YAKLAŞIMLARI İLE DEPREM HASAR TESPİTİ: 2023 ŞUBAT, KAHRAMANMARAŞ, TÜRKİYE DEPREM DİZİSİNDEN BİR VAKA ÇALIŞMASI**

## ÖZET


Son yıllarda, derin öğrenme tekniklerinin, uzaktan algılama teknolojisinin ve yapay zeka (AI) teknolojisinin birleşimi, afet yönetimi ve hasar tespiti alanını kökten değiştirmiştir. Yüksek çözünürlüklü uydu görüntülerinin artan kullanılabilirliği ve gelişmiş bilgisayarlı görü teknikleri ile yer gözlem verilerinin büyük ölçekte ve benzersiz bir hassasiyetle incelenmesi artık mümkün hale gelmiştir. Bu tez, bilgisayarlı görü kullanarak deprem sonrası hasar sınıflandırması yapmak için uzaktan algılama ve derin öğrenme tekniklerinin uygulanmasını incelemektedir ve özellikle 6 Şubat'ta gerçekleşen Kahramanmaraş depremlerine odaklanmaktadır.

Bu tezin amacı, çeşitli derin öğrenme tekniklerinin uygulanabilirliğini araştırmak, yapısal olarak hasar görmüş binaları bölütleme ile değerlendirmek ve deprem çalışmalarını geliştirmek amacıyla uydu görüntüleri ile çeşitli açık kaynaklı mekânsal verileri birleştirmektir. Bu yüksek lisans tezi, özellikle jeofizik ve deprem çalışmaları alanında uzaktan algılama, bilgisayarlı görü ve yer gözlem tekniklerinin birleştirilmesini ele almak, deprem sonrası hasarın analizinde bilgisayarlı görünün kullanımını sergilemek ve böylesine kritik anlarda hızlı müdahalenin önemini vurgulamayı amaçlamaktır.

Bu tezde, afet hasar tespiti için görüntülerin sınıflandırılmasında uydu görüntüleri ve piksel bazlı sınıflandırmanın kullanımı ana yöntem olarak kullanılmakta ve bunun önemi vurgulanmaktadır. UNet, DeepLabV3 ve PSPNet mimarileri, bilimsel araştırmalar için yenilikçi ve destekleyici bir araç olan ArcGIS Pro Python API yazılımı kullanılarak piksel tabanlı sınıflandırma araçları ile segmentasyon modelleri tasarlamaktır. Bu modeller, depremler sonrası toplanan uydu verilerinde hasar gören bölgeleri verimli bir şekilde tespit edebilir ve çözümlemenin hızını ve doğruluğunu artırır. Bu yöntem, hasar tespiti hızını ve doğruluğunu artırmakla kalmaz, aynı zamanda yıkımın coğrafi yayılımı ve şiddeti hakkında faydalı bilgiler sunar. Araştırma için birincil veri kaynağı Maxar Technologies'den alınan RGB görüntüleridir. Araştırma, 6 Şubat 2023 Kahramanmaraş deprem dizilerinden etkilenen üç şehir olan Kahramanmaraş, Hatay ve Gaziantep'i incelemektedir.

Hasar tespiti yapılan veri noktaları Yer Çizenler Sivil Toplum Kuruluşu (STK) sayesinde alınmış ve yakın zamanda güncelenen bina ayak izleri Humanitarian OpenStreetMap'ten (HOTOSM) alınmış ve hepsi hasar analizi için kullanılmıştır. Hasar noktalarına 5 metre uzaklığa kadar mesafede etiketli poligonlar oluşturulmuştur. Ancak, daha uzak ve yakın mesafeler için değerler atanması model doğruluğu üzerinde olumsuz bir etki yaratmıştır. Uydu görüntüleri ve hasar değeri atanan veri noktaları baz alınarak oluşturulan eğitim verileri, bina ayak izlerinin görüntülerle en etkili şekilde eşleştiği Kahramanmaraş ili için dengeli bir veri seti sağlamıştır. Hatay'da, hasar değeri atanan veri dağılımı en dengeli olduğu halde, bina ayak izlerinin görüntülerle iyi uyum göstermediği ve istenildiği gibi çakışmadığı görülmüştür. Gaziantep, bina ayak izleri ve görüntüler arasında iyi bir eşleşme sunmaktadır, ancak hasarlı veri sınıflarının dağılımı oldukça dengesizdir. Sonuç olarak, araştırılan depremden etkilenen bölgedeki çatı ve bina tiplerindeki benzerlik nedeniyle modelin Kahramanmaraş ili için eğitilmesine odaklanılmasına karar verilmiş ve modelin bölgedeki diğer şehirlere de

uygulanabileceği düşünülmüştür. Görüntü boyutlarının 256x256 piksel, 128 adım ve 4 yığın (batch) olması, DeepLabV3 modeli ve ResNet50 kodlayıcı (encoder) ile diğer seçenekler arasında bize en uygun model sonuçlarını vermiştir.

Ayrıca, kullanılan yazılım altyapısı sayesinde, özellikle uzaktan algılama görevleri için faydalı olan çeşitli görsel temsil seçenekleri sunulmuştur. Kullanılan yazılım 2D ve 3D görüntüler gibi uzaktan algılama verilerini görselleştirmek ve analiz etmek için gelişmiş araçlar sunar. Bununla birlikte, ArcGIS Pro verilerin görselleştirmeleri, grafikler gibi çeşitli görselleştirmelerin coğrafi bilgi sistemi iş akışlarına entegrasyonunu destekleyen bir yazılımdır. Veri görselleştirmelerini dahil etmek, karmaşık bilgileri ve modelleri etkili bir şekilde iletebilme, daha iyi karar verme ve işbirliği yapma olanağı sağlamıştır. Ayrıca, uzaktan algılama verilerini farklı boyutlarda görselleştirebilme yeteneği, derin öğrenme sonuçlarının analizini ve yorumunu geliştirerek içgörü ve keşifleri kolaylaştırmaktadır.

Ancak, ArcGIS Pro derin öğrenmeyi desteklese de, öncelikle derin öğrenme yapısına özel olarak olarak tasarlanmamıştır. Bu nedenle, özellikle PyTorch veya TensorFlow gibi uzman derin öğrenme altyapıları mevcut olan birçok karmaşık yetenek ve optimizasyonlar konusunda konusunda eksiklik taşımaktadır. Bu sınırlama, derin öğrenme modelleri için kullanılabilirlik ve önceden eğitilmiş modeller gibi özelleştirilme imkanını kısıtlayabilir. Ayrıca, en güncel geliştirilmiş derin öğrenme mimarileri ve tekniklerini desteklemeyebilir. Buna ek olarak, hesaplama açısından yoğun, derin öğrenme uygulamaları için özellikle GPU gibi yüksek teknoloji bilgisayar kaynaklarına sahip olunması önem taşır. Aksi durumda, özellikle karmaşık derin öğrenme altyapılarına göre, yapılan işlemler daha yavaş eğitim ve çıkarım süreleriyle sonuçlanabilir. Ayrıca, ArcGIS ekosistemine bağımlılık, GIS ile ilgili olmayan geliştiriciler için dezavantaj olabilir, çünkü ek kurulum, eklentiler, ArcGIS araçları (tool) ve kavramları hakkında ek bilgi gerektirebilir. Örneğin, bazı veri tipleri (JSON, vb.) ESRI yazılım sisteminde her araçta doğrudan desteklenmez, bu da ek olarak veri önişleme adımlarını gerektirebilir.

Bu çalışmada, ArcGIS Pro yazılımının büyük bir önemi bulunmaktadır. Özellikle, bu tez için özel olarak tasarlanan verilerin kullanımı açısından ArcGIS Pro, çok değerli bir araç sağlamıştır. Çalışmanın temel amacı, deprem sonrası hasar tespiti için yapay zeka ve derin öğrenme tekniklerini kullanarak uydu görüntülerini analiz etmek olduğu için, bu amaçla, veriler üç farklı ilde, yani Kahramanmaraş, Hatay ve Gaziantep'te toplandı. Bu iller, 6 Şubat tarihinde gerçekleşen Kahramanmaraş depremleri sonrasında etkilenen illerden bazıları olarak çalışmamızda seçilmiştir.

Toplamda, Maxar Technologies'den elde edilen 6 farklı uydu görüntüsü kullanılmış ve bu görüntülerin analizi ArcGIS Pro üzerinde gerçekleştirilmiştir. ArcGIS Pro, bu görüntülerin işlenmesi, görselleştirilmesi ve analiz edilmesi için mükemmel bir platform sağlamıştır. Verilerin bu şekilde bu tez için özel olarak tasarlanmıi ve farklı avantaj ve dezavantajı olan 3 ayrı veri seti oluşturuldu. Oluşturulan illerden değil de görüntü boyutlarından bahsederken, bu çalışmak kapsamında daha fazla veri seti üretmek ve deney yapmak zorunda olduğumuz söylenebilir. Bu süreçte, araştırmamızda mevcut olan çeşitli toolları sayesinde ArcGIS Pro vazgeçilmez bir araç olmuş ve elde edilen sonuçların değerlendirilmesinde büyük bir rol oynamıştır. Çünkü her ne kadar bu çalışmada farklı disiplinler ve veri tipleri bir araya getirilmiş olsa da, özel üretilen veri setleri ile özelleştirilmiş bir çalışma yapılması da amaçlanmaktadır. Ayrıca, kullanılan derin öğrenme modelleri alt yapısal olarak hazır olsa da, farklı bir API kullanmanın verdiği uyum zorluğu burada da görülmüş, dengesiz verilerin ArcGIS Pro Python API’da eğitilmesi için de veri ön işlem kısmında birçok özelleştirme yapılmıştır.

Sonuç olarak, bu yüksek lisans tezi uzaktan algılama, bilgisayarlı görü ve yer gözlem tekniklerinin jeofizik ve deprem çalışmaları için birleştirilmesinin potansiyelini göstermektedir. Ayrıca, açık kaynaklardan farklı veri türlerinin kullanılması ve bu farklı veri türlerinin deprem sonrası hasar tespiti yapmak için kullanılması konuyla alakalı farklı bit çözüm yöntemi olarak öne çıkmaktadır. Bu bağlamda, jeofizik ve deprem çalışmaları bağlamında uzaktan algılama, bilgisayarlı görü ve yer gözlem tekniklerinin entegrasyonu incelenmiştir. Bu şekilde, deprem kaynaklı hasarı değerlendirmek ve yönetmek için bilgisayarlı görünün uygulanmasına ve deprem sonrası senaryolarda zamanında ve etkili müdahalenin önemine odaklanılmıştır. ArcGIS Pro Python API, uydu görüntüleri, piksel bazlı sınıflandırma ve etiketli eğitim verilerinin kullanımı, model eğitimi için odak noktası olarak Kahramanmaraş ili ile deprem sonrası hasar tespitlerine ilişkin içgörüler sağlamıştır. Bulgular, etkin ve doğru afet yönetimi stratejilerinin geliştirilmesine katkıda bulunmakta ve bu alanda daha fazla araştırma yapılması için temel oluşturmaktadır.

# 1. INTRODUCTION

In recent years, the combination of deep learning techniques, remote sensing technology, and artificial intelligence (AI) has revolutionized the field of disaster management and damage detection. With the growing availability of high-resolution satellite images and improved computer vision techniques, it is now possible to investigate Earth observation data on a massive scale and with incomparable precision. This thesis investigates the application of AI and deep learning techniques to damage classification using computer vision, with a particular focus on the Kahramanmaraş earthquakes that occurred on February 6th.

The main purpose of this thesis is to design segmentation models with pixel based classsification tools using ArcGIS Pro Software, a robust geospatial analytic platform. These models can efficiently detect and outline damaged regions in the satellite data, collected after the earthquakes by employing deep learning techniques. This method not only improves the speed and accuracy of damage identification, but it also offers useful information about the geographical extent and severity of the devastation.

In summary, this thesis integrates the domains of deep learning, remote sensing, and artificial intelligence to investigate their potential for improving disaster management, notably in the context of damage identification in the Kahramanmaraş earthquakes. Additionally, the goal is to utilize various data types obtained from open sources and apply them in post-earthquake damage detection processes. The use of ArcGIS Pro, in conjunction with pixel categorization tools and powerful computer vision algorithms, seeks to deliver accurate and fast information to assist decision-makers in responding to and managing the aftermath of such natural catastrophes.

## 1.1 Purpose of Thesis

The objective of this thesis is investigation of the usability of various deeplearning methods, determination of the accuracy in detecting collapsed buildings, and showing the usage of different open-source spatial datas and satellite images in the earthquake studies. From this point of view, we investigated the integration of remote sensing, computer vision, and earth observation techniques in the context of geophysics and earthquake studies. Thus, it is demonstrated the application of computer vision for assessing and managing earthquake-induced damage, with a focus on the importance of timely and efficient response in post-earthquake scenarios.

Computer Vision (CV), Deep Learning (DL), and Artificial Intelligence (AI) methods for remote sensing applications can help to support and resolve challenges for large satellite image datasets by utilizing high-performance-based models to collect and identify features in an environment with precision as well as rapidity. To overcome the limitations of remote sensing data, computer vision algorithms may enhance and eliminate noise from satellite and aerial image data, allowing for better analysis of broad regions and the classification of objects, features, and changes, as well as data fusion, cloud removal, and spectrum analysis from imagery.

The importance of quick and efficient disaster management in the aftermath of earthquakes is emphasized after major earthquakes in parts of the world with high tectonic activity, as seen in the Kahramanmaraş-Gaziantep epicenter earthquakes in Turkey. Every authority, the government ministries of Turkey, and even volunteer researchers followed this approach as soon as possible. Earth Observation (EO) is quite crucial immediately after or days later after an earthquake, as seen in Turkey. This research intends to deal with the rapid earthquake assessment process and contribute to the development of effective multi-feature approaches for resource allocation and decision-making to aid in timely response efforts by merging remote sensing, computer vision, and earth observation approaches.

Under the support of TUBITAK 2210-D National Industrial MSc Scholarship Program and ESRI Türkiye, the collaboration of Yer Cizenler and Humanitarian OpenStreetMap as our main data sources gave us beneficial outputs. The thesis leverages the resources, including recently adjusted building footprints, to enhance the accuracy and efficiency of damage assessments with Deep Neural Networks (DNN) based cutting-edge technology to benefit geophysics.

Finally, the application of the forefront CV algorithms to the Kahramanmaraş-Gaziantep epicenter earthquakes was our greatest achievement. The thesis focuses on the specific cases of the Kahramanmaraş, Gaziantep, and Hatay epicenter earthquakes, utilizing satellite imagery and labeled data to create and train DNN models. So, it is analyzed the feasibility and effectiveness of these DNN models for damage identification in earthquake-affected regions, as well as their potential applicability to other similar places. By addressing the issues of earthquake damage assessment and emphasizing the necessity of early and efficient action, the research intends to contribute to the development of effective disaster management techniques, ultimately strengthening resilience and lowering the impact of earthquakes.

## 1.2 Literature Review

In a study on assessing earthquake damage, using remote sensing data and deep learning approaches is steadily growing, reflecting the increasing interest and potential of this interdisciplinary field. Earth Observation (EO) is generally an area supported with Remote Sensing (RS) and Computer Vision (CV) applications. Some researches with CNN-based models work at automatically locating and mapping earthquake-damaged areas. They were able to identify structural problems with accuracy and efficiency by training their models using satellite imagery, which facilitated quick disaster management and response (Qing et al., 2022).

For detecting earthquake-related building damage, Ghasem Abdi and Shabnam Jabar (University of New Brunswick Libraries) suggested a deep transfer learning approach for multi-feature fusion (Abdi and Jabar, 2021). To increase the precision of damage identification, their study concentrated on using deep learning models to extract characteristics from several sources, including satellite imagery.

A dataset gathering process, as well as several features and statistics for post-disaster damage assessment are covered in another study. The high resolution and low altitude dataset provided by UAV photos is particularly important for carrying out computer vision tasks. The dataset has classification and semantic segmentation annotations (Rahnemoonfar, et al., 2021). To determine the earthquake-caused damage in the buildings, VHR satellite photos of Haiti and significant updates to the UNet algorithm were used (Moradi and Shah-Hosseini, 2020).

Also, water-related calamities such as floods, tornadoes, hurricanes, and tsunamis pose a significant risk to human life. A cutting-edge deep-learning method that uses combinations of pre- and post-disaster satellite images to find locations affected by water-related disasters has been proposed. The stdies about these incidents can assist in directing resources to places most vulnerable to climate disasters, lowering their consequences while also promoting adaptive skills for climate-resilient development in the most vulnerable regions and successfully recognizing local devastation. (Kim et al., 2022).

The benchmark dataset utilized in another study for hurricane damaged building detection is sourced from FEMA (Federal Emergency Management Agency) and NOAA (National Oceanic and Atmospheric Administration) ( Choe et.a l.,2018).

Moreover, the XBD Dataset, which is the first multi-level damage dataset encompassing various disaster scenarios, is utilized in another study. This dataset provides valuable information for analyzing and understanding the impact of different disasters on buildings and infrastructure (Gupta et. al., 2019).

The SpaceNet 8 dataset, designed for the detection of flooded roads and buildings, is leveraged in a study to support earthquake risk assessment by identifying the probable impact of seismic hazards on infrastructure and buildings (Url-21).

The study introduces the PPM-SSNet, a novel benchmark model for assessing building damage using satellite imagery. It achieves high precision through residual and squeeze-and-excitation blocks and employs learned attention mechanisms for automated input and output. The model demonstrates strong performance on various building classes and shows potential for evaluating future disasters (Bai et.al., 2020).

There are many studies about the floods with the multidisciplinary help of RS and CV using DeepLabV3 and PSPNet and comparing the model differences in the literature (European Space Agency (ESA), 2023). Also, another study demonstrated a two-stage, machine-learning-based strategy that combines YOLOv4 with SVM to accurately identify small, dense objects and highly unbalanced data for the localisation of buildings after an earthquake and the evaluation of building damage in aerial photos (Weng et. al., 2022).

To observing the Antarctic coastline, Heidler et al. suggest HED-UNet, a segmentation and edge detection approach coupled. By combining the benefits of segmentation and edge detection approaches, their approach enables accurate delineation and monitoring of coastal changes. Despite not being specifically concerned with earthquake damage assessment, the study demonstrates the value of merging various computer vision techniques for monitoring and analysis (Heidler et. al., 2022).

Moreover, panoptic segmentation is used in the processing of remote sensing data, to give a thorough comprehension of remote sensing settings, the researchers mix semantic segmentation with instance segmentation. Their study highlights the potential of panoptic segmentation for in-depth analysis and interpretation of remote sensing data, including applications in disaster management and mapping land cover (Carvalho, et al., 2022).

Additionally, to overcome the time constraints of current techniques, an automated post-earthquake evaluation procedure is presented. The approach is built as a C# prototype and real-world damaged concrete column photos from Haiti's 7.0 earthquake in 2010 were utilized for validation (Paal et al., 2014). Also, the Haiti Earthquake is examined for the use of machine learning techniques for identifying earthquake damage, such as feed forward neural networks, radial basis function neural networks, and random forests (Cooner et al., 2016).

Other publications address current remote sensing technology and its use in earthquake investigations to the present (Rathje et al., 2008), produced building-seismic-resilience (BSR)-mapping models based on multiple categorization schemes employing random forest (RF) and a support vector machine (SVM) (Wen et al., 2023), enabled for actionable damage mapping by automatically selecting needed training samples and identifying damage level using a simple classification algorithm like SVM or MLP (Takhtkeshha et al., 2022).

Additionally, considering the widespread benefits of synthetic aperture radar (SAR), it was inevitable to use this imagery type for post-disaster studies. Another framework combines high-resolution building inventory data with maps of the intensity of ground shaking during earthquakes and surface-level alterations were discovered by comparing pre- and post-event InSAR (interferometric synthetic aperture radar) images. It is showed how ensemble models may be used in a machine-learning technique to categorize the condition of building damage in an earthquake-affected area (Rao et al., 2023).

In terms of technologies, UAVs and LIDAR represent an area of potential dramatic and rapid growth for both academia and industry. A study covers initiatives that use remote sensing methods to document damage patterns, gather three-dimensional failure geometries, and quantify ground motions during geotechnical earthquake reconnaissance. Satellite imagery, LIDAR, and UAV, the three most used remote sensing methods in geotechnical engineering, are described together with some recent instances of their application in reconnaissance operations (Rathje1 and Franke, 2015). In almost all cases, a comprehensive examination of a huge number of building damage detection systems revealed that they were created following the features of the applied data and the afflicted region. As a result, review articles are used to provide a quantitative comparative evaluation of all of these methodologies (Dong and Shan, 2013).

Also, DInSAR plays a crucial role in earthquake modeling as it provides valuable information about the spatial extent and magnitude of ground displacement caused by earthquakes. DInSAR can identify and measure surface deformations such as ground uplift, subsidence, and horizontal displacements by comparing SAR images recorded before and after an earthquake. This approach allows scientists to examine the distribution and patterns of ground deformation, which can aid in the identification of fault zones, the understanding of fault slide processes, and the assessment of overall seismic activity in an area. Another study compares the various data formats as well as image processing tools for mapping and monitoring earthquakes, faulting, volcanic activity, landslides, flooding, and wildfires, as well as the accompanying damages (Joyce et al., 2009).

High-resolution images obtained from Pléiades and SPOT satellites of Adana and Osmaniye, two of the cities where the earthquake disaster occurred, were published as a web map service and satellite images were presented in the ITU-CSCRS labs (ITU CSCRS, 2023).

Melgar et al. (2023) stated that the results of earthquake relocations for the first 11 days of aftershocks, as well as the inferred rupture models for both events, were presented in this study. These models were obtained through a joint kinematic inversion of HR-GNSS and strong motion data, considering a multi-fault and 3D rupture geometry.

The General Directorate of Geographical Information Systems has data produced and updated by geographical data-producing institutions and organizations within the scope of Turkey's National Geographical Information System (TUCBS) on behalf of the units of The Republic of Türkiye’s Ministry of Environment and Urbanization. These platforms such as ATLAS Basic, and Metadata Portal are quite beneficial for damage assessment, especially with detailed 3D data sources of the earthquake affected areas (Url-5).

The Republic of Türkiye Ministry of National Defence General Directorate of Mapping presented VHR: Very High-Resolution satellite images via the national application of web mapping right after the earthquakes on 6 February 2023. Thus, the devastation and the buildings damaged by the earthquake are visible on the map (Url-20).

Moreover, ESRI Turkey within the scope of the Esri DRP (Disaster Response Program) program, they provided software and workforce support to all institutions and organizations in need of assistance in the disaster area and supported our citizens in reaching them in the fastest way during search, rescue, and coordination processes (Esri Turkiye DRP, n.d.).

Also, many relevant expert authorities released detailed observation and analysis of the impact reports about the 6 February earthquakes (Url- 2-7).

As can be seen in Url-20 various remote sensing datas are served to those interested, such as optical images (NASA Earth Observatory, 2023; Airbus DS Intelligence, 2023; Url-20), radar imagery (Url 6-9), geospatial data (Url-10; Blackshark-Ai., n.d.), earthquake data (Url 13-15), and analysis results (Earthquake Damage in Türkiye, 2023; ArcGIS Dashboards, n.d.).

Also, after the Kahramanmaraş earthquake sequence occurred, numerous articles were published to analyze the seismic structure and kinematics of the earthquakes in that region. These articles stand as some of the most valuable contributions to the seismic literature, shedding light on the complex geological and tectonic processes at play in the aftermath of the seismic events (Wang et. al., 2023; Okuwaki et. al., 2023; Ding et. al., 2023; Wu et. al., 2023; Xu et. al., 2023; Rodkin et. al., 2023; Goldberg et. al., 2023a; Goldberg et. al., 2023b; Melgar et. al., 2023 and Turunçtur et. al., 2023).

## 2. STUDY AREA AND DATA

According to the Disaster and Emergency Management Presidency (AFAD), Press Bulletin About the Earthquake in Kahramanmaraş – 36, on February 6, 2023, two earthquakes of Mw 7.7 and Mw 7.6 occurred at 04:17 and 13:24, respectively, with epicenters in Pazarcık district (Kahramanmaraş) and Elbistan district (Kahramanmaraş). A total of 11,020 aftershocks occurred, and 45,089 people have lost their lives, according to the Press Bulletin, published on March 1, 2023. 1.971.589 people were removed by the Gendarmerie and with their own resources from Kahramanmaraş, Gaziantep, Şanlurfa, Diyarbakır, Adana, Adıyaman, Osmaniye, Hatay, Kilis, Malatya, and Elazığ and enrolled by submitting a formal deployment to the target provinces' governorships and district governorships (Press Bulletin-36).

Both of the epicenters of the major intense earthquakes are located in Kahramanmaraş province by the AFAD Presidency, and these earthquakes are officially recorded as Kahramanmaraş earthquake sequences internationally.

To provide further details, the Kandilli Observatory and Earthquake Research Institute (KOERI) located the first earthquake epicenter in the Sofalaca neighborhood of the Şehitkamil district in Gaziantep Province, which is quite close to the Pazarcık district in Kahramanmaraş Province. Both authorities agreed that the second earthquake, with a magnitude of Mw 7.6, occurred in Kahramanmaraş Province, but the localization of the districts varied, as Ekinözü for KOERI and Elbistan for AFAD, at 13:24 on the same day. Finally, another earthquake with a magnitude of Mw 6.4 struck on February 20, 2023 in Hatay Province (Kandilli Observatory and Earthquake Research Institute, 2023).

The Hatay earthquake was an aftershock; besides the loss of lives, it caused the collapse of some damaged buildings. The earthquakes were felt over a wide area covering Southeastern Anatolia, Eastern Anatolia, Central Anatolia, and the Mediterranean, causing heavy damage to settlements. According to a review by officials from the T.C. Ministry of Environment, Urbanization, and Climate Change, 202,000 buildings in the region urgently needed demolition, were severely damaged, or have collapsed. On March

14, 2023, AFAD also, announced that 48,448 people died in the earthquake (Kandilli Observatory and Earthquake Research Institute, 2023).

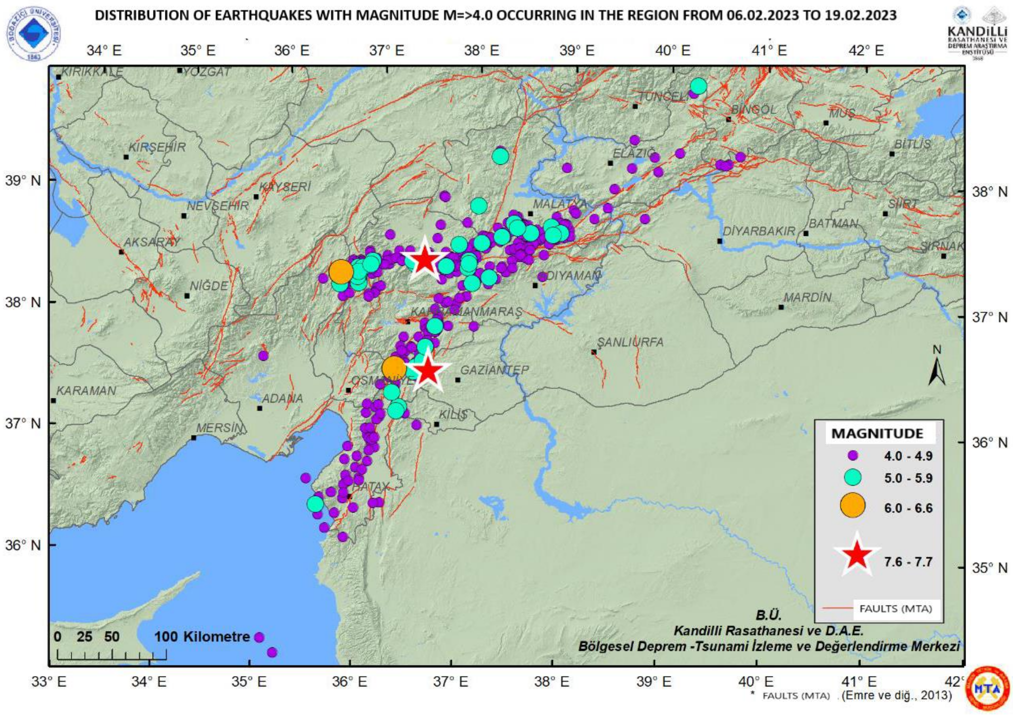


**Figure 2. 1.** Kahramanmaraş epicentered earthquakes (Kandilli Observatory and Earthquake Research Institute, 2023).

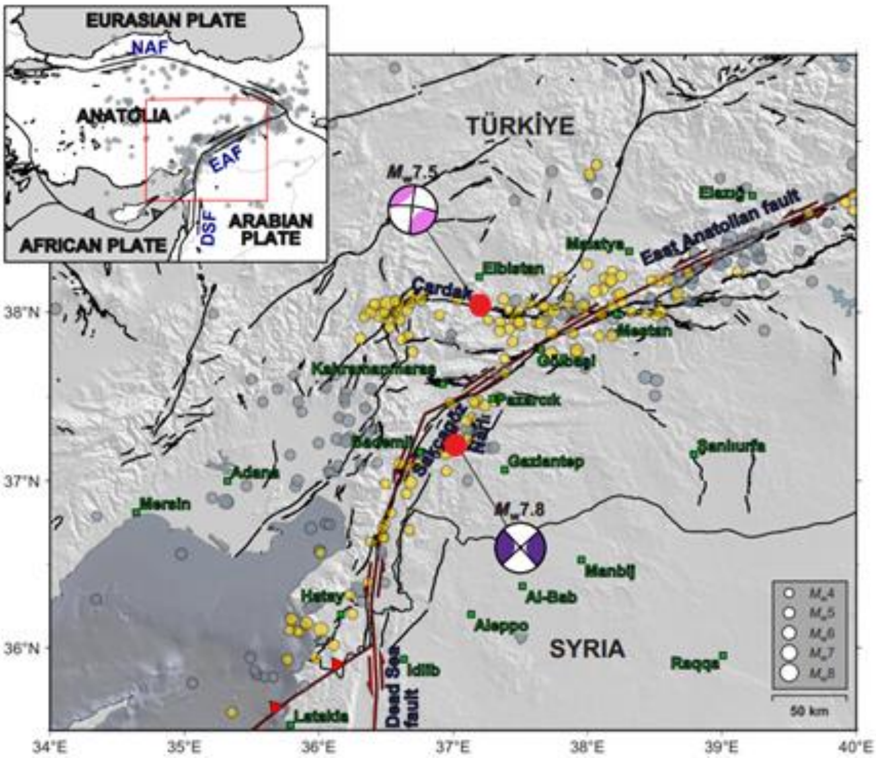


**Figure 2. 2.** The research area is depicted on a map (Goldberg et al., 2023a).

**Table 2. 1.** Kinematics of the Kahramanmaraş Earthquakes (Url-22).

| **Kahramanmaraş Earthquake Sequences** | **Pazarcık Earthquake (Şehitkamil)** | **Elbistan Earthquake (Ekinözü)** |
|---|---|---|
| Moment magnitude scale (Mw) | 7.7 | 7.6 |
| Date time (Turkey, GMT+3) | 01:17 | 10:24 |
| Location | Pazarcık (Kahramanmaraş) | Elbistan (Kahramanmaraş) |
| Depth (km) | 8.6 | 7 |
| Vs30 (m/s) | 541 m/s | 246 |
| PGA(cm/sn2) | 2039.20 (TK.4614 EW) | 635.45 (TK.4612 NS) |
| PGV(cm/sn) | 186.78 (TK.3123 NS) | 170.79 (TK.4612 NS) |
| PGD(cm) | 142.08 cm (TK.3137 NS) | 90.99 (TK.4631 EW) |

In this thesis, we will utilize the local terms used by KOERI because they are more convenient, given the similarity between the damage assessed data points by Yer Çizenler NGO.

Major tectonic plates and boundaries are depicted in the inset, including the North Anatolian Fault (NAF), East Anatolian Fault (EAF), and Dead Sea Fault (DSF). The gray circles represent historical earthquake epicenters.The primary tectonic boundaries are depicted in red on Figures 2.2 with additional mapped faults highlighted in black. Gray circles reflect seismicity during the previous 50 years (Mw between 4 and 5), scaled by earthquake magnitude. The Mw 7.7 Pazarcık and Mw 7.6 Elbistan earthquake sequence, as well as their NEIC Wphase centroid moment tensor (WCMT), are shown in purple and pink, respectively. Additional Mw between 4 and 5 earthquakes in the 2023 series are indicated in yellow (Figure 2.2.). Locations of relevant faults, EAF, DSF, Çardak fault, and Sakçagöz, and Narlı segments are given in dark blue. Nearby city locations are shown in green (Figure 2.2).

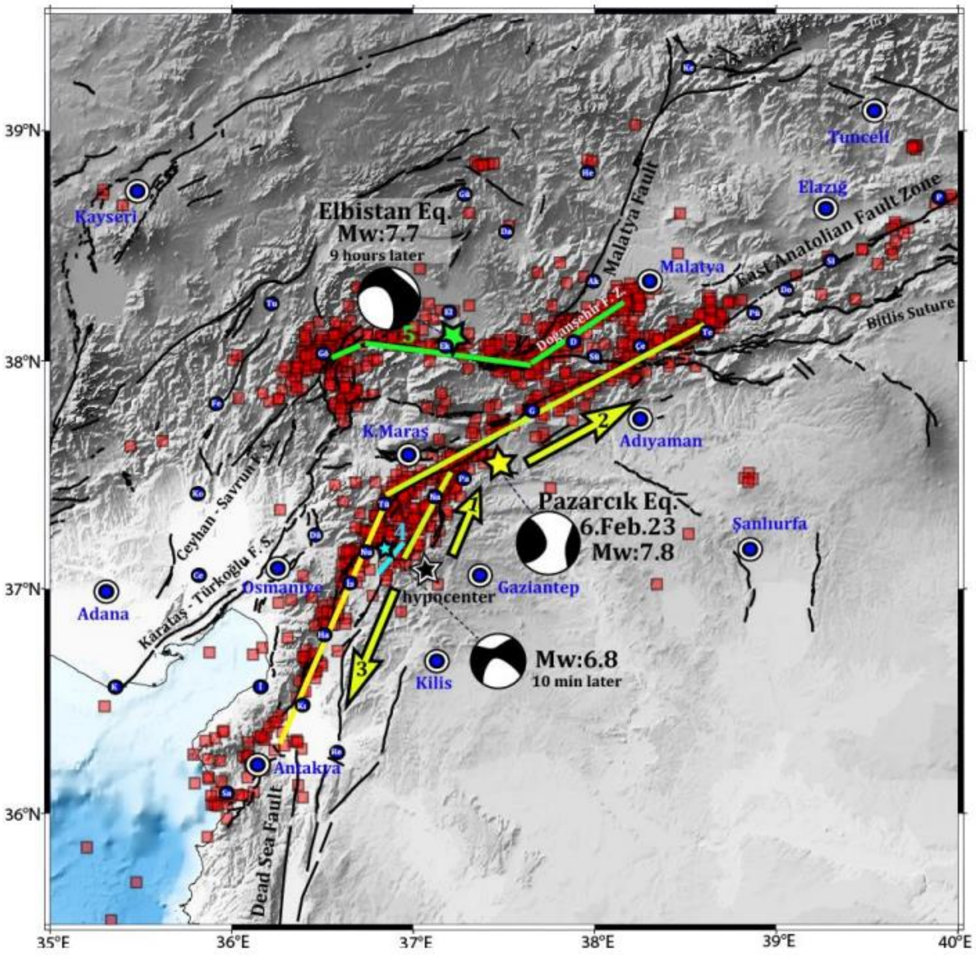


**Figure 2. 3.** The research area is depicted on a map (Goldberg et al., 2023a).

After the earthquake series, surface ruptures have been mapped using publicly available satellite imagery, aerial images provided by the General Directorate of Mapping (Turkey), and fieldwork conducted by geologists. Images related to the left-lateral displacements of 2.4 m observed on the road near Pazarcık and 6.7 m observed in the Sürgü region are presented in Figure 2.3.

Examples of seismotectonic maps depicting recent large earthquakes' global moment tensor solutions, rupture planes, and aftershocks can be found in Url-3. These maps include arrows that indicate the predicted rupture direction of the original Pazarcık earthquake with a magnitude of Mw 7.8, showcasing directivity and discontinuous rupture progression. The ruptures are numbered in chronological order, and further details can be found in (Çetin, 2023).

**Table 2. 2.** Number of Total Buildings in Earthquake-Affected Provinces (Presidency of The Republic of Turkey Presidency of Strategy and Budget, 2023).

| **Status** | **Number of Buildings** | **Number of Detached Units** |
|---|---|---|
| Undamaged | 860.006 | 2.387.163 |
| Lightly Damaged | 431.421 | 1.615.817 |
| Moderately Damaged | 40.228 | 166.132 |
| Severely Damaged | 179.786 | 494.588 |
| Collapsed | 35.355 | 96.100 |
| Requiring Urgent Demolition | 17.491 | 60.728 |
| Not Assessed | 147.895 | 296.508 |
| **Total** | 1.712.182 | 5.117.036 |

**Table 2. 3.** The number of structures included in the structural damage estimation (March 6, 2023) (Presidency of The Republic of Turkey Presidency of Strategy and Budget, 2023).

| Province | Resident | Workplace | Public | Other | Overall Total |
|---|---|---|---|---|---|
| Adana | 404.502 | 29.920 | 8.916 | 7.779 | 451.117 |
| Adıyaman | 107.242 | 5.765 | 4.370 | 3.119 | 120.496 |
| Diyarbakır | 199.138 | 11.412 | 11.964 | 3.165 | 225.679 |
| Elazığ | 106.569 | 7.221 | 2.872 | 7.051 | 123.713 |
| Gaziantep | 269.212 | 22.829 | 5.480 | 8.162 | 305.683 |
| Hatay | 357.467 | 33.511 | 10.382 | 5.489 | 406.849 |
| Kahramanmaraş | 219.351 | 12.358 | 6.879 | 4.565 | 243.153 |
| Kilis | 33.399 | 1.526 | 1.651 | 736 | 37.312 |
| Malatya | 159.896 | 8.370 | 6.670 | 4.051 | 178.987 |
| Osmaniye | 128.163 | 9.428 | 3.105 | 2.384 | 143.080 |
| Şanlıurfa | 347.902 | 18.847 | 11.790 | 4.089 | 382.628 |
| **Total in 11 Provinces** | 2.332.841 | 161.187 | 74.079 | 50.590 | 2.618.697 |

The southward bending of aftershocks at the western end of the rupture in Figure 2.3 indicates the possible activation of different fault segments. The total length of the fault formed by the main shock is approximately 160 km, and significant surface displacements of 2 to 8 meters have been observed in the field.

In our approach, we opted for a 31 cm resolution when merging the satellite images using ArcGIS Pro. The images were collected with the WV02 sensor on February 28, sourced from Maxar Technologies. This resolution was chosen for its suitability in achieving the desired level of detail and accuracy in our analysis and subsequent applications (ITU CSCRS, 2023).

In our approach, we opted for a 31 cm resolution when merging the satellite images using ArcGIS Pro. The images were collected with the WV02 sensor on February 28, sourced from Maxar Technologies. This resolution was chosen for its suitability in achieving the desired level of detail and accuracy in our analysis and subsequent applications (ITU CSCRS, 2023).

As of March 6, 2023, damage assessments for 1,712,182 structures in the 11 provinces impacted by the earthquake had been completed. As a result, 179,786 buildings were severely damaged, 40,228 structures were moderately damaged, and 431,421 buildings had minor damage. Additionally, 35,355 buildings were demolished, 17,491 buildings required urgent destruction, and 179,786 buildings were severely damaged. In addition to structures used as homes, other buildings that collapsed or sustained significant damage included historical and cultural structures, schools, office buildings, hospitals, and hotels (Presidency of The Republic of Turkey Presidency of Strategy and Budget, 2023).

While the epicenters of the earthquakes differ according to AFAD and Kandilli Observatory, the selected areas in this thesis refer to the regions within the scope of the study. In this regard, the Şehitkamil district of Gaziantep Province, the Ekinözü district of Kahramanmaraş Province, and the Antakya district of Hatay Province were analyzed in this thesis.

## 2.1 Şehitkamil District, Gaziantep Province

On February 6, 2023, a very strong earthquake with a magnitude of Mw=7.7 (Ml=7.4) occurred at the epicenter Sofalaca-Şehitkamil-Gaziantep at 04:17 local time. The focal depth of the earthquake was about 8 km and it was a shallow focused earthquake. The earthquake was felt in a vast area, including Southeastern Anatolia, Eastern Anatolia, Central Anatolia, and the Mediterranean (Kandilli Observatory and Earthquake Research Institute, 2023).

KOERI-BDTIM rapidly reported the earthquake's local magnitude as ML=7.4 and moment magnitude as Mw=7.7 shortly after its occurrence. Following the swift announcement of the preliminary evaluation, the location was more accurately identified as 37.1757 North - 37.085 East using data from more distant earthquake recorders (Figure 2.5). The revised position information was then estimated using both Kandilli Observatory and AFAD's near-field earthquake stations, and the results are shown in Figure 2.5. The analysis utilized data from Kandilli and AFAD's near-field seismic monitoring stations to establish the position as 37.2318 North - 37.0029 East. This position also falls within the boundaries of Gaziantep Province.


**Figure 2. 4.** Location map of Sofalaca neighborhood-Şehitkamil district -Gaziantep province (Mw=7.7) earthquake (Kandilli Observatory and Earthquake Research Institute, 2023).

In light of this information, an area of interest that will facilitate our study has been determined by taking into account the data points we have assigned damage levels, and the study area has been customized in line with the need, as seen in Figure 2.6.

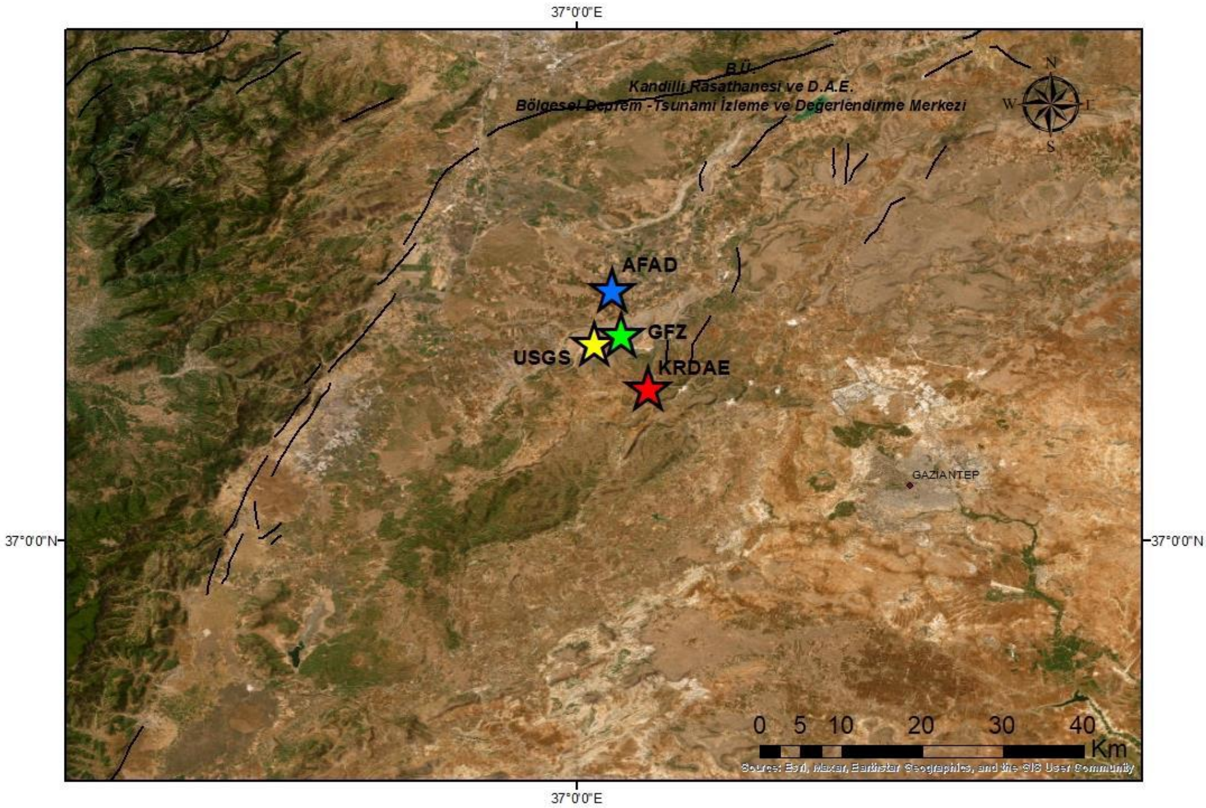


**Figure 2. 5.** February 6 2023, 04:17 Location map of Şehitkamil-Gaziantep earthquake given by different centers (KRDAE, 2023).

**Table 2. 4.** Location and magnitude information of Sofalaca-Şehitkamil -Gaziantep (Mw=7.7) earthquake given by different centers.

| Date | KRDAE | AFAD | USGS |
|---|---|---|---|
| **06.02.2023 - 04:17** | 37.17-37.08 | 37.28-37.04 | 37.22-37.02 |
| **Mw** | 7.7 | 7.7 | 7.8 |
| **Depth (km)** | 10 | 8.6 | 10 |
| **Moment Tensor** |  |  | 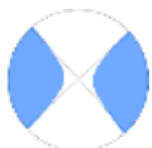 |

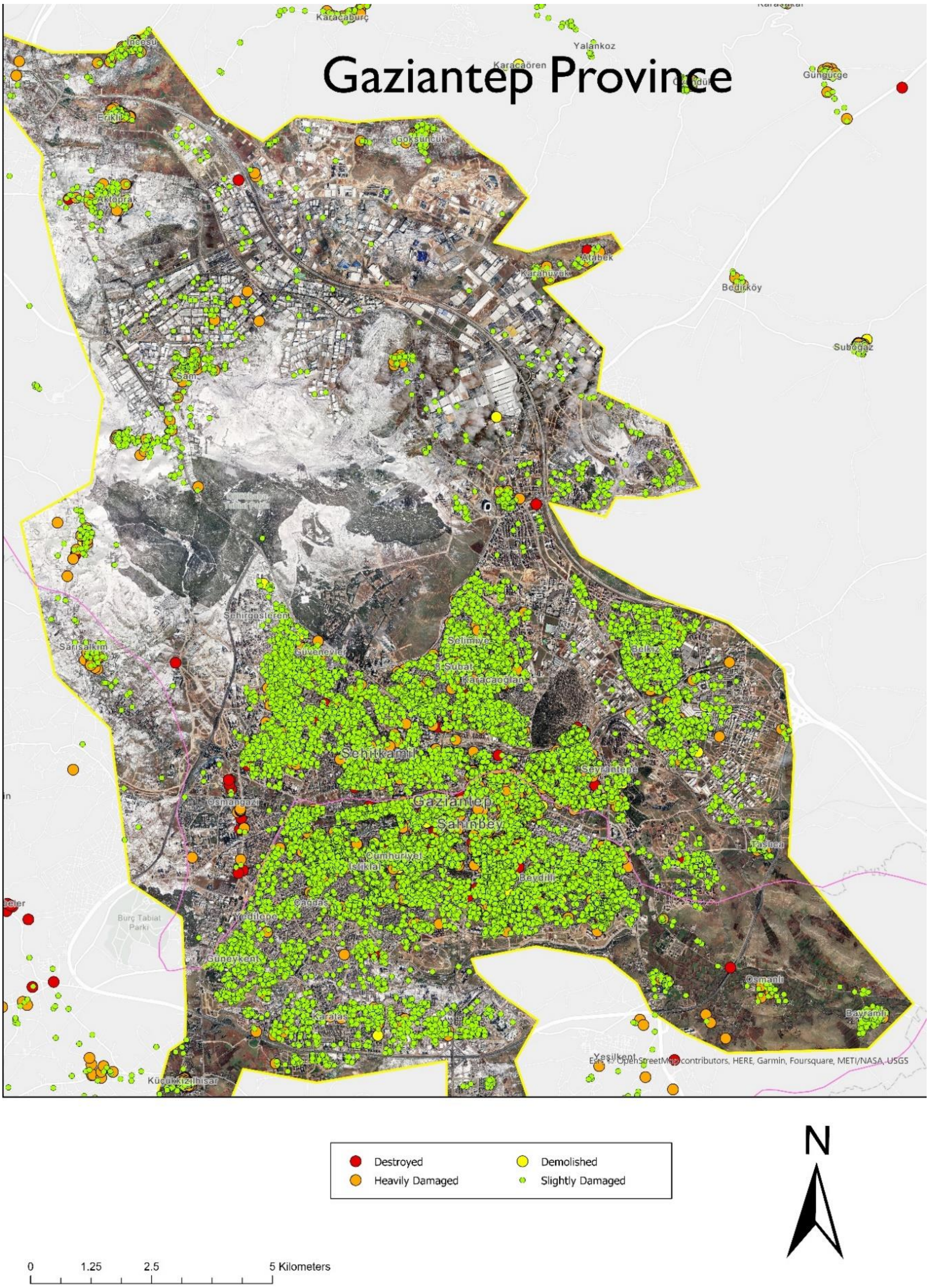


**Figure 2. 6.** Gaziantep assessed damaged points on Maxar images.


**Figure 2. 7.** Şehitkamil District, Gaziantep Province.

### 2.2 Ekinözü District, Kahramanmaraş Province

On February 6, 2023, in the middle of Ekinözü district, Kahramanmaraş province (38.0717 N- 37.2063 E), at 13:24 local time with a magnitude of Ml = 7.5 and Mw = 7.6, an earthquake occurred. The earthquake's focal depth was 7.6 km. It is a shallow-oriented earthquake. The earthquake struck Southeastern Anatolia, Eastern Anatolia, and Central Anatolia, and it was felt throughout the Mediterranean region (Kandilli Observatory and Earthquake Research Institute, 2023).

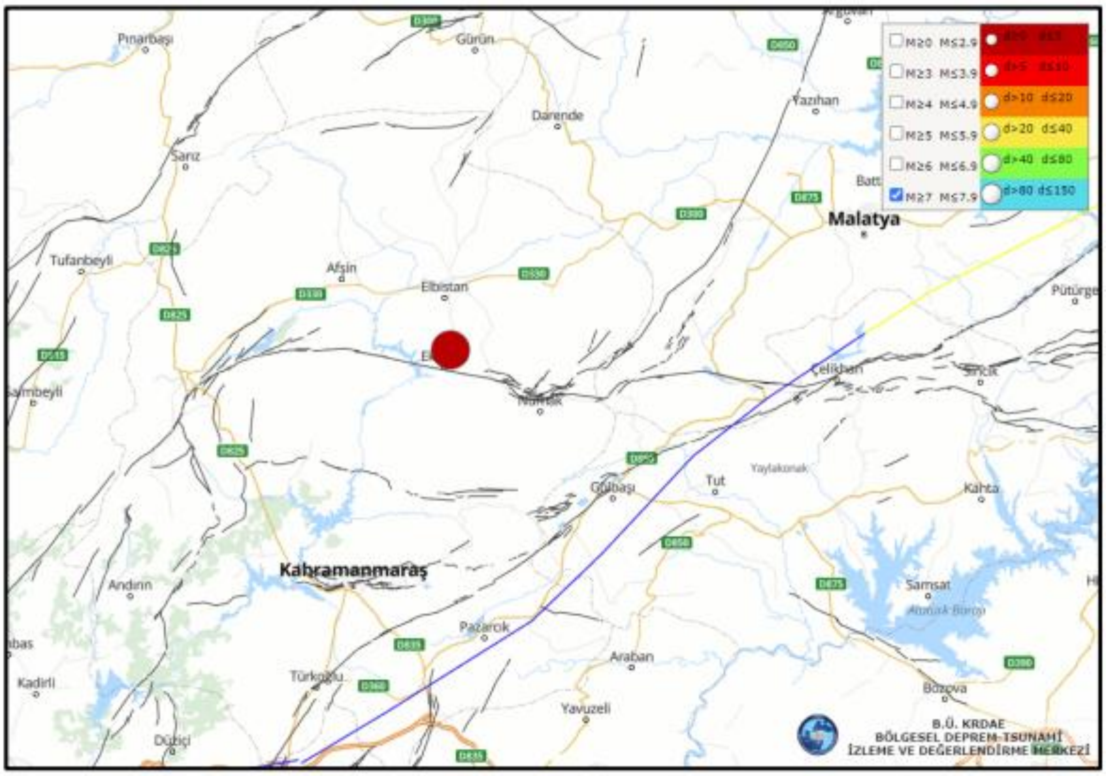


**Figure 2. 8.** Location Map of the Ekinözü-Kahramanmaraş (Mw=7.6) Earthquake (Kandilli Observatory and Earthquake Research Institute, 2023).

Initial solutions are sent to the European Mediterranean Seismological Center (EMSC) by different seismological centers. Location information from different seismological centers is shown in Figure 2.5 and 2.9.

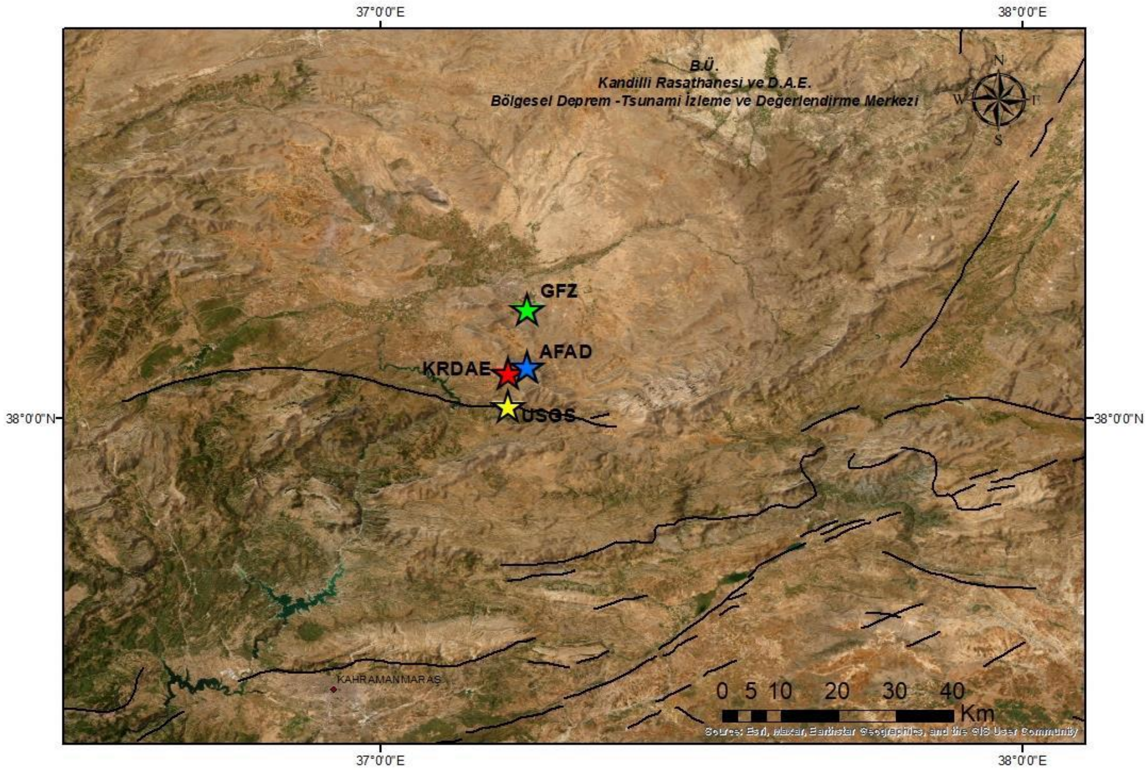


**Figure 2. 9.** February 6 2023, 13:24 Location information of Ekinözü-Kahramanmaraş earthquake given by different seismology centers (KRDAE, 2023).

**Table 2. 5.** 06.02.2023 13:24 Location and magnitude information of Ekinözü-Kahramanmaraş earthquake given by different centers.

| Date | KRDAE | AFAD | USGS |
|---|---|---|---|
| **06.02.2023 - 04:17** | 38.07-37.20 | 38.08-37.23 | 38.02-37.20 |
| **Mw** | 7.6 | 7.6 | 7.5 |
| **Depth (km)** | 10 | 7 | 10 |
| **Moment Tensor** |  | 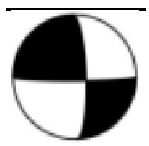 | 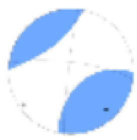 |

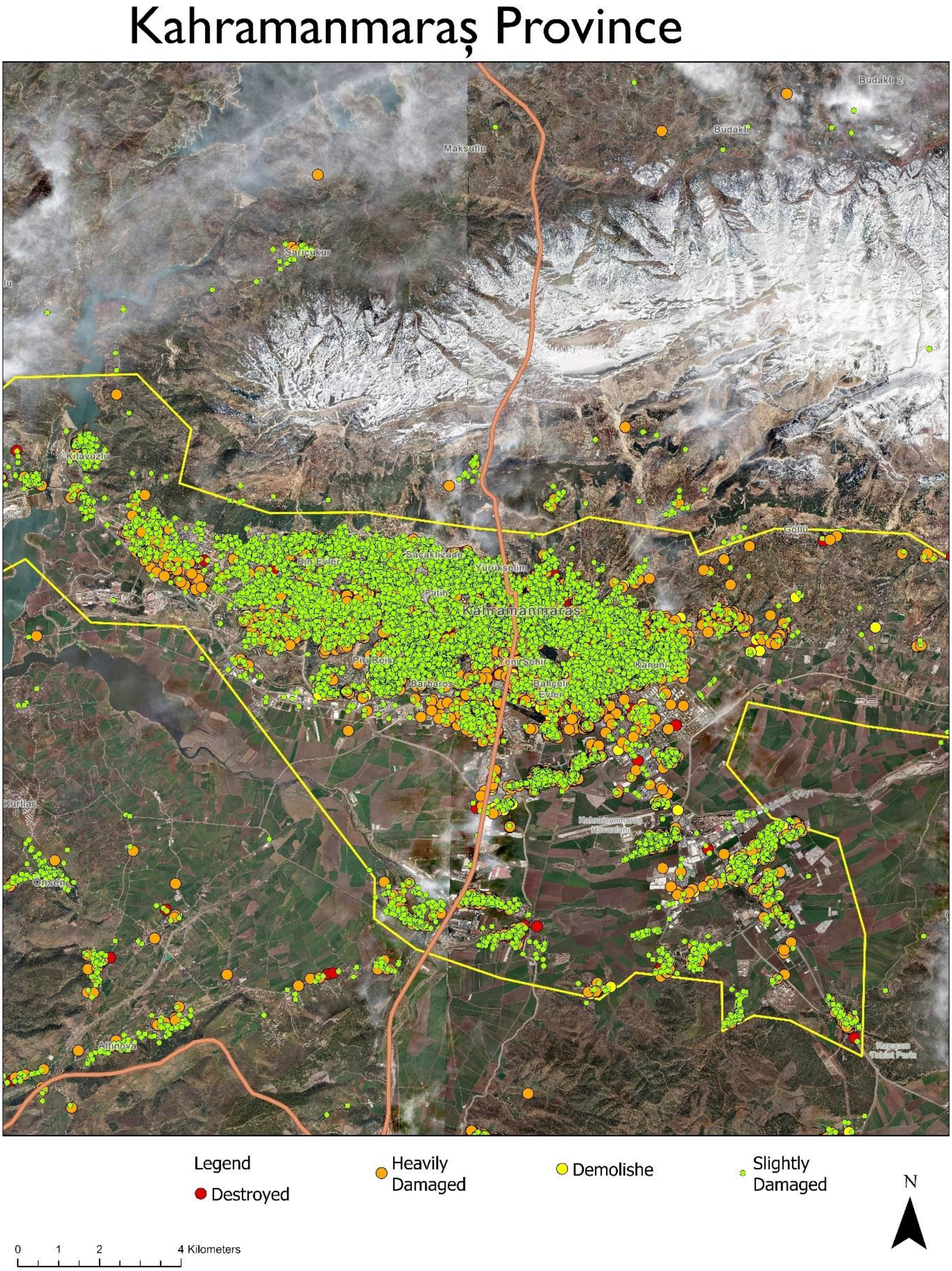


**Figure 2. 10.** Kahramanmaraş assessed damaged points over Maxar imagery.

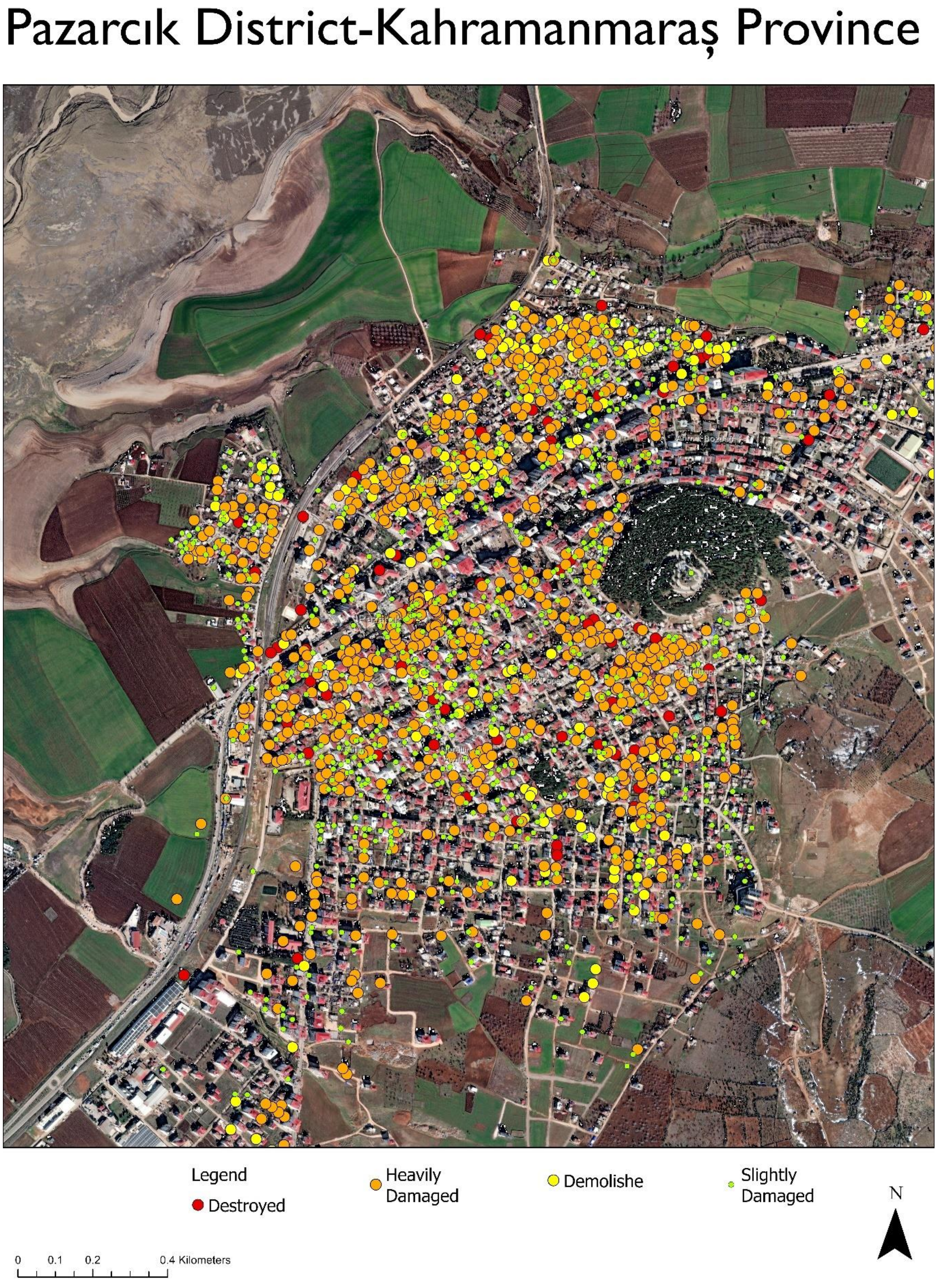


**Figure 2. 11.** Pazarcık District, Kahramanmaraş Province

Approximately 9 hours after the first earthquake, at 13:24, a second earthquake with a magnitude of Mw7.6 occurred in Ekinözü district with the rupture of the Sürgü-Çardak fault. Although the magnitude of this earthquake is close to the magnitude of the first earthquake, the total length of the fault segments broken (ruptured) in the first earthquake is about 300 km, while the total length of the fault segments broken in the second earthquake is around 100–120 km. While the total rupture time of the fault segments was around 80 seconds in the first earthquake and it was 30-35 seconds in the second earthquake (Figure 2.2). Relatively lower seismic moments were also observed in the eastern and western parts of the Sürgü-Çardak fault. Although the general character of the fault is strike-slip, the GCMT moment tensor solution shows that the fault plane is inclined 42 degrees to the north. (Tanırcan and Kaya Eren, 2023).

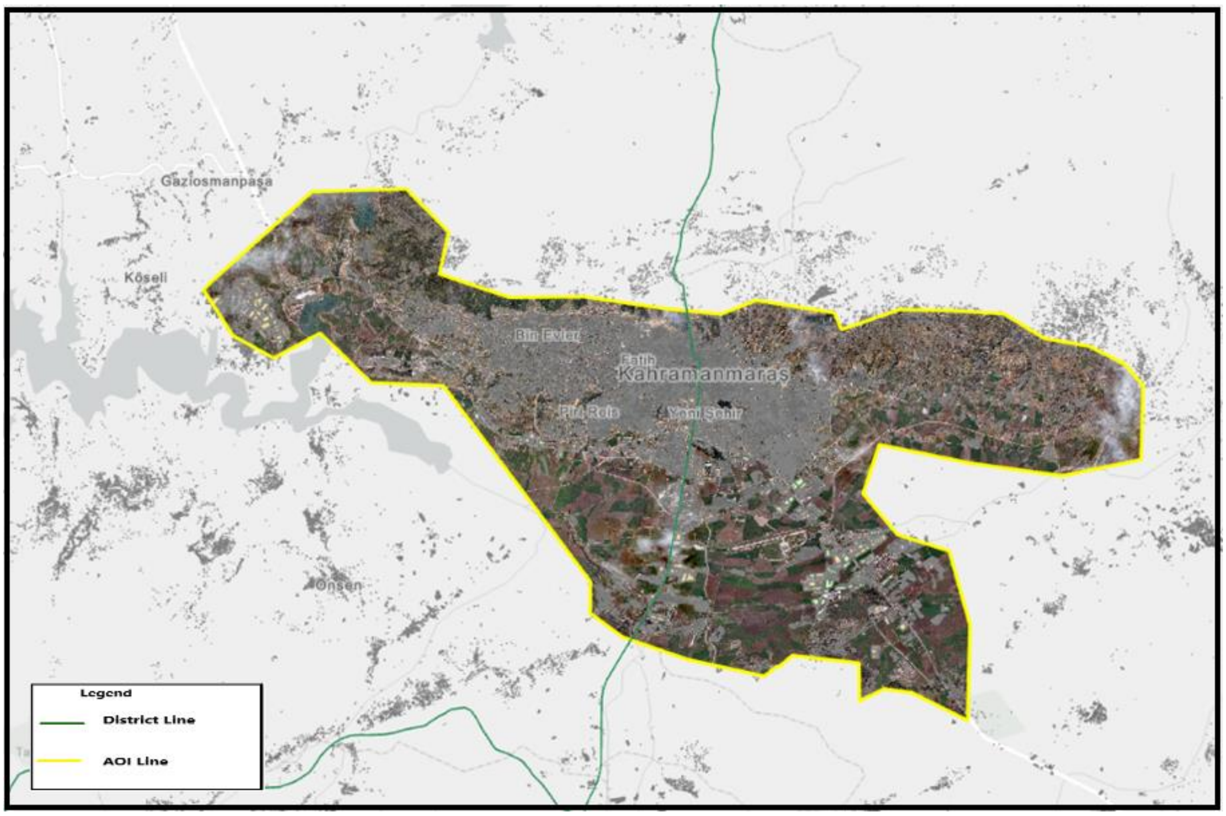


**Figure 2. 12.** Kahramanmaraş with Area of Interest.

## 2.3 Antakya District, Hatay Province

On February 20, 2023, a very strong earthquake with an instrumental magnitude of Mw=6.4 (local magnitude ML=6.4) struck at 20:04 local time at the epicenter of Büyükçat-Samandağ-Hatay according to the primitive solutions. The focal depth of the earthquake was 20 km. The earthquake was felt in the Mediterranean, Eastern, and Southeastern Anatolia regions, Syria, Israel, Palestine, Jordan, Lebanon, and Egypt. (Tanırcan and Kaya Eren, 2023).

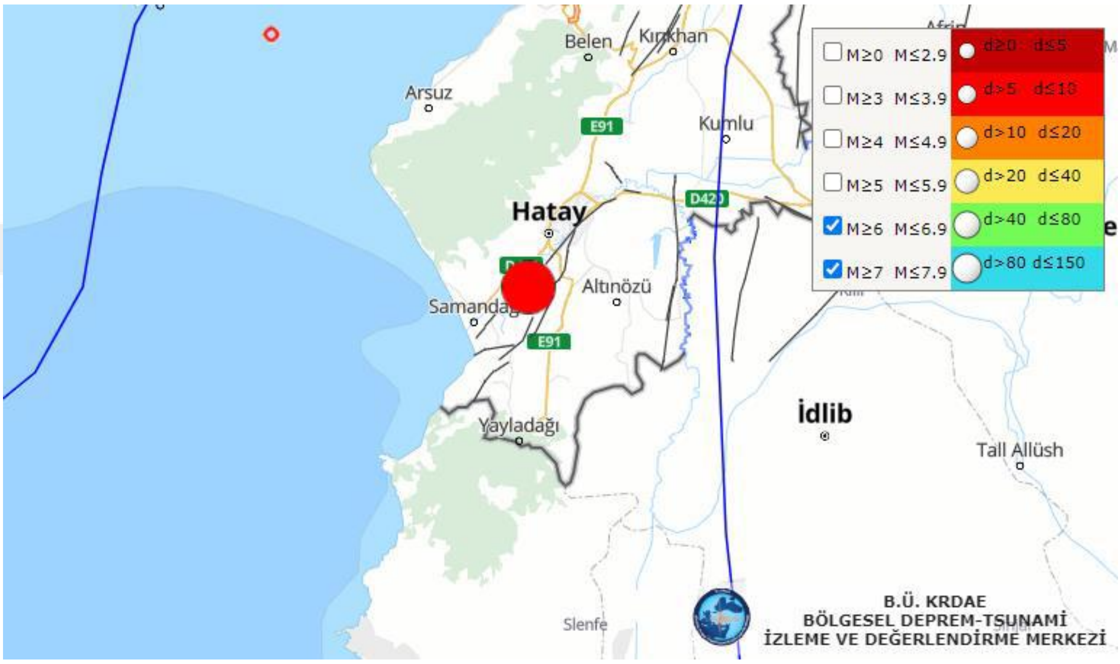


**Figure 2. 13.** Primal solution location of the Büyükçat-Samandağ-Hatay (Ml=6.4) earthquake Earthquake (Kandilli Observatory and Earthquake Research Institute, 2023).

After the preliminary assessment was quickly announced, the location was more precisely determined as 36.0077 North - 36.1310 East using data from remote earthquake recorders.

To sum up, this earthquake sequence is a singular example of a complex rupture with a multi-event nature since it exhibits directivity effects along the rupture's margins and discontinuous temporal evolution over several fault segments. The distribution of aftershocks shows that the earthquake rupture reached as far as Antakya District Hatay Province in the south and ended in the north on the Pütürge fault section near the Doğanyol, Elazığ earthquake in 2020 (Figure 2. 3). The total length of the mainshock-generated rupture is just over 300 km and large surface displacements of 3-7 m are observed at the surface (Url -29).

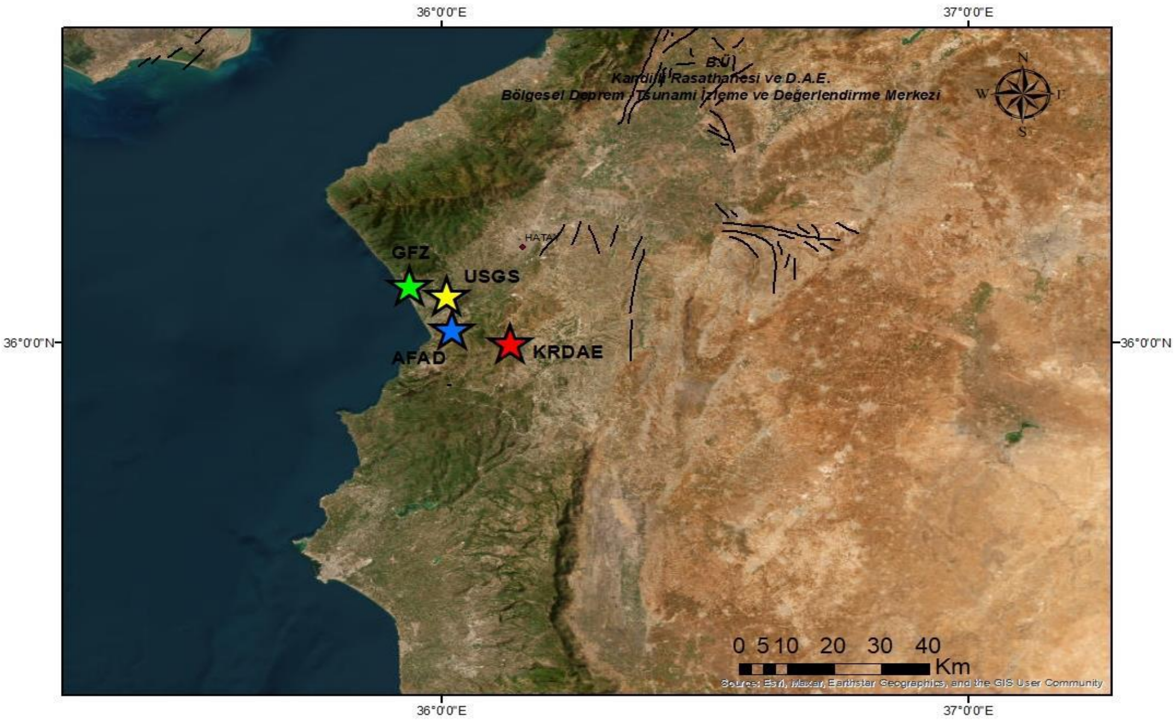


**Figure 2. 14.** Büyükçat-Samandağ-Hatay (ML=6.4) location information given by different seismology centers Earthquake (Kandilli Observatory and Earthquake Research Institute, 2023).

**Table 2. 6.** Location and magnitude information of 20.02.2023 20:04 Samandağ-Hatay earthquake given by different centers.

| Date | KRDAE | AFAD | USGS |
|---|---|---|---|
| **06.02.2023 - 04:17** | 36.00-36.13 | 36.03-36.02 | 36.10-36.01 |
| **Mw** | 6.4 | 6.4 | 6.3 |
| **Depth (km)** | 20.2 | 21.73 | 36.10-36.01 |
| **Moment Tensor** |  |  | |

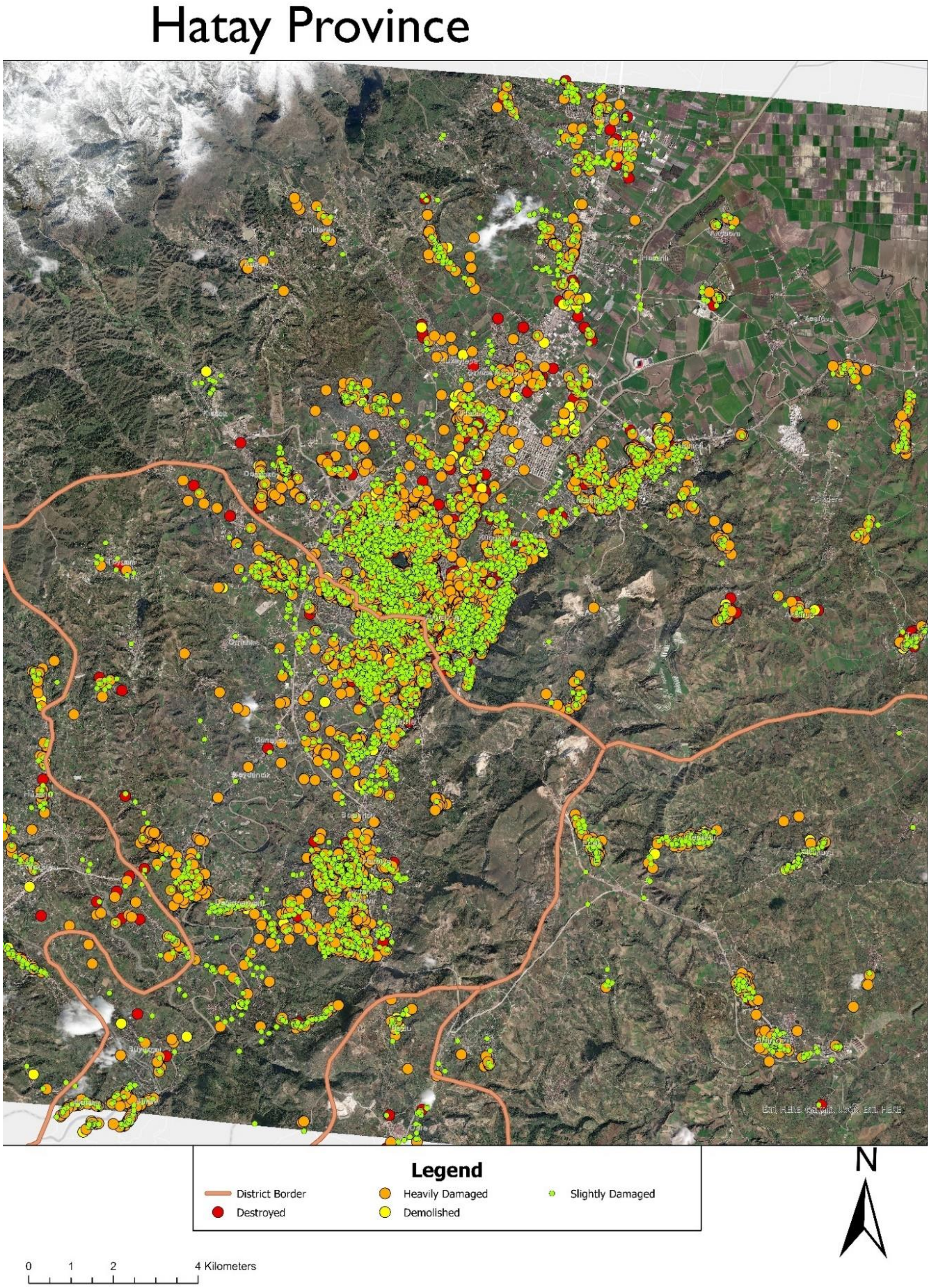


**Figure 2. 15.** Hatay, Antakya city centre with assessed damage points.

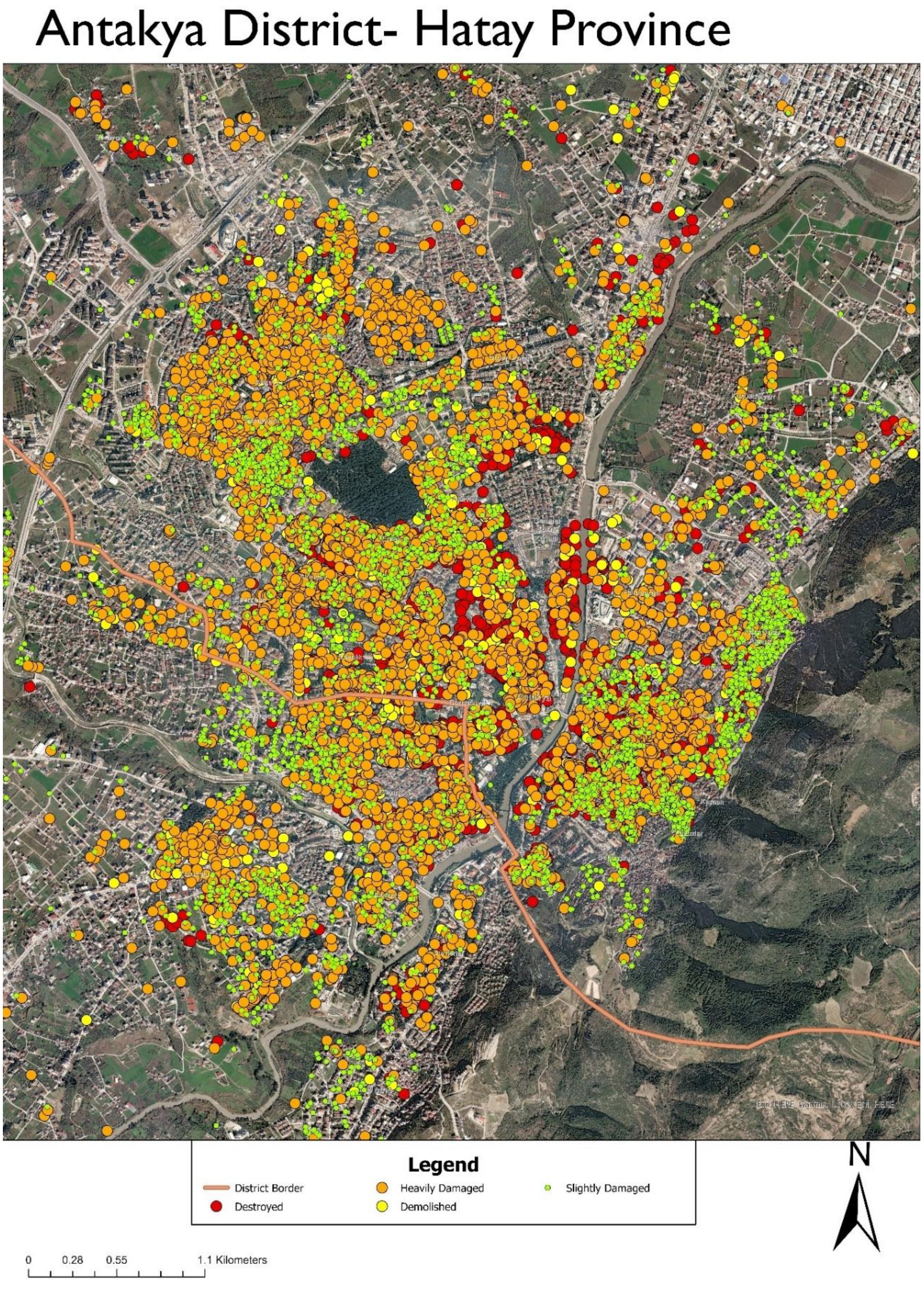


**Figure 2. 16.** Antakya District, Hatay Province.

### 2.4 Data

In this thesis we used various customized datasets, ranging from chip size to earthquake affected provinces.

#### 2.4.1 Satellite images

On Monday, February 6, 2023, at 4:17 a.m. local time, a devastating magnitude 7.7 earthquake hit the Turkish province of Kahramanmaraş, around 23 kilometers east of Nurdağı in the Gaziantep province near the Syrian border, followed by a 7.6 magnitude aftershock nine hours later (Url-4). More than 50,000 people have perished and tens of thousands have been injured in Turkey and Syria. These figures are expected to grow as search and rescue activities continue. Millions of people in the region have been impacted by the earthquake and its aftershocks. In the ten most severely affected areas, millions of people in the region have been affected by the earthquake and its aftershocks. Turkey's president declared a three-month state of emergency in ten earthquake-ravaged districts (Presidency of The Republic of Turkey Presidency of Strategy and Budget, 2023).


**Figure 2. 17.** Before and after the Kahramanmaraş earthquake (Stadiums Become Shelters: Satellite Pics Show Turkey Earthquake Damage, 2023).

**Table 2. 7.** The parameters of the satellite images received from Maxar Technologies for the study areas.

| Province | Image ID | Sensor Source | Collected | Image off Nadir | Bands | Image Clouds | Max Target Azimuth |
|---|---|---|---|---|---|---|---|
| **Hatay** | 10300100E18CB600 | 0.67 m | WV02 | 2023/02/11 | 8 bands | 34.6° | 139.5° |
| **Hatay** | 10300500D9F8D500 | 0.78 m | WV02 | 2023/02/08 | 8 bands | 40.2° | 85.6° |
| **Kahramanmaraş** | 10300100E3154100 | 0.66 m | WV02 | 2023/02/28 | 8 bands | 34.0° | 193.3° |
| **Kahramanmaraş** | 10300100E2C66F00 | 0.69 m | WV02 | 2023/02/28 | 8 bands | 36.1° | 195.6° |
| **Gaziantep** | 10300500D9F8D100 | 0.83 m | WV02 | 2023/02/08 | 8 bands | 41.8° | 99.8° |
| **Gaziantep** | 10300100E2226200 | 0.67 m | WV02 | 2023/02/12 | 8 bands | 34.4° | 342.7° |

On February 7, 2023, Maxar shared pre- and post-earthquake satellite imagery of earthquake zones provided by the WV02 sensor with various resolutions through the Open Data Program Turkey and Syria Earthquake 2023, (2023, February 8), and these satellite images are provided resampled at 31 cm resolution, 3 bands, and 8 bit unsigned with OpenStreetMap as well (Url-25).

Although we only utilized Maxar images for this study, we specifically chose satellite images from Kahramanmaraş city to present the optimum models and metrics, as we will elaborate on later in the study.

### 2.4.2 Damage points

For the earthquakes that occurred on February 6, 2023, data on building damages was extracted by Gece Yazilim from hasar.cbs.gov.tr and demonstrated by Yer Cizenler NGO and İhtiyaç Haritası which was updated on February 20, 2023. Damage levels are indicated by the colors on a map of damaged buildings received from (Url-25).

On February 7, 2023, Maxar shared pre- and post-earthquake satellite imagery of earthquake zones provided by the WV02 sensor with various resolutions through the Open Data Program Turkey and Syria Earthquake 2023, (2023, February 8), and these satellite images are provided

resampled at 31 cm resolution, 3 bands, and 8 bit unsigned with OpenStreetMap as well (Url-25).

Although we only utilized Maxar images for this study, we specifically chose satellite images from Kahramanmaraş city to present the optimum models and metrics, as we will elaborate on later in the study.

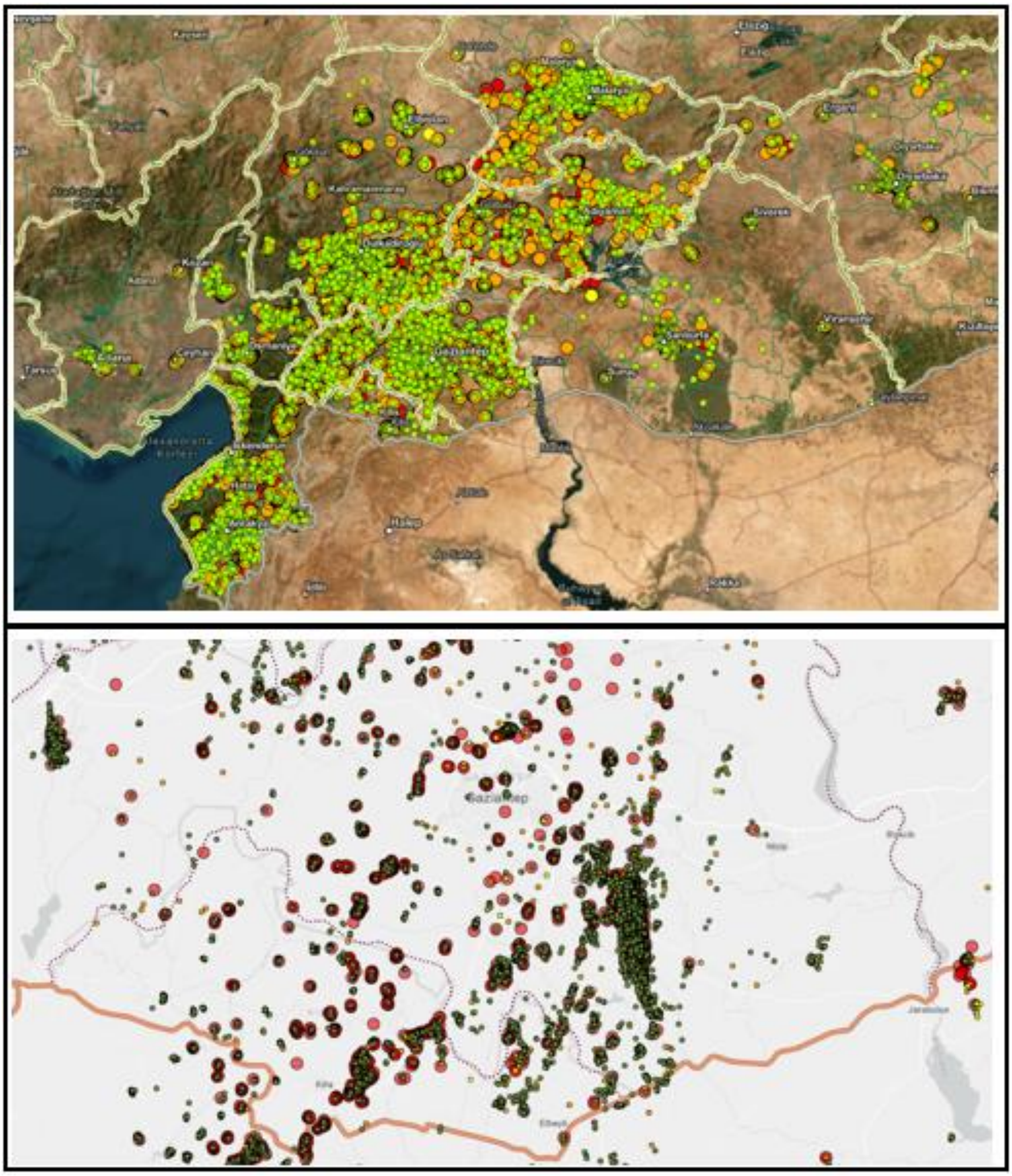

**Figure 2. 18.** Assessed four scaled damage points for Kahramanmaraş earthquakes (Url-25).

There are 4 damage grades: as Collapsed, Heavily Damaged, Damaged and Slightly Damaged and in our study, the attributes were coded as Col, HevDam, Dam, and Slig (Url-25).

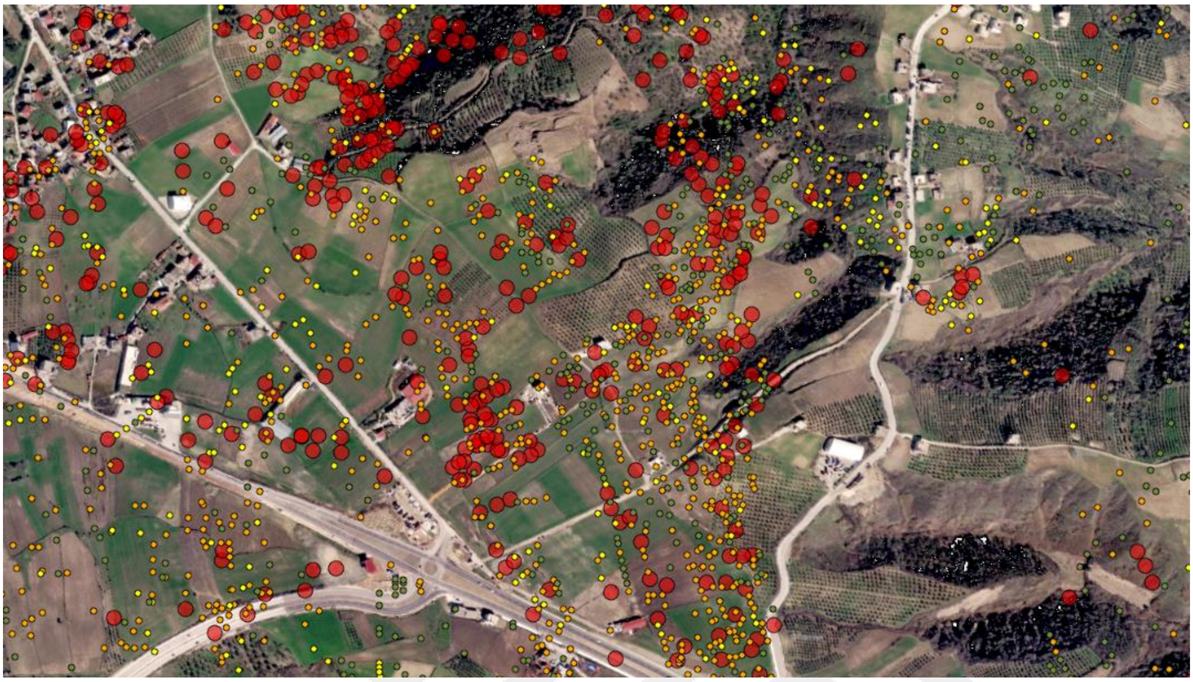

**Figure 2. 19.** Four scaled damaged points.

These damage assessment points are the essential foundation of this study. We have gratefully obtained these data points through the invaluable contribution of Yer Çizenler NGO.

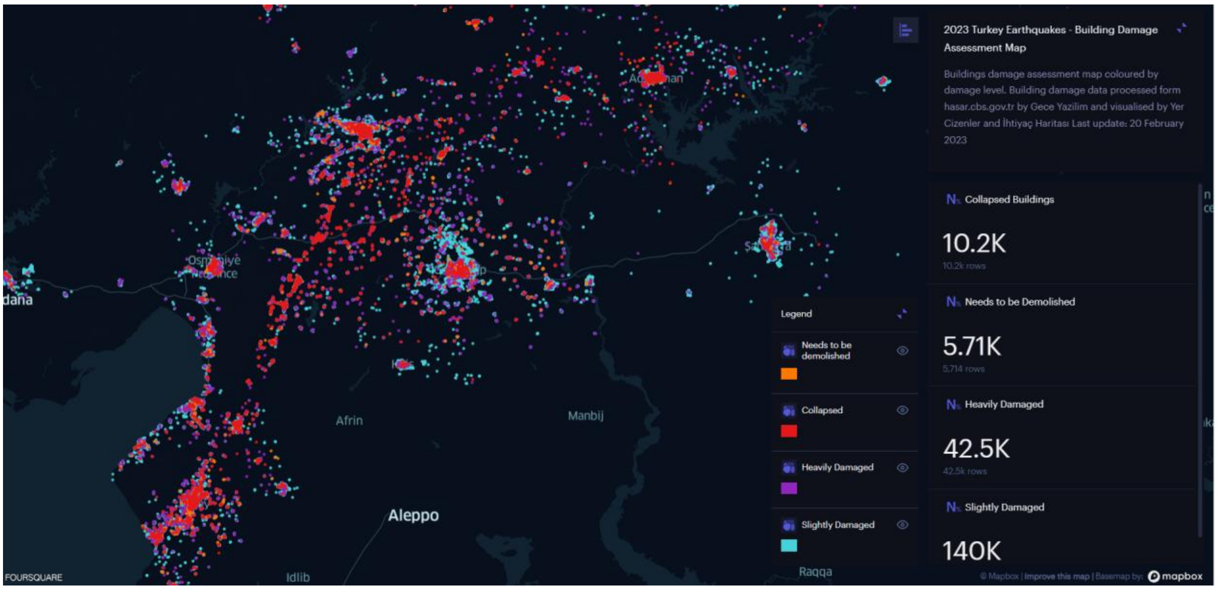


**Figure 2. 20.** Damage point taken from (Url-25).

### 2.4.3 Building footprints

Humanitarian OpenStreetMap Team (HOTOSM) is utilized for obtaining updated and customized building footprint extracts from OpenStreetMap. These exports come in various formats suitable for GPS and GIS applications, such as shapefile and geojson.

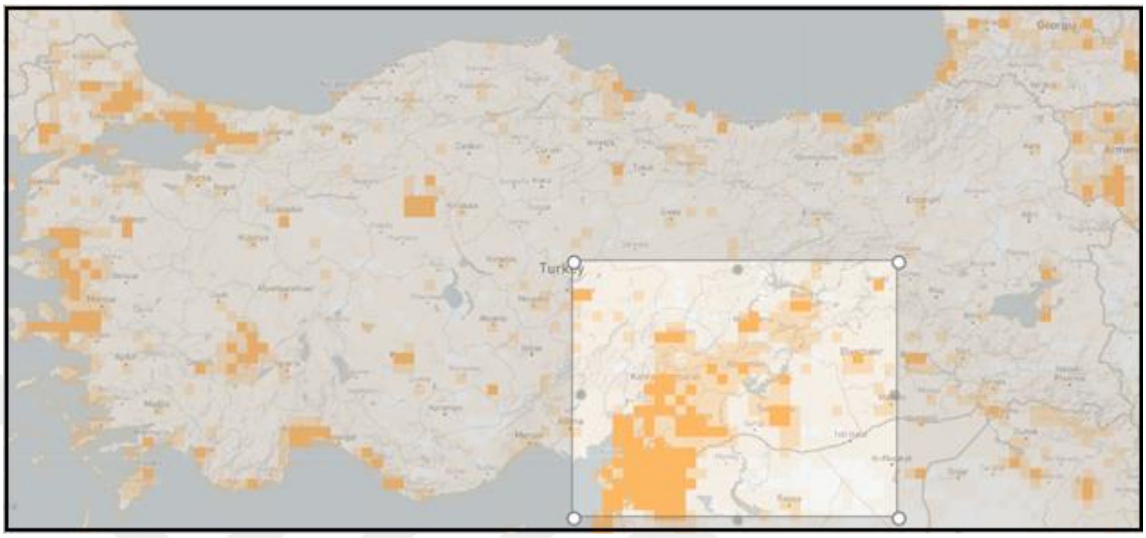

**Figure 2. 21.** Recent info building intensity of HOTOSM (HOT Export Tool, 2023).

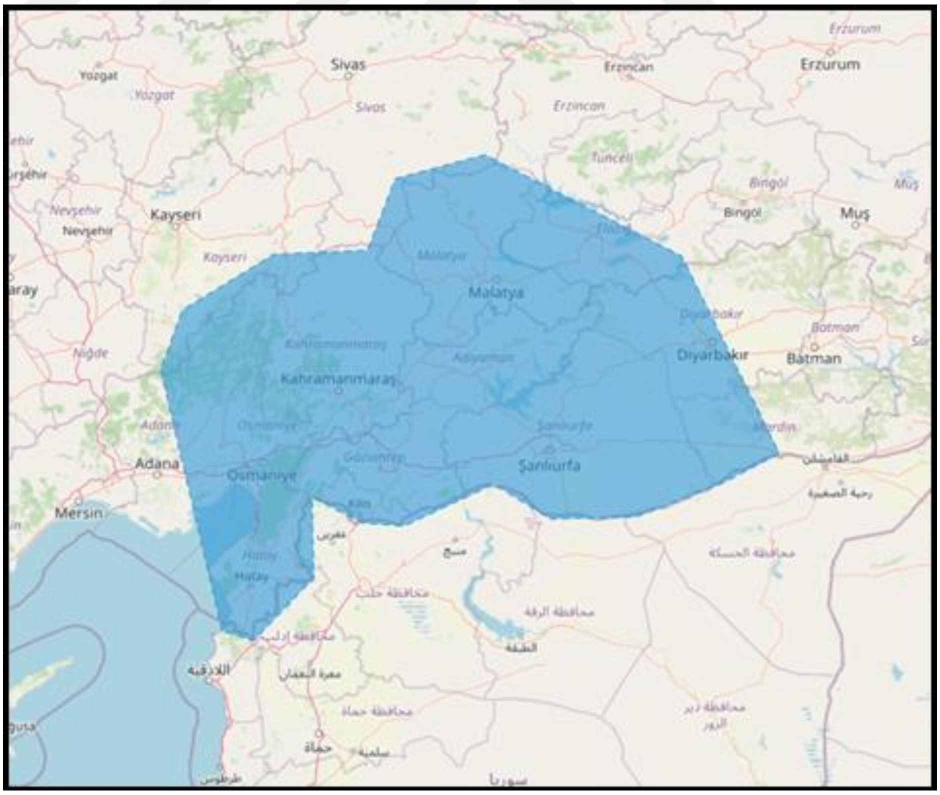


**Figure 2. 22.** The custom area we extracted building shapefiles from (HOT Export Tool, 2023).


**Figure 2. 23.** All building polygons and buildings with damage assessment overlaid on the satellite image.

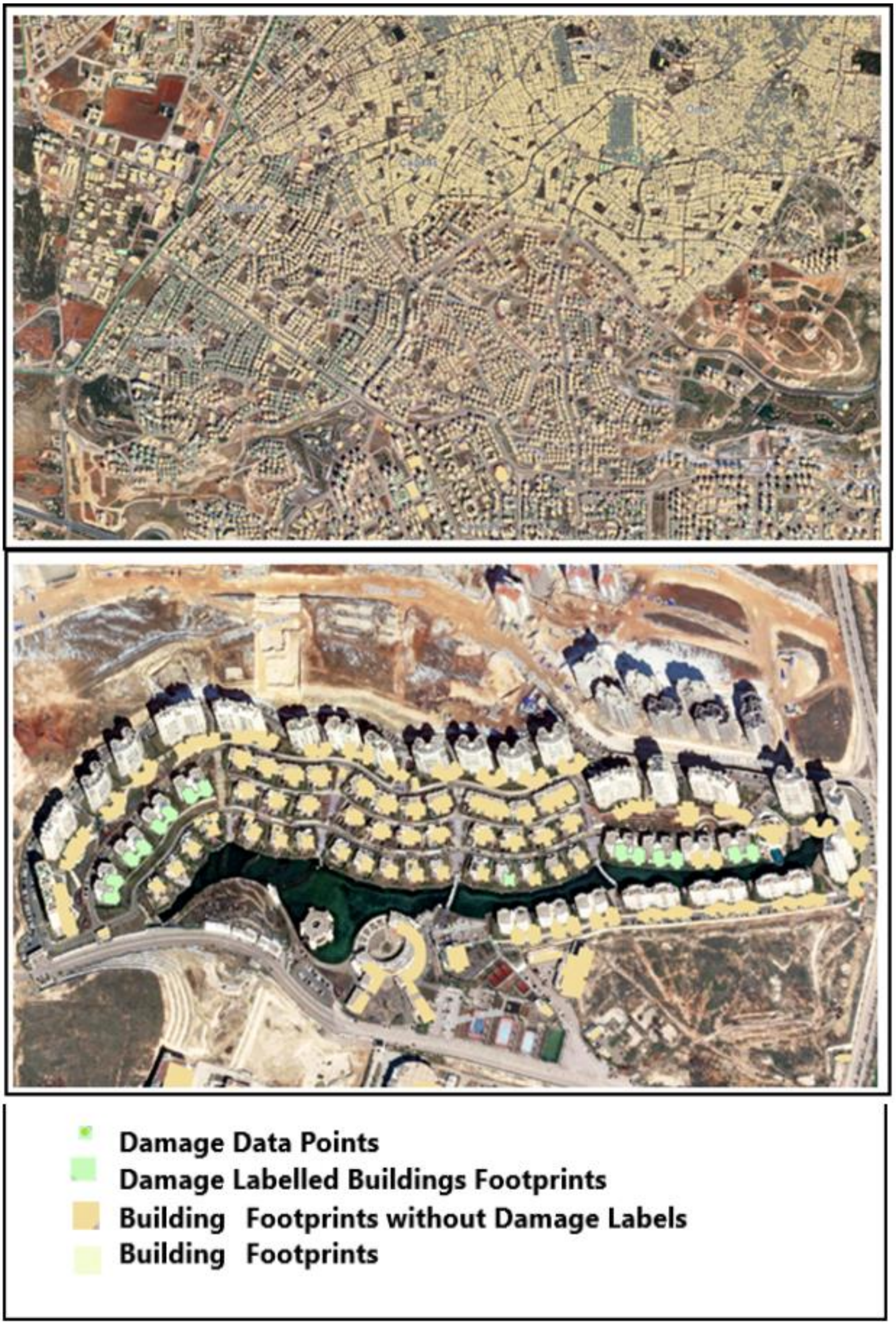


**Figure 2. 24.** Buildings with damage assessment based on post-earthquake images do not match here.

We possess polygonal data representing building footprints and point data indicating four-scaled damages. Now, the challenge is to assign the features of the point data as labels to the recently acquired building footprints. To accomplish this task, we employ *the Spatial Join (Analysis) Tool,* which proves to be a convenient solution within ArcGIS Pro (Esri, n.d.).

**Figure 2. 25.** Building footprints and damage data points close up.

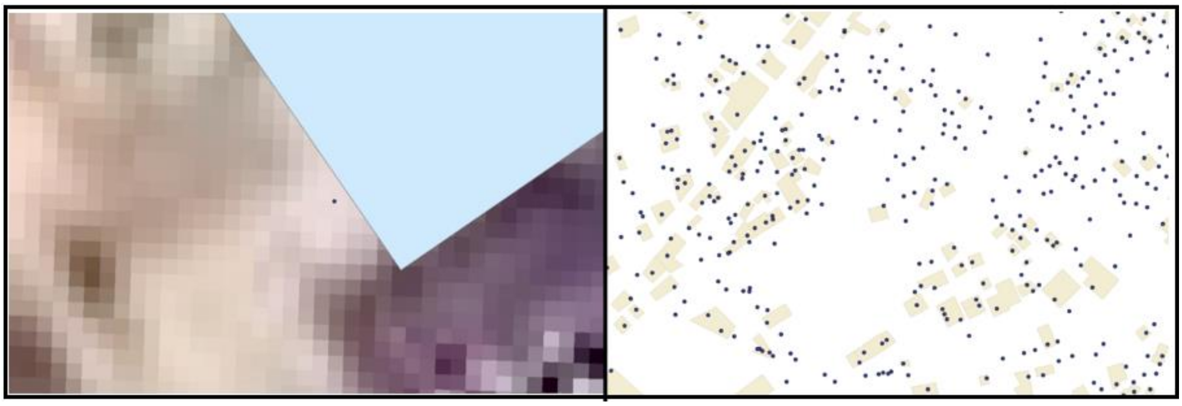

**Figure 2. 26**. Results of intersection match option.

So instead of 12,000 buildings at the intersection, we have 29,000 labeled building footprints within a 5-meter distance. We tried a 10-meter distance as well, and we had more than 36 thousand data points, but if we include the buildings that do not overlap with the building pixels on the satellite images, this decision did not seem like a logical step. Moreover, the training accuracy significantly improved with the 5-meter distance option, reaching around 90 percent, compared to approximately 80 percent accuracy with the 10-meter distance option. This improvement in accuracy reinforces the decision to choose the 5-meter proximity for labeling the building footprints.

The first method that came to mind was to perform an intersection between the points and building footprints. Through this approach, we successfully obtained over 12,000 labeled building footprints. However, when using the intersection match option, numerous closely located data points were not added to the building footprints (refer to Figure 2.25-2.26). This poses a potential challenge since some buildings may not precisely align with the post-earthquake image when they are initially drawn, resulting in significant data loss.  So, we went to another method, which is the within a distance match option. Thus, we examine and visualize labeled building footprints within 5, 10, 20, and meter distances. The further we move away from the established damage points, the less realistic the results will be

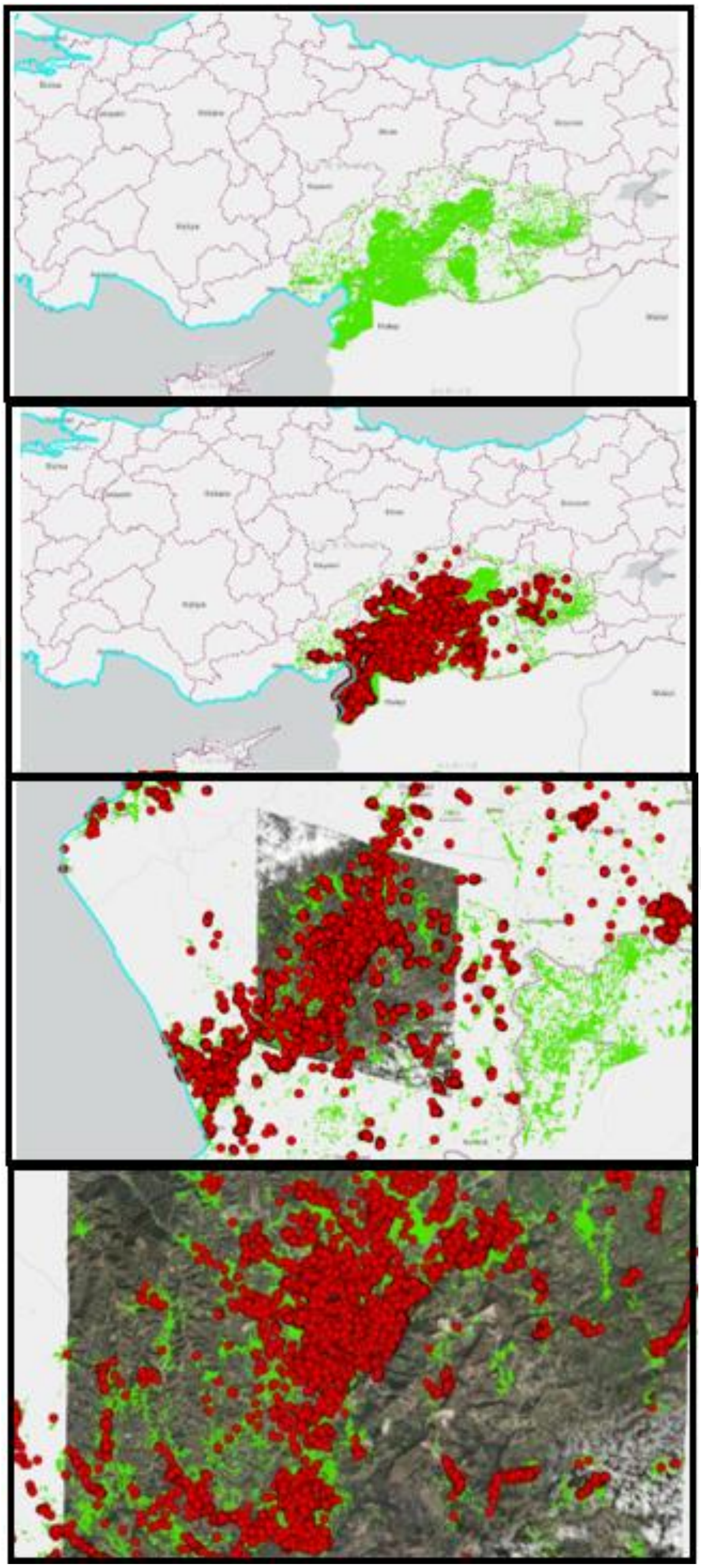

**Figure 2. 27.** Building footprints (green polygons) and damage data points (red points).

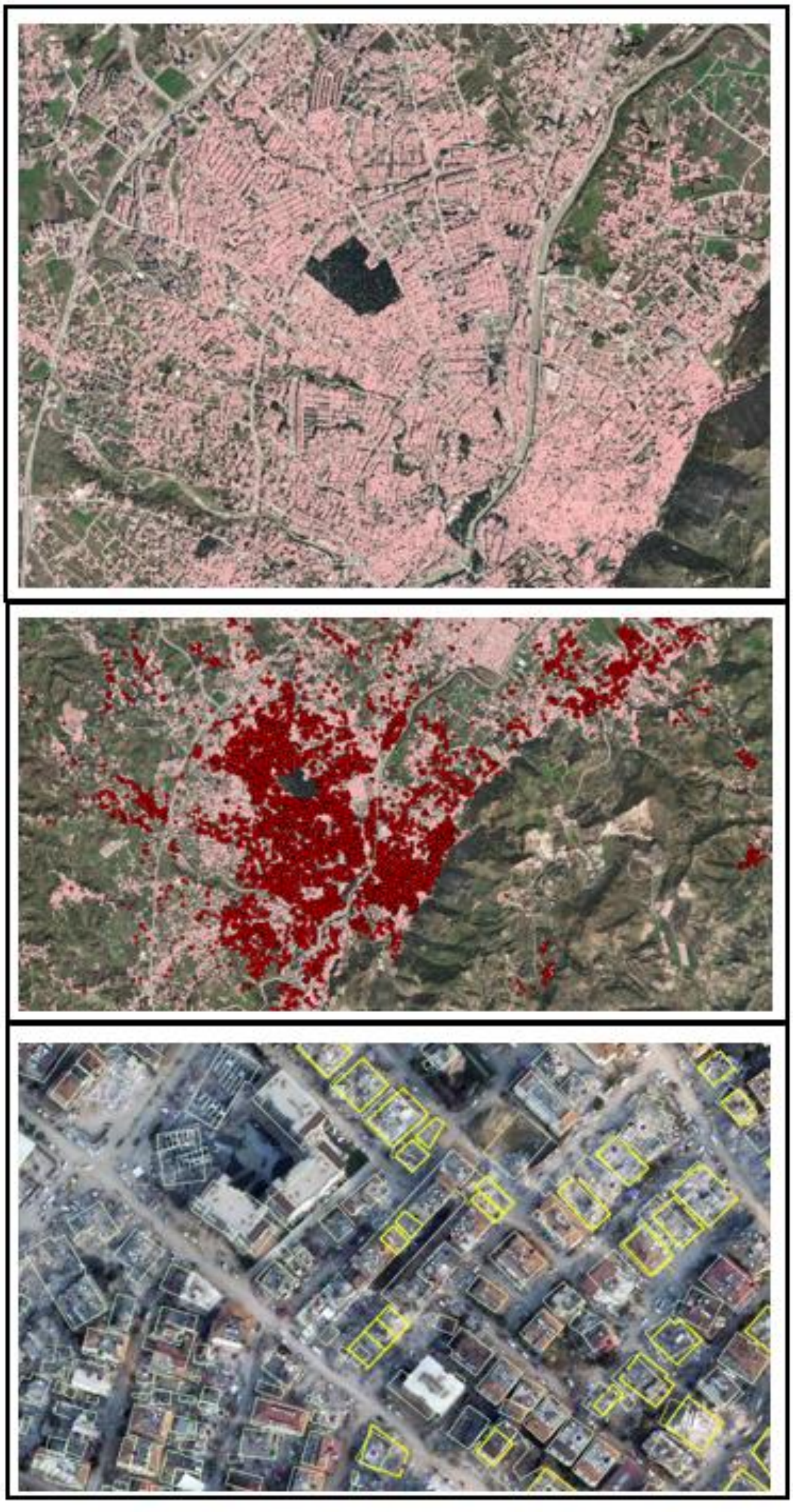

**Figure 2. 28.** Antakya City Center building footprints, damage points and, close up demonstration.

# 3. METHODOLOGY

After we reached out to the imagery data, it was decided that Kahramanmaraş would be the best option for model training. Because comparing the building footprint overlap ratio of the images and the damage level data point distribution balance would affect the model accuracy, and it was a time-consuming and crucial process to choose the best imagery data.

## 3.1 Deep Neural Networks (DNN)

Semantic segmentation (pixel-based classification) in deep neural networks is a procedure that assigns pixels in an image to one of several classes. In remote sensing, pixel-based classification can be used to identify different types of land cover or to separate roads and structures from satellite images. It also includes two inputs: a raster image with multiple bands and a labeled image with the label for each pixel, also, models such as U-net, DeepLabV3, Feature Pyramid Network, and Pyramid Scene Parsing Network (PSPNet).


**Figure 3. 1.** Deep Learning approach in ArcGIS Pro ("How U-Net Works," n.d.).

### 3.1.1 Unet

Biomedical image segmentation was the initial application for which U-net was created. Its architecture consists mostly of an encoder network and a decoder network. Unlike classification, where the final output of the deep network is the only factor that matters, semantic segmentation necessitates a mechanism for projecting the discriminative features learned at various stages of the encoder onto the pixel space in addition to pixel-level classification ("How U-Net Works," n.d.).

The encoder is the first half of the architecture diagram. The input image is frequently encoded into feature representations at many levels using a pre-trained classification network like VGG or ResNet and convolution blocks, followed by maxpool downsampling. The decoder is the second component in the design. The goal is to create a dense classification by semantically projecting the encoder's learned discriminative features (lower resolution) onto the pixel space (higher resolution). The decoder is composed of upsampling, concatenation, and typical convolution algorithms.

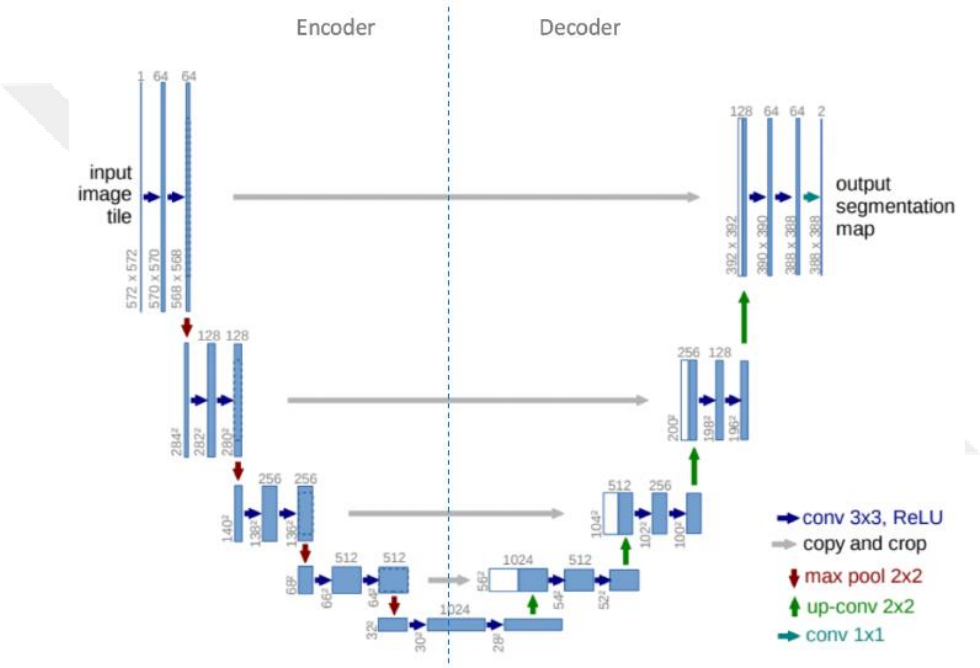


**Figure 3. 2.** Unet Architecture ("How U-Net Works," n.d.).

### 3.1.2 DeepLabV3

DeepLabV3 is a highly renowned deep learning model for semantic image segmentation, widely acknowledged for its exceptional accuracy and state-of-the-art performance across various computer vision applications.

Based on a fully convolutional network (FCN) architecture, DeepLabV3 has the remarkable ability to analyze images of any size. Given an input image, the model generates a pixel based classification map, where each pixel is assigned a label identifying the class to which it belongs. This capability makes DeepLabV3 an ideal choice for tasks requiring precise and detailed segmentation, enabling it to provide valuable insights into complex visual data.

The utilization of DeepLabV3 in our study will enhance the accuracy and efficiency of damage identification in earthquake-affected regions, further solidifying our objective to integrate deep learning, remote sensing, and earth observation techniques for improved disaster management and geophysical studies.

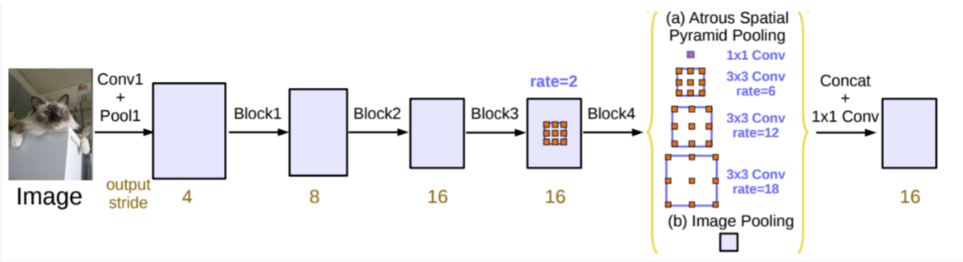


**Figure 3. 3.** DeepLabV3 Model ("How DeepLabV3 Works," n.d.).

DeepLabV3's primary breakthrough is the use of atrous convolution, also known as dilated convolution or sparse convolution. The model can collect multi-scale information using atrous convolution without considerably increasing computing complexity. DeepLabV3 can successfully widen the receptive field by altering the dilation rate of convolutions, allowing the model to catch both fine-grained details and the wider context in the image.

DeepLabV3 also includes a feature known as "atrous spatial pyramid pooling" (ASPP), which improves the model's capacity to gather context at many scales. ASPP is made up of parallel atrous convolutions with varying dilation rates, which are then followed by global pooling operations. This enables the model to successfully capture and integrate context information at different scales.

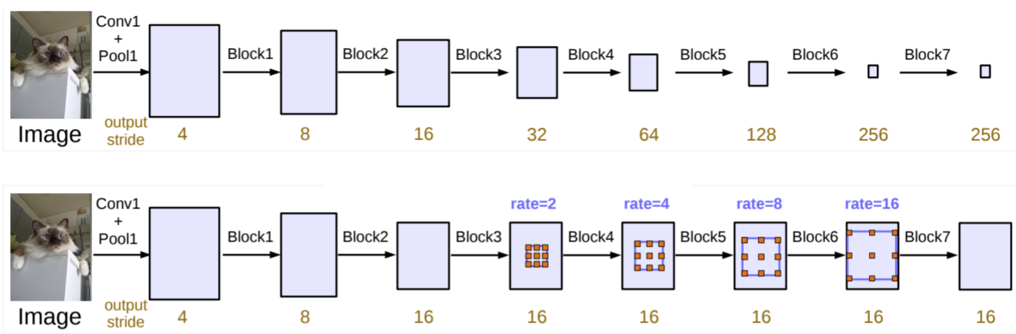


**Figure 3. 4.** DCNN without Atrous Convolution & with Atrous Convolution ("How PSPNet Works," n.d.).

PointRend enhancement is a powerful semantic segmentation augmentation technique employed in DeepLabV3. It operates by selecting a subset of pixels, known as "rend points," based on the confidence of the original predictions. It then refines these points using small "rend fields" surrounding them. This unique approach allows the model to improve predictions by considering both local and global context, thereby enhancing accuracy in regions that are uncertain or ambiguous.

The selected refinement process leads to more precise and comprehensive segmentation masks, significantly improving tasks like object detection and image segmentation. By leveraging PointRend, DeepLabV3 can achieve superior segmentation results, making it an essential tool for our study's goal of damage identification in earthquake-affected regions. It also enables us to handle complex and challenging scenarios, ultimately advancing the effectiveness of our research in disaster management and geophysical studies.

### 3.1.3 Pyramid Scene Parsing Network (PSNET)

PSPNet (Pyramid Scene Parsing Network) is a deep learning network used to segment semantic images. It is intended to categorize each pixel in an image into separate groups.

Primary distinction of the PSPNet is the usage of a pyramid-like structure to promote scale compatibility. Traditional segmentation algorithms that use a single scale struggle to represent objects of varying sizes and levels of detail. PSPNet addresses this by combining feature maps at multiple scales to improve scale Convolution ("How PSPNet Works," n.d.). PSPNet is made up of two primary parts: an encoder and a decoder. The encoder shrinks the input image while creating feature maps at different scales. The feature maps are then combined by the decoder to create a higher-resolution segmentation map.

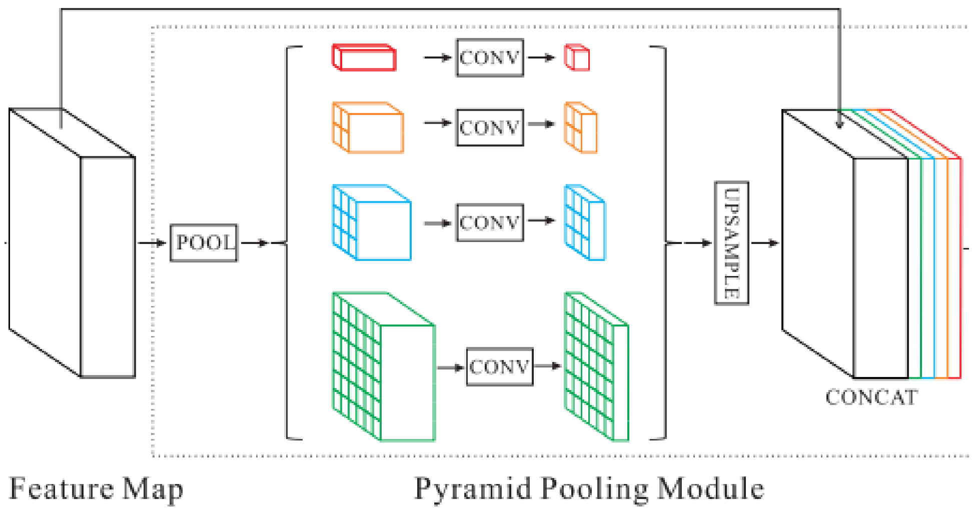


**Figure 3. 5.** PSPNet Architecture ("How PSPNet Works," n.d.).

The "pyramid pooling" module is one of PSPNet's distinguishing features. This module collects contextual information by pooling and combining features from several scales. This allows the network to grasp the context of each pixel, resulting in more accurate segmentation.

PSPNet is built on Convolutional Neural Networks (CNNs), which are widely used for image processing. To extract features from input data, CNN layers use techniques such as convolution, pooling, and activation functions Convolution ("How PSPNet Works," n.d.). PSPNet is widely employed in a variety of applications including as autonomous driving, medical imaging, and remote sensing. PSPNet can generate accurate and thorough segmentation results by successfully exploiting contextual information at different scales.

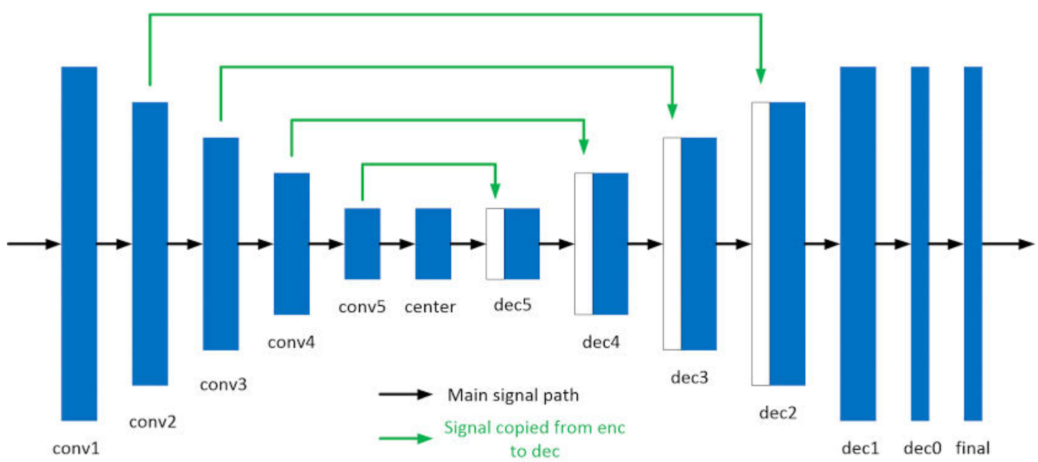


**Figure 3. 6.** Skip connections from encoder to U-Net like decoder ("How PSPNet Works," n.d.).

## 3.2 Software

ArcGIS Pro (ESRI Inc.) is a geographic information system software produced by ESRI, and the most recent version, ArcGIS Pro 3.1, is preferred for these theses. ArcGIS Pro offers a wide range of tools for deep learning and computer approaches, making it a valuable resource for research in these areas. Imagery and Remote Sensing play a crucial role in various fields, including scientific research, environmental studies, business applications, government operations, and disaster assessments. The advanced capabilities of ArcGIS Pro enable efficient and accurate analysis of spatial data, making it a popular choice for researchers and professionals working with geographic information systems. ArcGIS Pro has Deep Learning toolsets that are used for many purposes, such as classifying pixels of the images and exporting training datasets, extracting features, postprocessing the inferenced outputs, and so on. Especially the *Image Anaylst Toolbox* is very beneficial for many custom dataset preparations such as tiling, sizing, rotating, and deep learning for imagery datasets.

### 3.2.1 Arcgis Pro and software libraries

ArcGIS API for Python is a Pythonic GIS API that proves to be highly effective for Deep Learning approaches, as well as utilizing its toolboxes. The integration of modern Pythonic libraries such as Jupyter Notebook, Fastai, PyTorch, and TensorFlow is seamless and successful in ArcGIS Pro. This integration empowers users to leverage the capabilities of these open-source libraries within ArcGIS Pro.


**Figure 3. 7.** Arcgis Pro Python API ("Overview of the ArcGIS API for Python," n.d.).

Specifically, Jupyter Notebook is used for custom data augmentations, metrics visualizations, and modifying model options that default toolboxes cannot support, all facilitated via the arcgis.learn module. This enables researchers and practitioners to tailor their Deep Learning workflows to suit specific requirements and achieve more accurate and precise results.

The hardware system used for these operations consists of NVIDIA Geoforce RTX 2060 Intel® UHD GPU graphics cards, an i7-10750H processor, 16 GB of memory, and the Windows 10 operating system. This hardware configuration ensures a robust and efficient computing environment, allowing for the seamless execution of Deep Learning tasks within the ArcGIS environment.

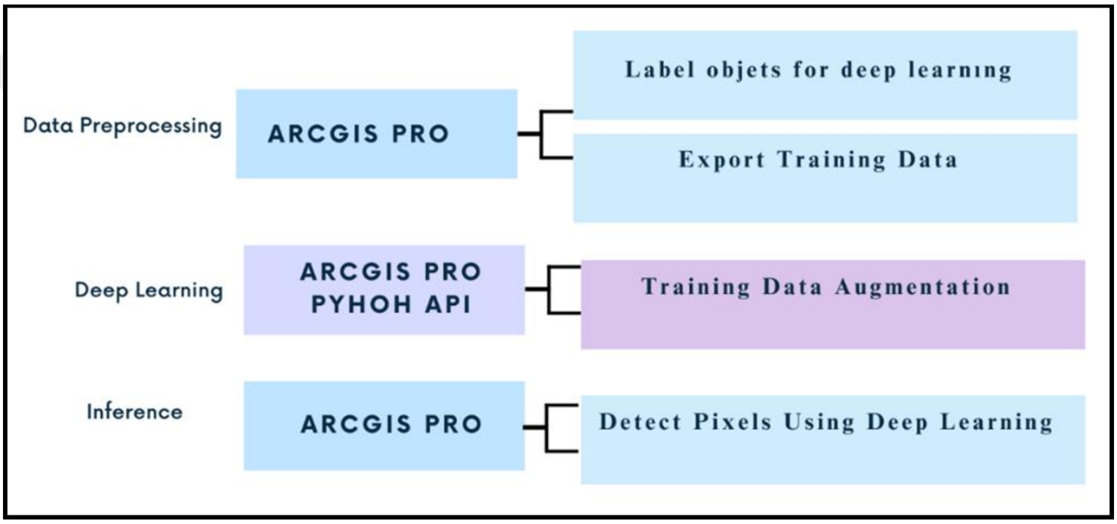


**Figure 3. 8.** Deep Learning Approach in ArcGIS Pro.

### 3.2.2 Preparation of the training data

Labels are just as crucial as the data in the training dataset when it comes to deep learning models. For this thesis, labeling data is derived from the damage-assessed data points used for making sense of the information. As previously mentioned, these damage scales are utilized as classes (labels) for training the models. Before feeding our custom dataset into the model, we underwent detailed and time-consuming preprocessing of different data types. Each step of this preprocessing is explained below.

To begin with, we received the damage-assessed data points in both csv and geojson data formats, thanks to the generous assistance of Yer Çizenler NGO. Using the *XY*

*Table To Point (Data Management) Tool*, we constructed a point feature class based on the x-, y-, and z-coordinates from the input table. For our case, the input table consisted of four different damaged csv files. The resulting feature class was created with x values representing longitude, y values representing latitude, z values representing postcode, and the Coordinate System value set as WGS 1984, based on the knowledge obtained from the raw csv and geojson data.

Subsequently, we obtained four different damages as point feature class data types, all ready to be merged. Our data source provided us with damage assessments for ten different earthquake-affected regions. At an early stage, we made the wise decision to remove unnecessary columns, such as geojson numerical value, district, neighborhood, open address, building details, etc., since numerous column calculations were expected to be performed. Among the columns, the most important ones were the province and damage value field types, which were crucial for our analysis and model training.

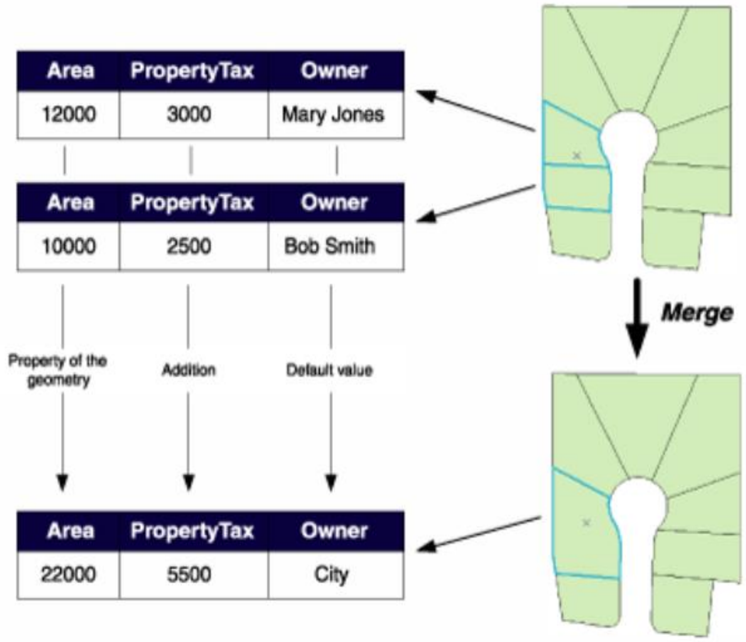


**Figure 3. 9.** Merge explanation in attributes ("An Overview of Attribute Domains", n.d.).

As expected, human-recorded data sources may vary, even when they pertain to the same features. For instance, city name columns may be written in different cases (upper-case, lower-case) and may include Turkish characters. To merge the damage points for each city effectively, we needed to standardize the city name column and ensure consistency.

In ArcGIS Pro Software, attribute domains play a vital role in managing attribute values for tables or feature classes. They allow us to limit or expand the possible values for a given attribute. With this functionality, we were able to divide the feature class data city by city, enabling us to examine the earthquake-affected cities individually.

To manage the attribute domains and add values while associating them with a feature class, we used the *Add Coded Value To Domain (Data Management) Tool*. This tool facilitates the creation of coded value domains that can be applied to attributes of various types, such as text, numeric, or date. Coded value domains define a set of valid values for an attribute, making it easier to work with and understand the data.

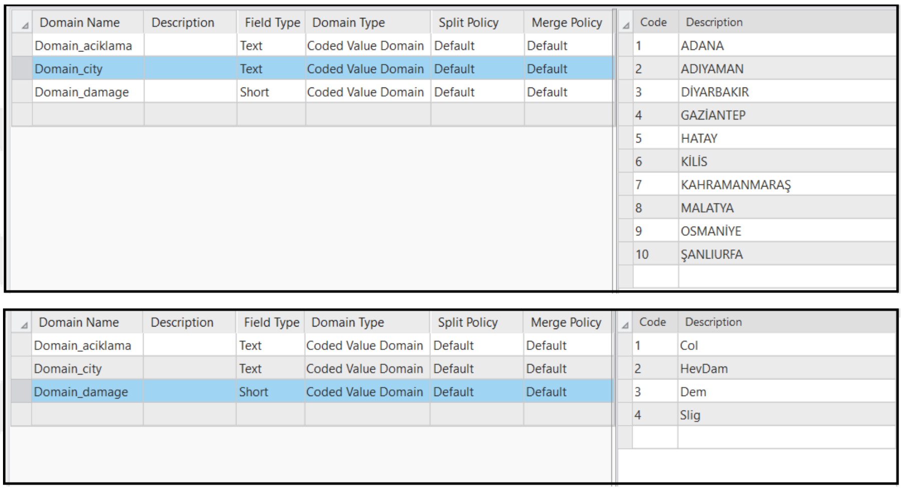


**Figure 3. 10.** Coded Value Domains ("Add Coded Value To Domain", n.d.).

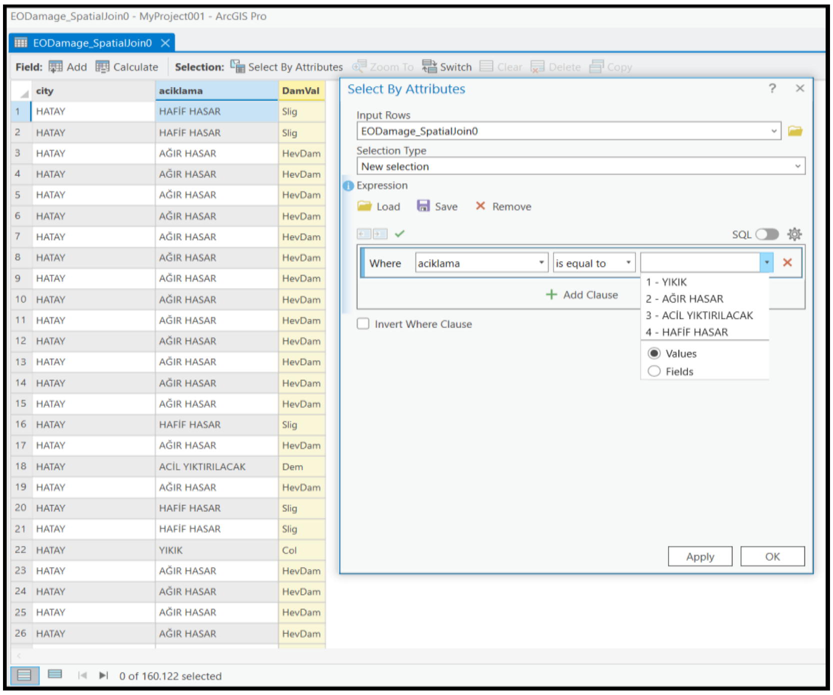


**Figure 3. 11.** SQL query for attribute management ("Add Coded Value To Domain", n.d.).

In our training data, the polygon class label representing the damage level is denoted by variables ranging from 1 to the total number of classes. The coded value domain contains both the database value (e.g., 1 for the damaged class) and a more user-friendly description of what the value signifies (*"*Add Coded Value To Domain*"*, n.d.).This improves the interpretability and user-friendliness of our data, making it easier to work with and comprehend during the analysis and model training processes.

We can select features using attributes use this tool for creating a SQL query to choose features from a layer or database that fulfill a selection criteria.

ArcGIS Pro offers another essential classification tool, called *Label Objects for Deep Learning,* available in the Image Analyst extension. This tool proves to be invaluable for our purposes, as it enables the labeling and preparation of imagery datasets for exporting as training datasets according to our specific requirements and preferences ("Label Objects for Deep Learning" n.d.).

Among the various data sources we have, the most significant and valuable one is the point data, which was meticulously collected building by building in the disaster-affected area. We are immensely grateful for the tremendous assistance provided by Yer Çizenler, as they have contributed the four-staged damage data, which will play a pivotal role in our study (Url-25).

By utilizing the *Label Objects for Deep Learning Tool* and incorporating the detailed point data from Yer Çizenler, we can ensure the accurate labeling and preparation of our imagery datasets, which is crucial for the success of our deep learning models in damage identification and earthquake assessment. This collaboration and data contribution enhance the effectiveness and reliability of our research in disaster management and geophysical studies.

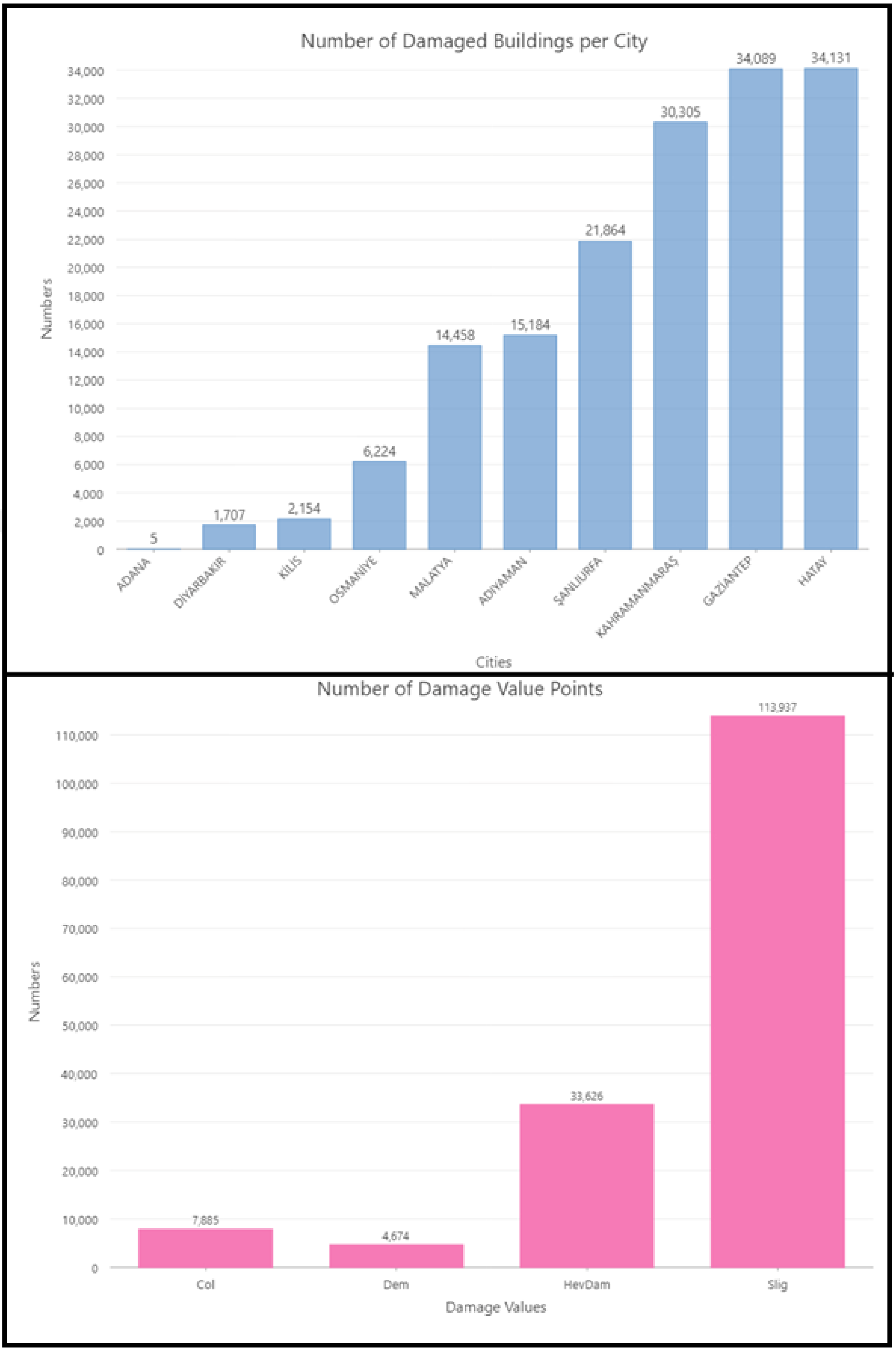


**Figure 3. 12.** Results of attribute calculations.

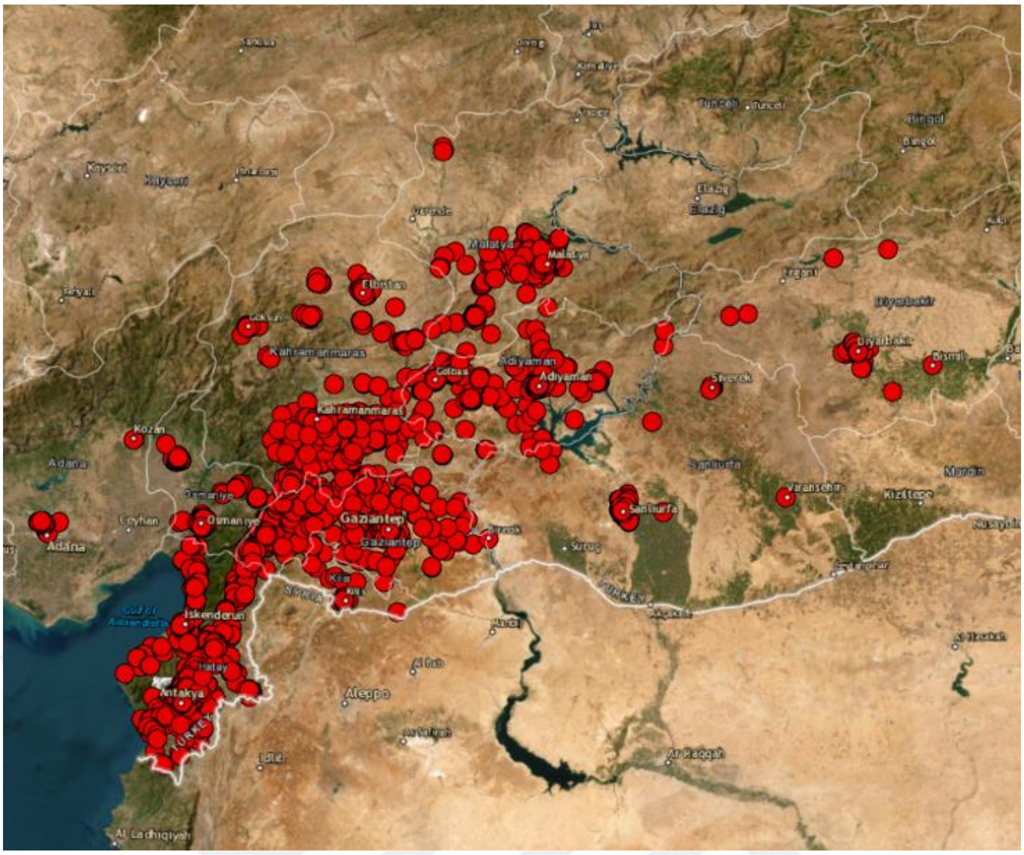


**Figure 3. 13.** Damaged data points received from Yer Çizenler NGO.

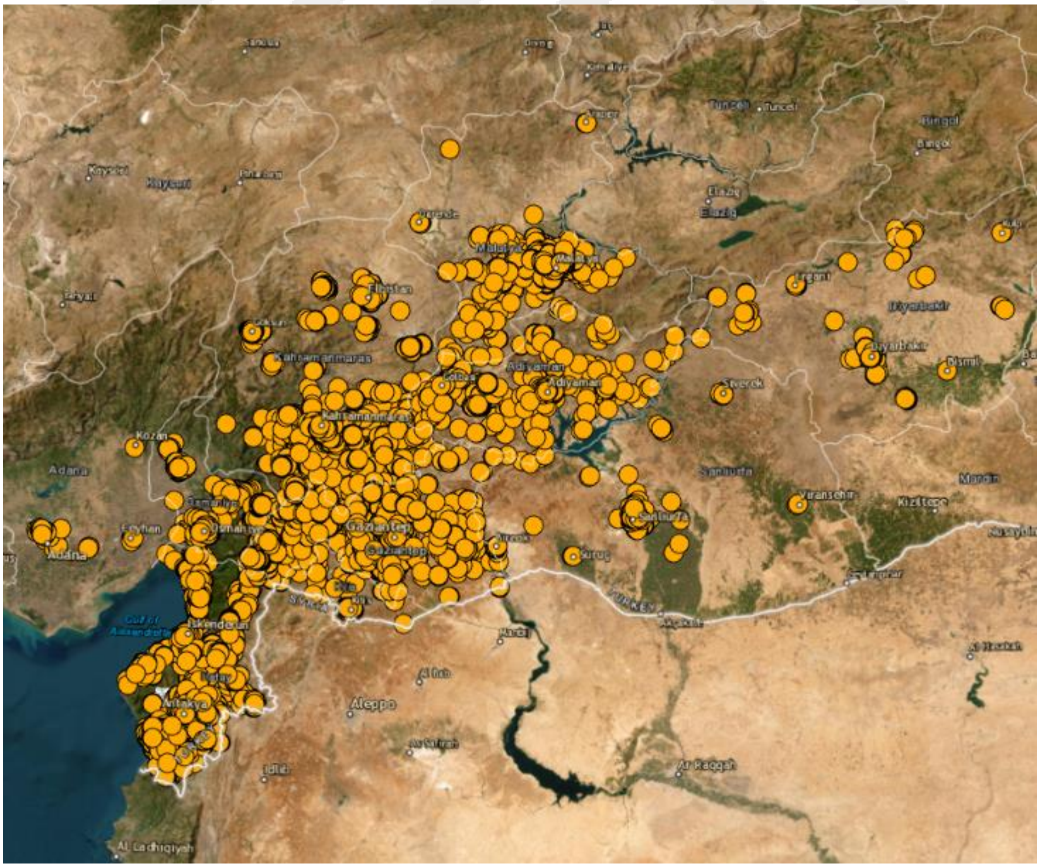


**Figure 3. 14.** Heavily Damaged data points received from Yer Çizenler NGO.

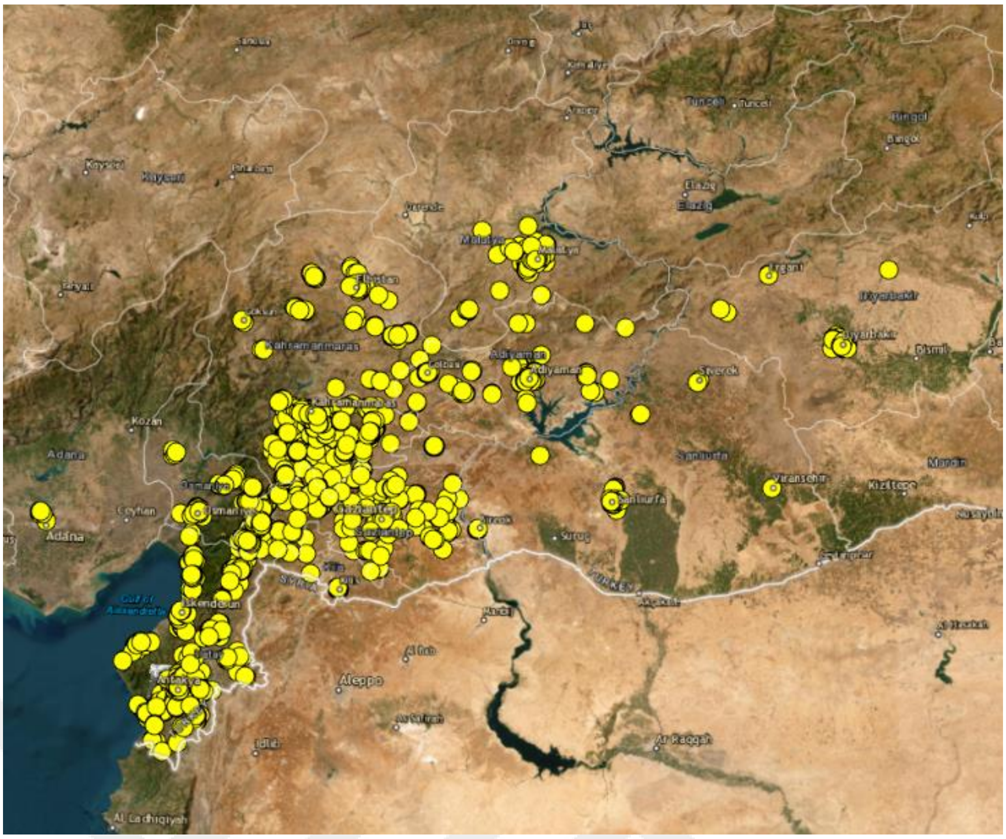


**Figure 3. 15.** Slightly Damaged data points received from Yer Çizenler NGO.

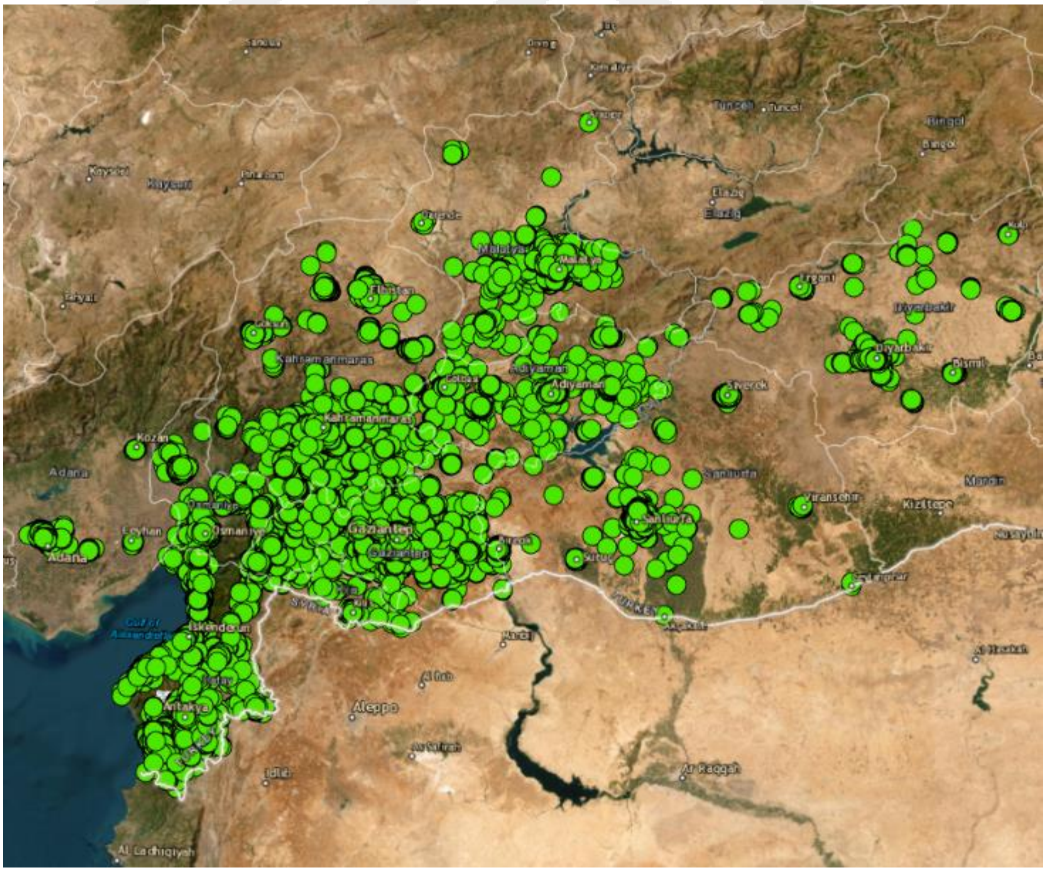


**Figure 3. 16.** Demolished data points received from Yer Çizenler NGO.

After collecting data points, we needed the building footprints to be labeled in our dataset. Thankfully, the Humanitarian OpenStreetMap Team (HOTOSM) (*HOT Export Tool*, n.d.) enables an open source that was done by the volunteer contributors to the MapRoulette challenges of Yer Çizenler. This way, we could achieve recently adjusted building footprints starting from February 7th to today over the pre-earthquake images taken from ("Spatial Join", n.d.).

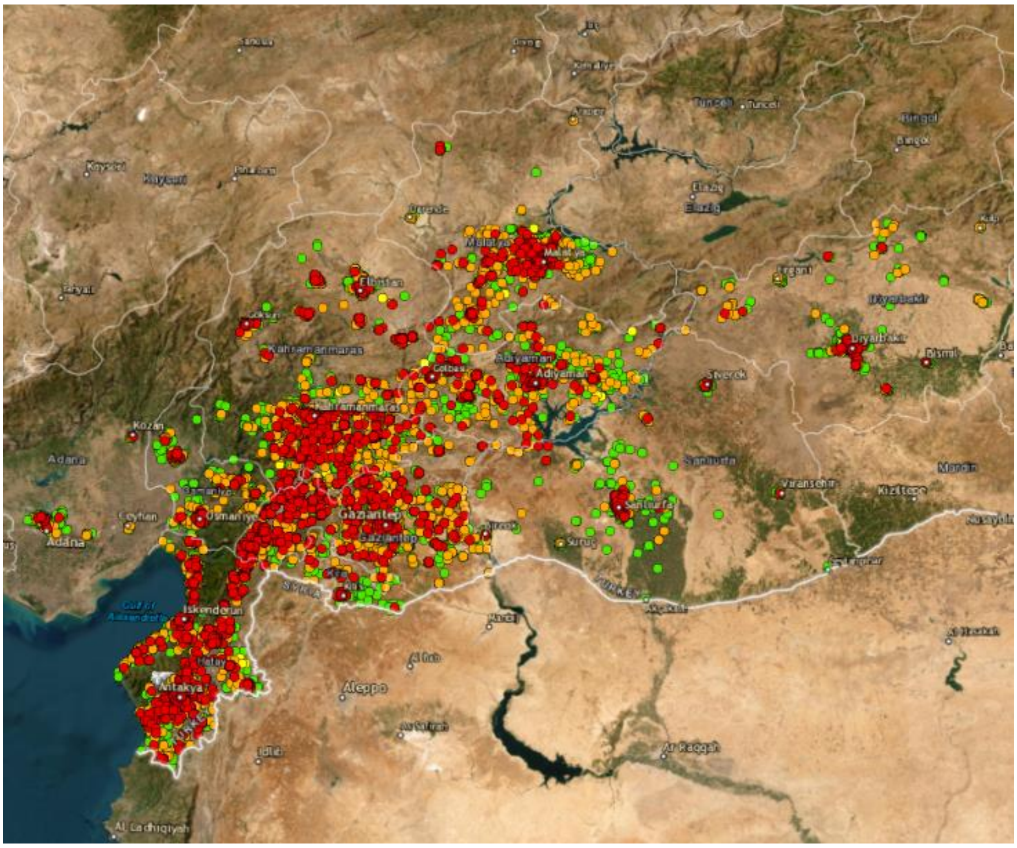


**Figure 3. 17.** Four scales of damage points are merged.

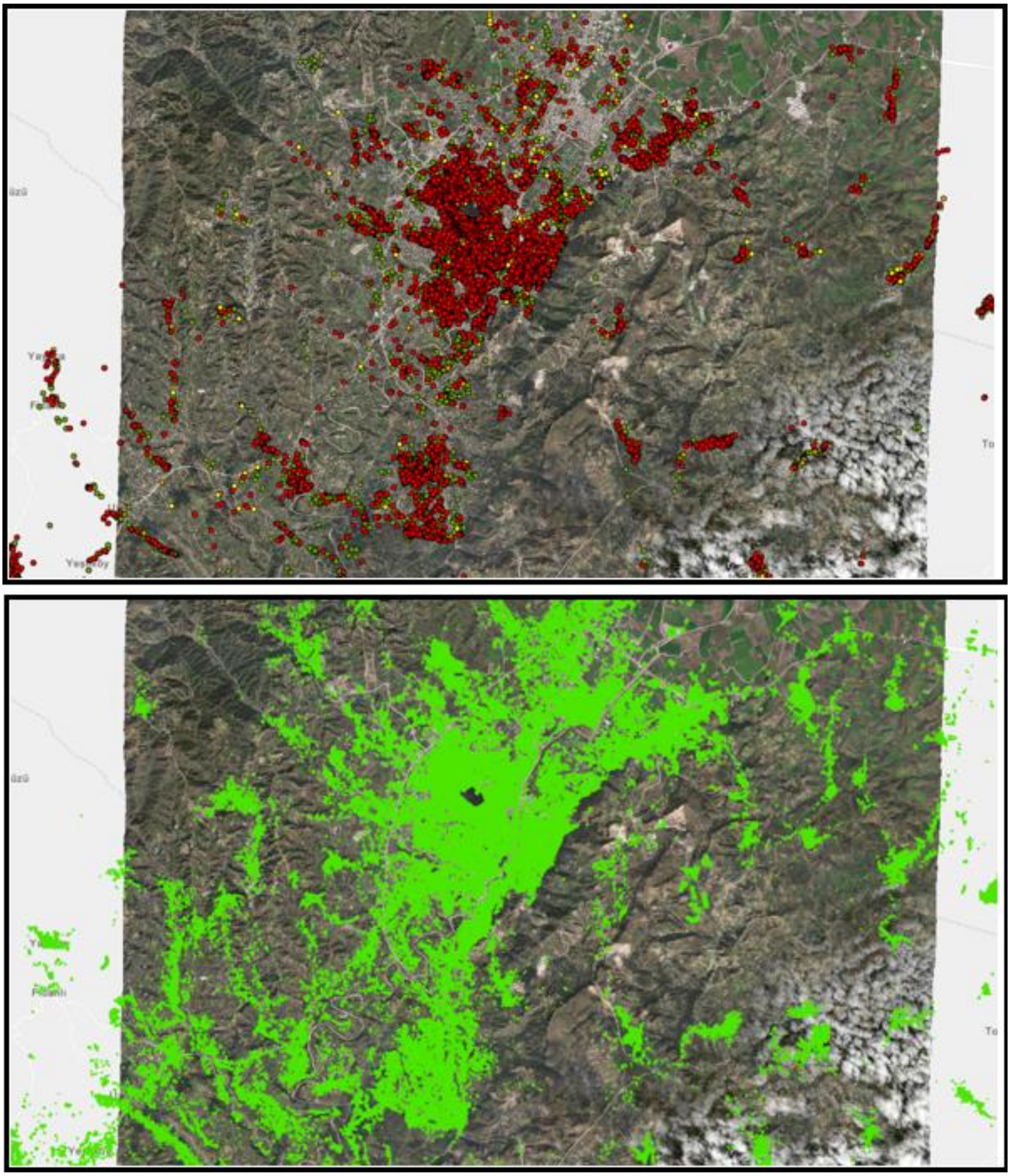

**Figure 3. 18.** Damage points and building footprints in Hatay, Antakya district.

**Imagery Characteristics and Limitations**

**Figure 3. 19.** Choosing the optimum imagery out of the options was crucial.

Now, finally, we can label building footprints based on the damage points. Thanks to ArcGIS Pro's *Spatial Joint Analysis Tool*, recently adjusted building footprints are determined as target features and merged damage point data as join features ("Spatial Join", n.d.). So, we create new labeled polygon data with the File Geodatabase Feature Class type. But again, a new setback occurred. If we decided our match option was intersect, we would lose a large amount of information, as seen in Figure 3.21. Considering the fact that building footprints and building locations will not match 100% due to the nadir angles, we had to find a reasonable match at the end. But the images we used have different nadir angles, even though Maxar Technologies enabled us to capture multiple images on multiple days after the earthquakes.

**Figure 3. 20.** Intersect option causes information loss.


**Figure 3. 21.** Data loss due to intersection match (before and after selection).

To deal with this, we used the within-distance match option in the *Spatial Joint Analysis Tool* rather than intersect. Thus, features of the target and joint sections will overlap within a selected distance. So we tried this match within 1m, 5m, 10m, 20 m, and further distances. When the distance was 1 m, it created a similar effect as when it intersected; a 10 m distance created more than 36 thousand building polygons, and a 5m distance created more than 29 thousand building polygons. When we trained the model based on the labeled data within a 10-meter distance, accuracy and other metrics became poorer. So, we decided to opt longer distance matches at the expense of losing information and stick to 5m in the *Spatial Join Tool*. Besides, even 10m would be a large distance, and values may change drastically in a disaster-affected area considering the sizes and dimensions of the building structures.

As a final challenge, particularly in Antakya district, Hatay province, we encountered a problem where building footprints and the buildings on the imagery could not overlap. Hatay imagery has the worst footprint mismatch among the three provinces we examined. Even though we tried different post-earthquake images and used pretrained building footprint extraction models in ArcGIS Portal Living Atlas, the results were very poor compared to the hand-made, adjusted building polygons (ArcGIS Living Atlas of the World, n.d.).

**Figure 3. 22.** An example of the best match of the building footprints in Hatay.

**Figure 3. 23.** Kahramanmaraş and Gaziantep province footprint match demonstration, respectively.

As it is seen in Figure 3.22 and 3.23, Kahramanmaraş and Gaziantep have better polygon matches compared to Hatay province. The reason why Gaziantep is not chosen for the model training is that, unfortunately, the affected area has an imbalanced damage distribution, which will be demonstrated below (Figure 3.25).

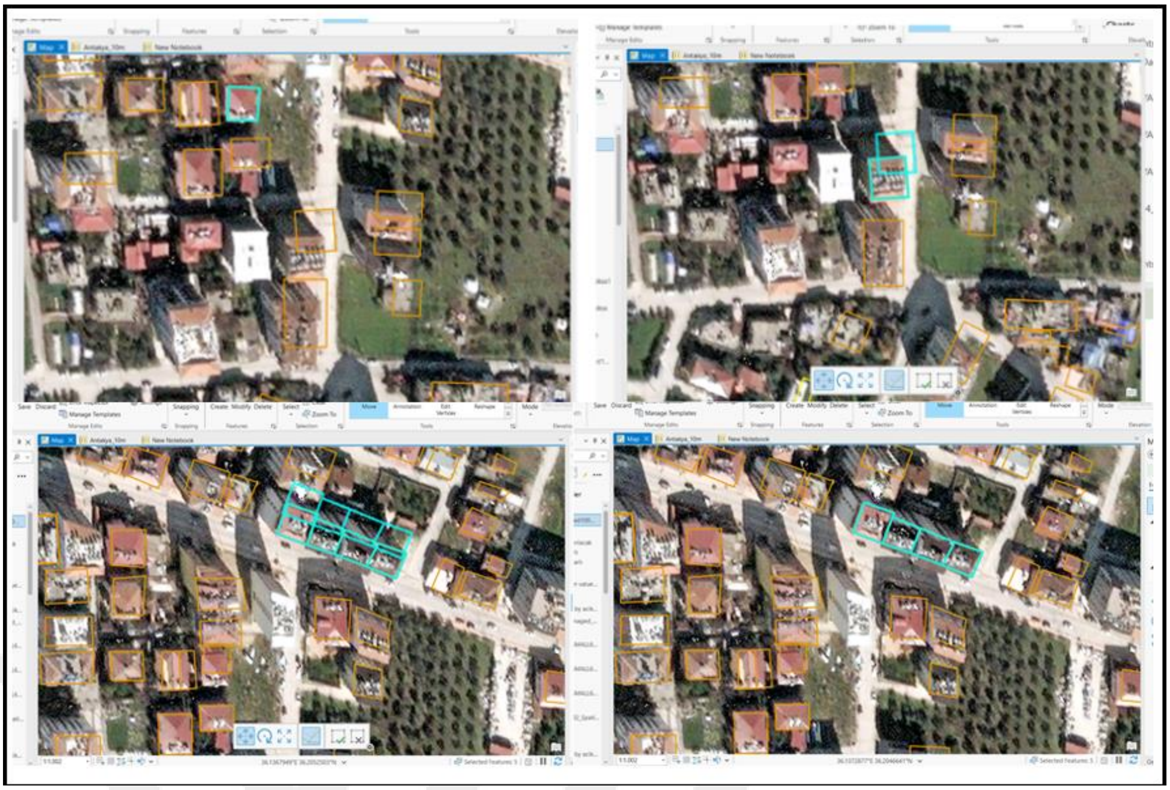

**Figure 3. 24.** Blue polygons are chosen to move and displaced.

In our efforts to improve the dataset and align the polygons properly, we attempted manual rotation for some polygons, as depicted in Figure 3.24. However, we soon realized that this approach was impractical for thousands of polygons due to the sheer volume of data. Furthermore, despite Hatay having a well-balanced class distribution, we faced challenges with the image's usability. Specifically, we encountered problems with the proper alignment of building polygons in the satellite images, as illustrated in Figure 3.22. As a result, we had to exclude this particular image from our dataset, as it did not meet the required alignment standards. Despite these challenges, we continued to refine the dataset, focusing on other earthquake-affected regions and utilizing the most suitable images with accurately aligned building polygons. Such efforts were crucial in ensuring the dataset's quality and subsequently improving the accuracy and effectiveness of our deep learning models in damage identification and earthquake assessment tasks. In the end, no artificial building footprint model was as successful as the polygons drawn by volunteer experts. Obviously, it was not a method to be pursued because it was not the aim of this thesis. Moreover, considering the roof and the building types are locationally quite similar in the provinces of Turkey, it was plausible to train the model in one city and use this pre-trained model for other neighboring cities. And assuming that, our data preparation approaches helped us increase the accuracy and other metrics in the models, we could double-check that our choice to use the pre-trained models is appropriate.

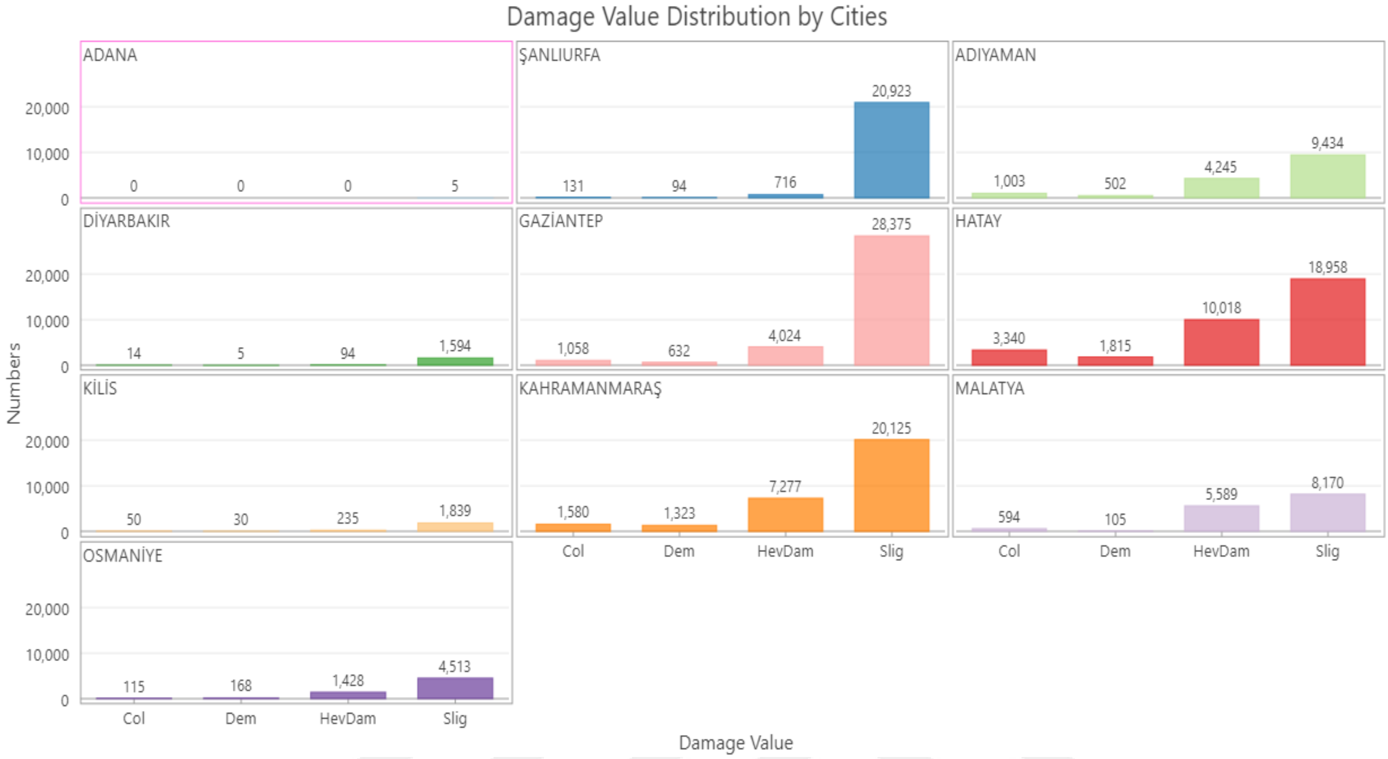


**Figure 3. 25.** Damage level Distribution by earthquake affected cities.

Damage detection datasets are indeed among the most imbalanced datasets, primarily due to the natural distribution of damage levels after an earthquake. The classes we are interested in (e.g., severely damaged buildings) are typically a minority in the class distribution compared to other classes (e.g., slightly damaged or undamaged buildings). This imbalance can pose challenges during model training and may lead to biased predictions.

To address this issue and improve class balance, various class balancing techniques can be employed. Some common techniques include weighted random sampler, SMOTE (Synthetic Minority Over-sampling Technique), and data augmentation. These methods can help to balance the class importance fed into the model and mitigate the impact of class imbalance.

As depicted in Figure 3.25, it is evident that slightly damaged buildings are assessed more frequently than other damage levels. Additionally, there is a noticeable inequality in the distribution between Gaziantep, Hatay, and Kahramanmaraş provinces. Gaziantep seems to have a considerably higher imbalance when compared to Hatay and Kahramanmaraş.

While Hatay may exhibit the most balanced distribution, it is essential to consider the trade-offs and potential loss of information in excluding certain regions from the examination. Each region may present unique challenges and insights, and by utilizing appropriate class balancing techniques, we can make the most of the available data and enhance the model's performance in damage identification tasks.

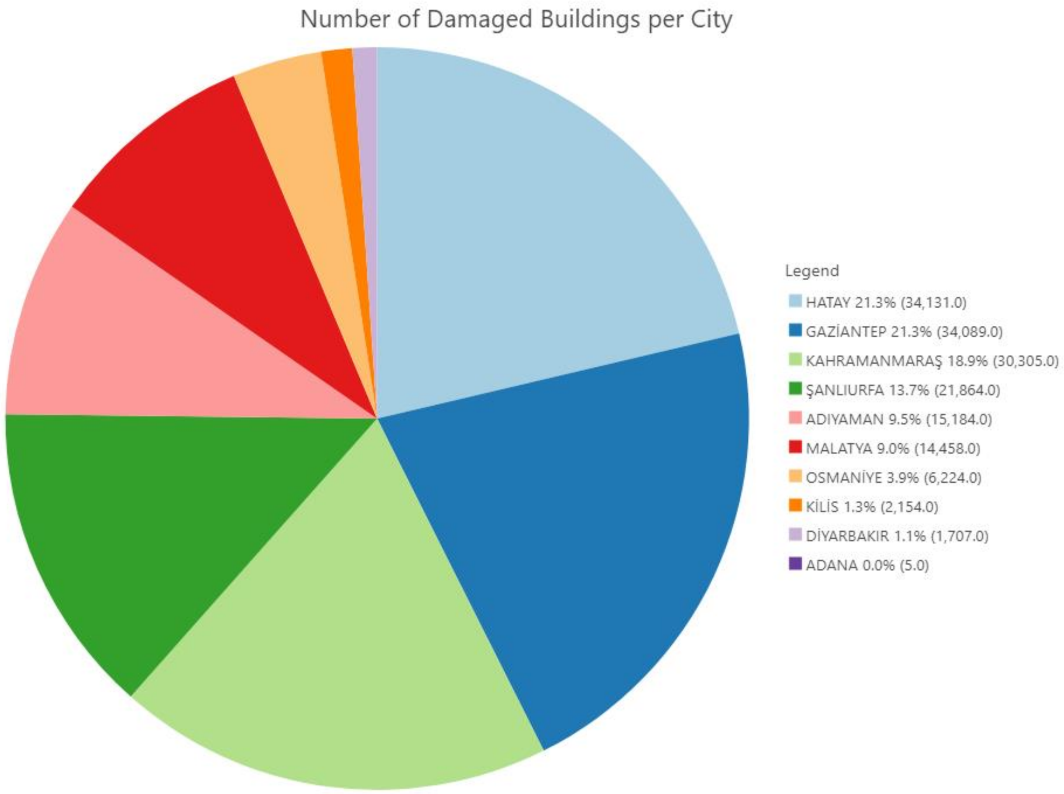


**Figure 3. 26.** Number of damaged buildings per city.

Among all the damage assessed data points and their dispersion for ten cities, our focus and concentration will be solely on the attributes within Kahramanmaraş province. By narrowing our analysis to this specific region, we aim to conduct a more targeted and in-depth investigation of the damage assessment for the earthquake-affected areas, thereby providing valuable insights for disaster management and recovery efforts in Kahramanmaraş.

160.122 polygons are selected within a 5m distance out of 1.575.244 polygon data points that are gathered from HOTOSM for all provinces in total. Building footprint distribution for within 5m, 10 m, and all the available polygons for the Antakya region for demonstration is seen in Figure 3.28.

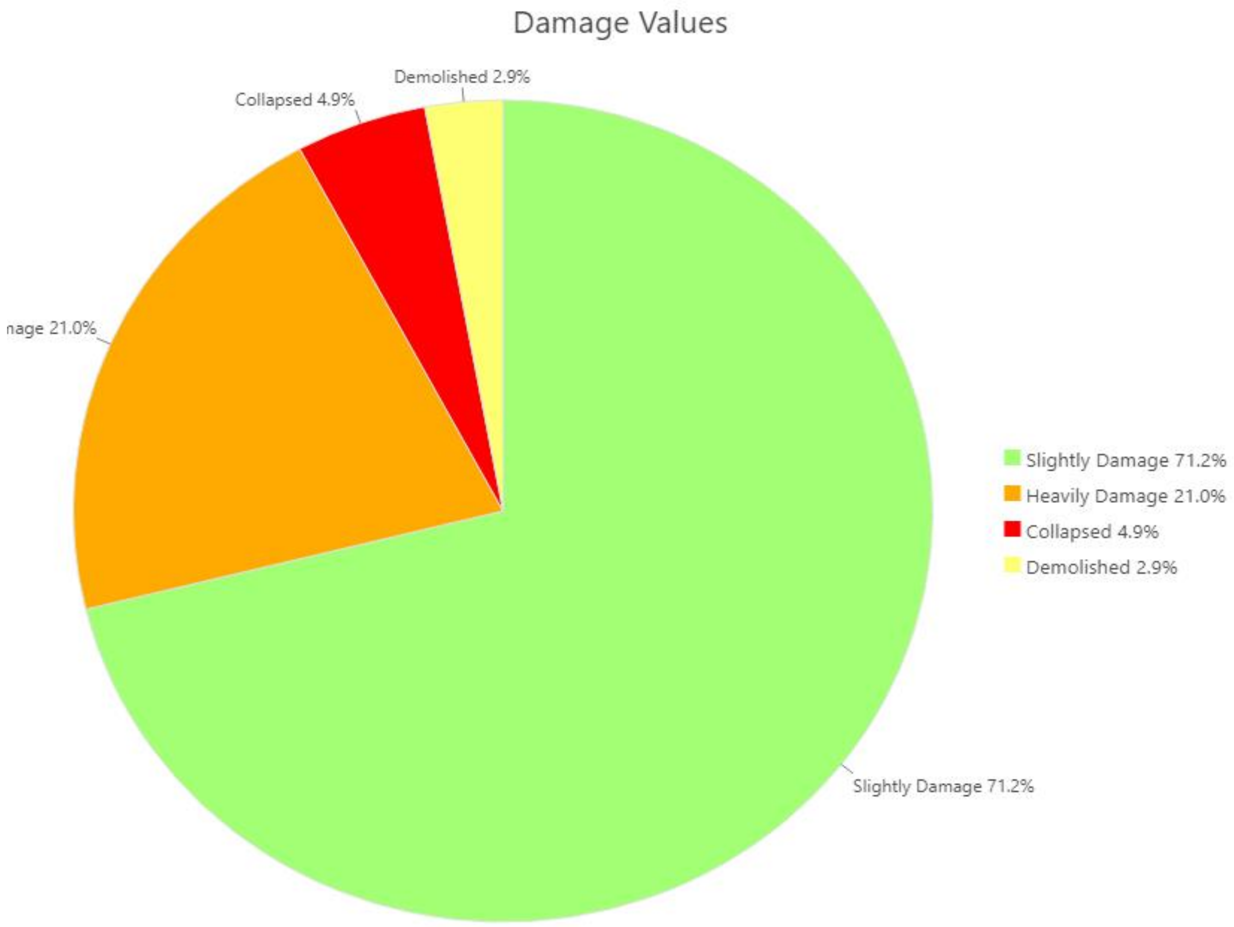


**Figure 3. 27.** Damage Distribution in total.

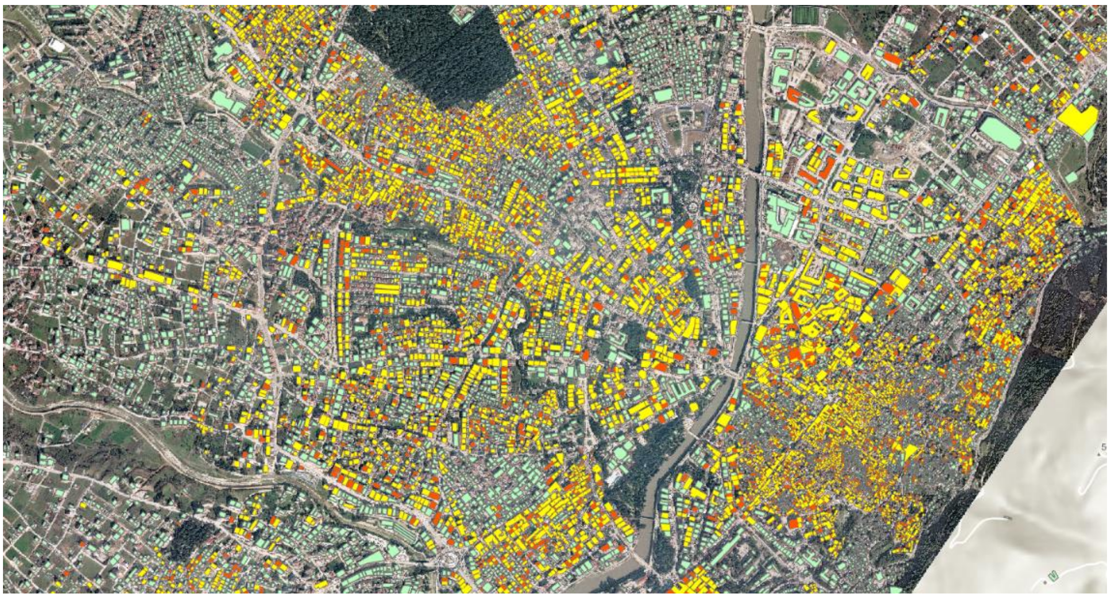

**Figure 3. 28.** Green: all the footprints, orange: within 10m and yellow: within 5m distance.

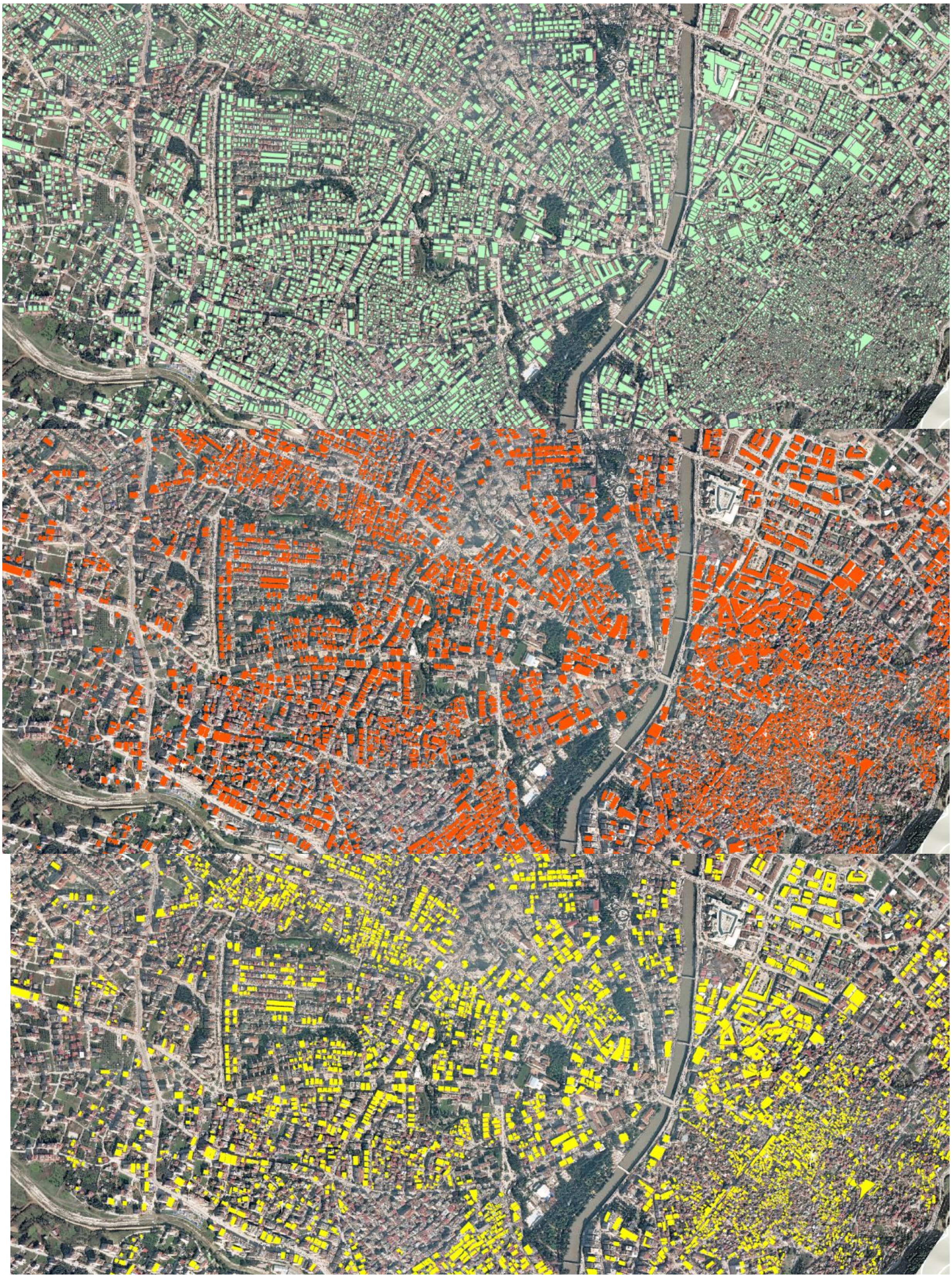

**Figure 3. 29.** Demonstration of the building footprints in detail (all of them, within 10m and 5m respectively).

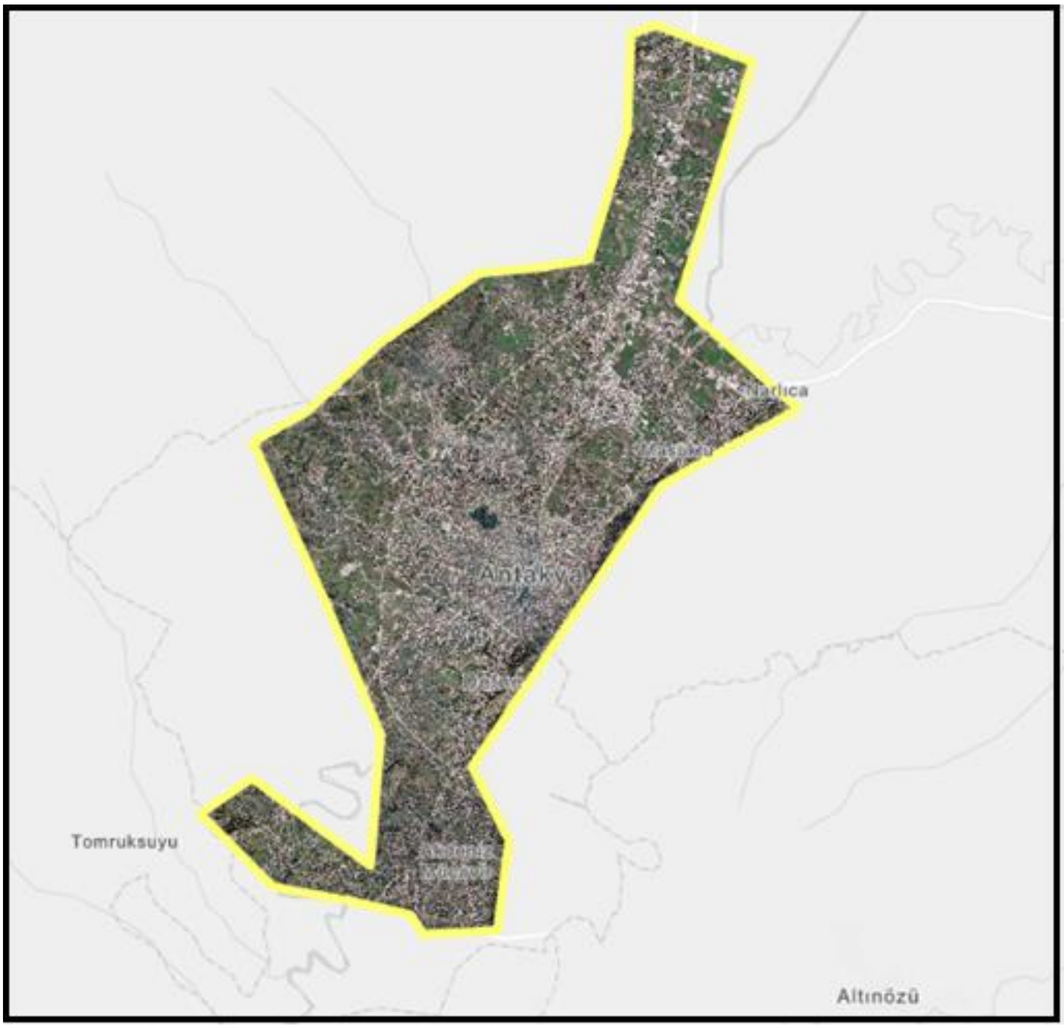


**Figure 3. 30.** Area of Interest (AOI) for Hatay Province.

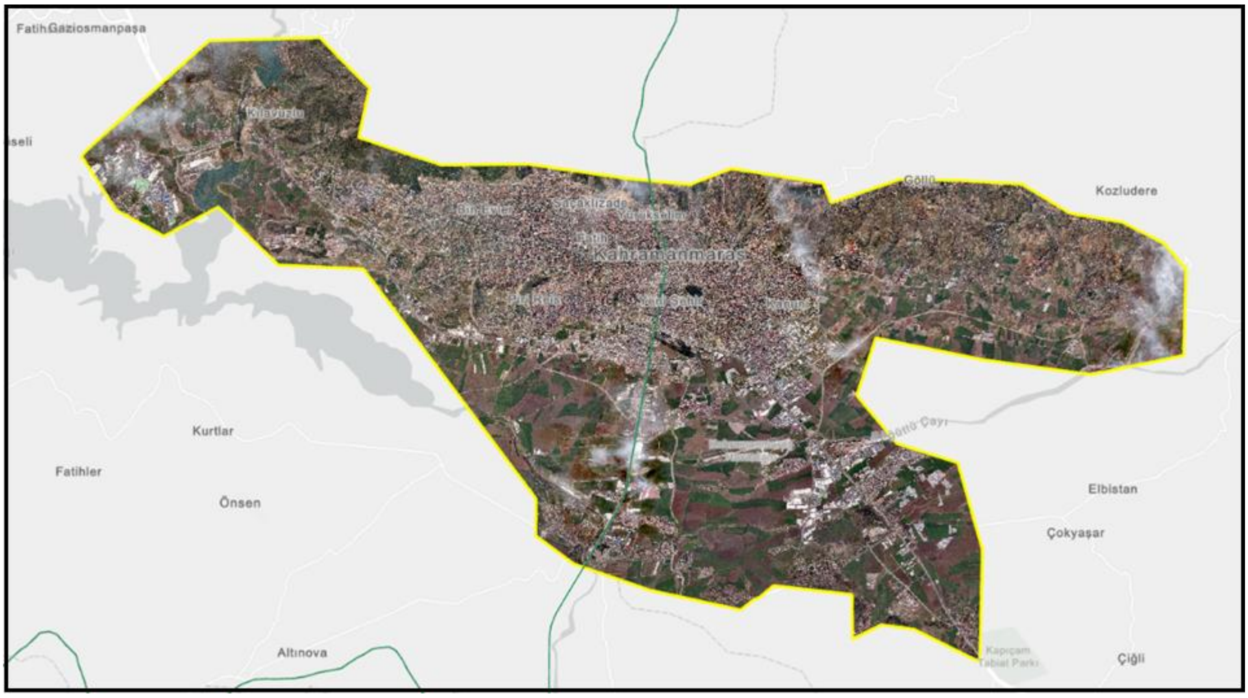


**Figure 3. 31.** Area of Interest (AOI) for Kahramanmaraş Province.

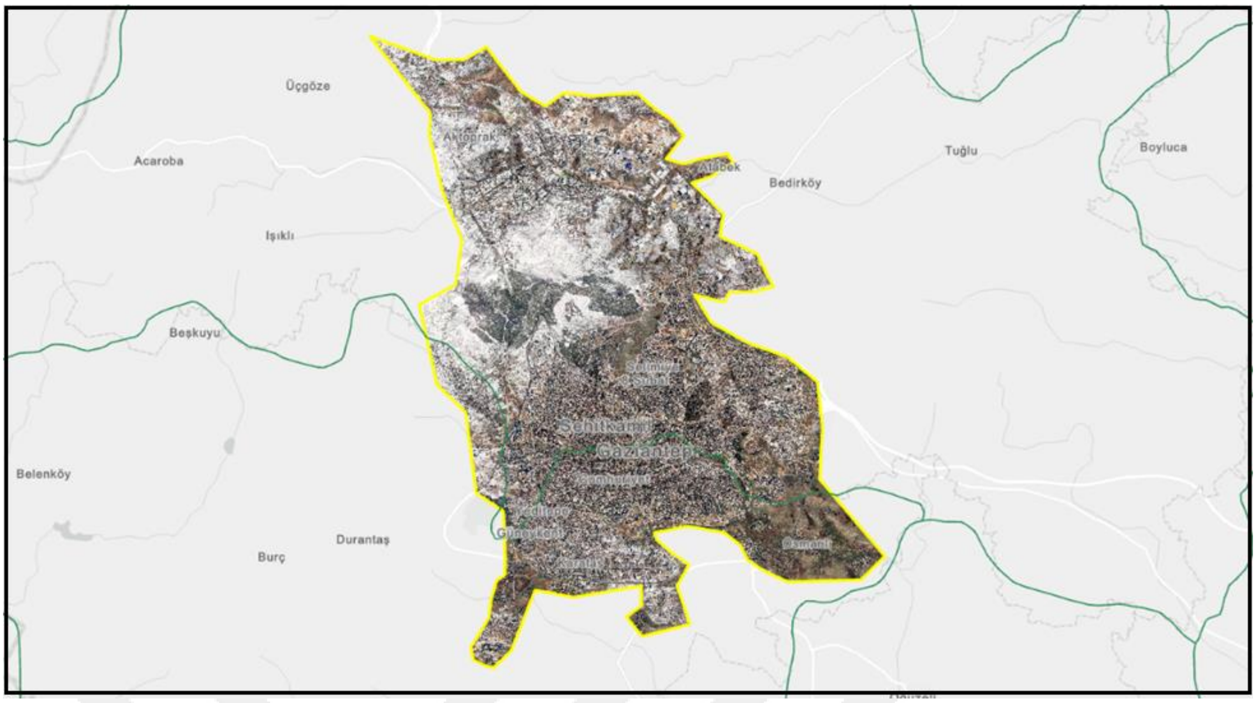


**Figure 3. 32.** Area of Interest (AOI) for Gaziantep Province.

Moreover, labeling some pixels by using the edges of the building footprints causes large undefinable areas as background in the images. ArcGIS Pro establishes a label for background, even though we did not mention that in the coded value domains.

The feature that is shown on the product and denotes the precise geographic scope of the instance is called the area of interest (AOI). To be able to ignore the background pixels and focus on the classes we would like more of, we choose to minimize the study area and work on only the area of our interest (AOI). Area of interest is an easy option for raster images with ArcGIS Pro tools. After we defined the feature class typed polygon that represents the area of interest, we clipped the raster based on this target polygon. Damage detection or classification datasets are one of the imbalance data types because damaged or destroyed classes will be rare among other classes. It was logical to eliminate the background class (index 0) that includes most of the classes in the dataset to make it more balanced.

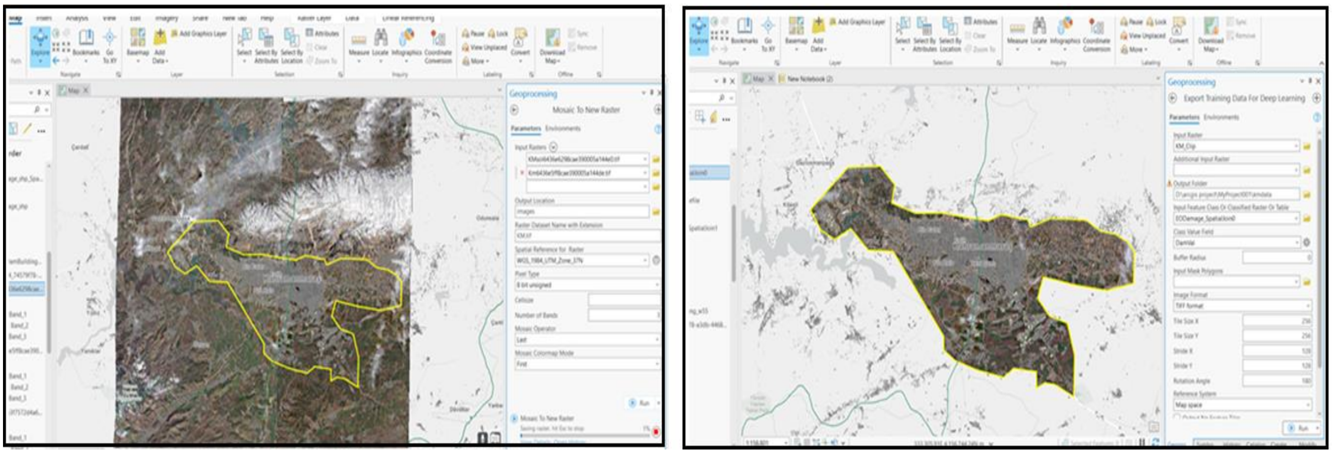

**Figure 3. 33.** Before and after clipping the raster.

### 3.2.3 Export training data

At last, our data preprocessing will come to a final end. Thanks to *ArcGIS's Export Training Data for Deep Learning (Image Analyst) Tool* in Image Analyst toolboxes, for remote sensing applications, we may convert labeled vector or raster data into deep learning training datasets. (Figure 3.34). The output folder will contain image chips and metadata files in the format specified.

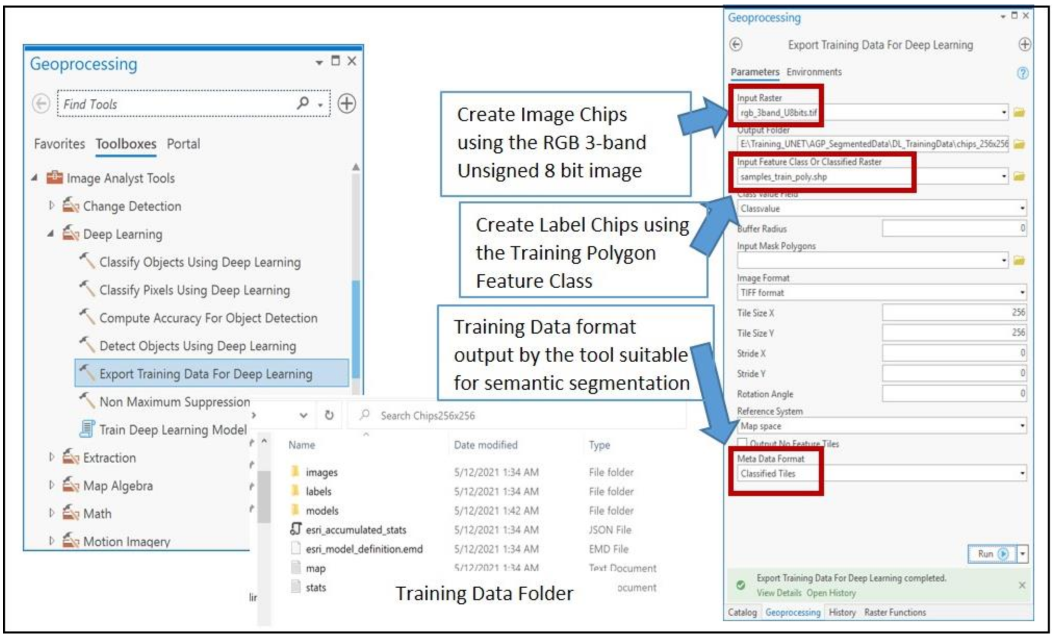


**Figure 3. 34.** Export Training Data for Deep LearningTool (Abd-Elrahman,et.al., 2021).

Maxar-originating satellite images are 8-bands images. We were able to produce the input raster as a three-band, unsigned 8-bit raster using ArcGIS Pro's *Export Training Data Tool.* The training data polygon shapefile (explained further in the Data Preparation section) comprises several instances of each of the four classes in the input feature class or categorized raster. The tool additionally requests the Class Value Field (damval feature file in our coded domain values), which specifies which property of the input feature class should be used as the label for each training feature. Actually, the class value field is the most important part because we will use the domain-coded values here. And all the image preprocessing was for assigning labels to the image batches.

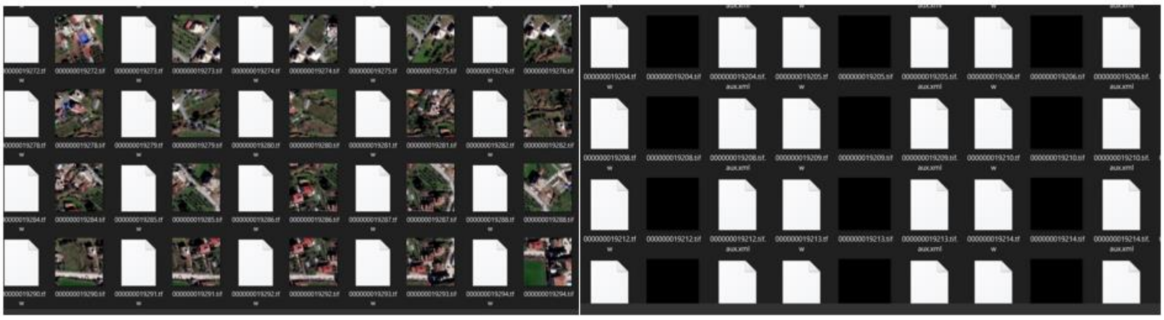

**Figure 3. 35.** Image and masks tiles created in training dataset.

```
images = 20529 *3*256*256

Class feature statistics:
features = 80364
features per image = [min = 1, mean = 3.91, max = 38]
classes = 4
cls name                                 cls value    images   features    min size   mean size    max size
Col                                              1      1616       3223        9.75      181.50     5153.99
HevDam                                           2      7216      16645        0.24      175.02     4980.66
Dem                                              3      1662       2742        5.60      186.96     6081.84
Slig                                             4     17560      57754        0.00      173.27     6103.46
```

**Figure 3. 36.** Training data statistics after exporting.

**Figure 3. 37.** 256x256 tile sized image batches after all augmentations labeling for Kahramaraş satellite image.

This powerful tool generates chips of images in desired sizes from the image and mask tiles, as we wish in this study: 256 × 256. Here, we can decide the rotation degree and the overlap tolerance based on the stride size of 128. Apart from other data augmentation strategies, these two factors enhance the size of the training dataset, resulting in a significant gain in classification accuracy in our experiment. The two tiles (referred to as image and label tiles) relate to the same location, with the first a raster representing the class value of the pixels based on the training polygons and the second the RGB values of the input features. Text documents in the folder have a list of each image and label as tiff files, as well as the statistics of the training dataset. This beneficial tool also creates datasets, whether we use Pixel based classsification, Object Detection, RCNN Masks, CycleGAN, or Panoptic Segmentation. We chose classified tiles to classify image chips per input image chip, ready for pixel based classification and possibly change detection.

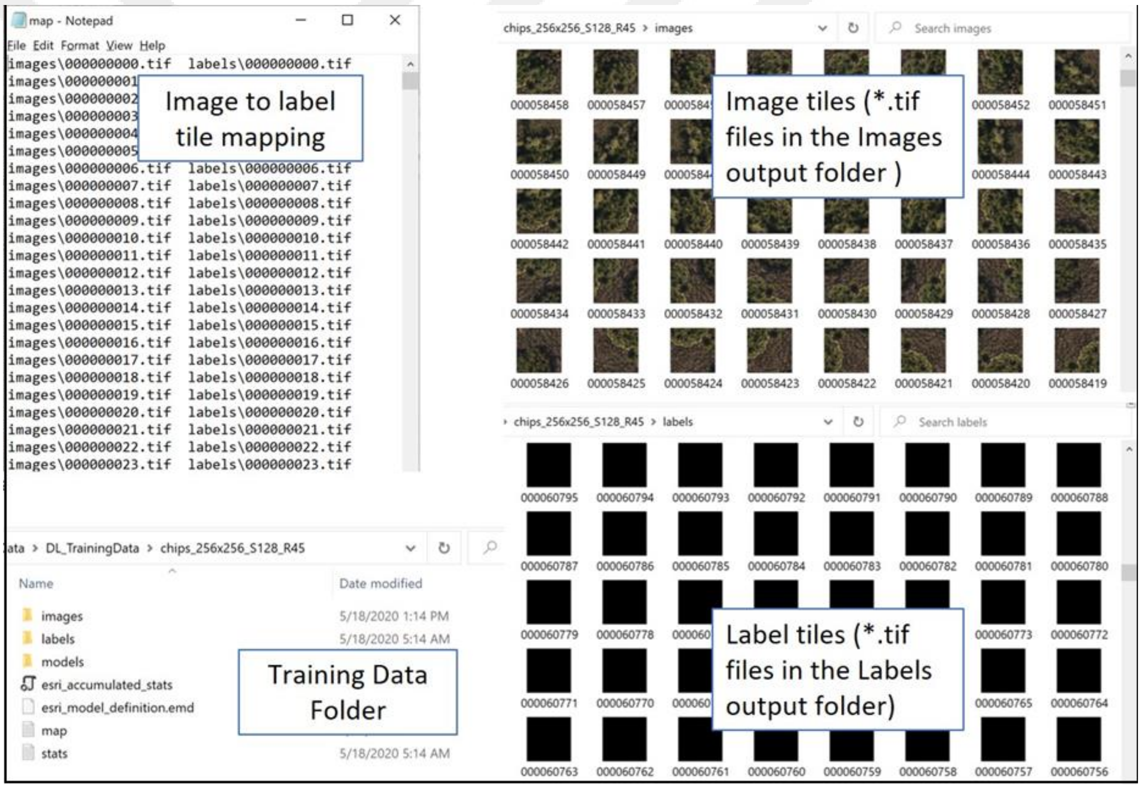


**Figure 3. 38.** Outputs of the Export Training Data tool (Abd-Elrahman,et.al., 2021).

In our attempt, we customized some parameters of this tool, as seen in Table 3.1. We did not use the rotation angle option considering image augmentations will be used in our customized training model. Also, for a richer result, we also created a 128x128 tile-sized dataset with 64 strides. But the result after training was drastically different, so we avoided using this version of the training dataset.

The best part of this tool is that it creates training datasets in any image format, such as tiff, png, or jpg. The size and the stride distance for the x and y dimensions in the image chips, the overlap ratio tolerated based on the stride, and the metadata option are some of the benefits. The metadata mentioned here defines the output as one classified image chip per input image chip. Because in this thesis we would use pixel based classification for damage classification, classified tiles are the chosen format in the tool. This format is also used for change detection when the output is one classified image chip from two image chips.

### 3.2.4 Training

The arcgis.learn module in the ArcGIS API in Python makes it easy to address challenging issues by quickly training a wide range of deep learning models on datasets. Besides, ArcGIS API Python includes numerous deep learning models and supports cutting-edge GIS and remote sensing workflows. These models also handle a wide range of data formats, including feature layers, LiDAR, video, point clouds, bathymetric data, and even tabular and free-form text data. The training process, as previously mentioned, is done in an ArcGIS Pro Python API Jupyter Notebook using the arcgis.learn module for specific requests. This module has Pytorch, Tensorflow, Keras, and Fastai support with the Jupyter Notebook API, where we customized our training model.

**Table 3. 1.** Parameters of the Export Training Data for Deep Learning Tool.

| Tool Parameters | Description |
|---|---|
| **Input raster** | Maxar 3 band 8 bit imagery |
| **Input feature class** | Merged and labeled building footprints |
| **Class value field** | Damage level field taken from coded domain values [1-4] |
| **Image format** | Tiff format (jpeg, png, mrf is also possible) |
| **Tile size x and y** | 256, 128 |
| **Stride size x and y** | 128, 64 |
| **Metadata Format** | Classified Tiles for semantic segmentation and pixel based classification |
| **Rotation angle** | The default rotation angle 0 is used |
| **Minimum polygon overlap ratio** | The default value 0 is usewd, which means that all features will be included. |
| **Cell size** | Resolution is chosen same as the clipped raster |
| **Reference System** | Map space is used (pixel space is possible) |


**Figure 3. 39.** arcgis.learn is a powerful module (Singh, 2021).

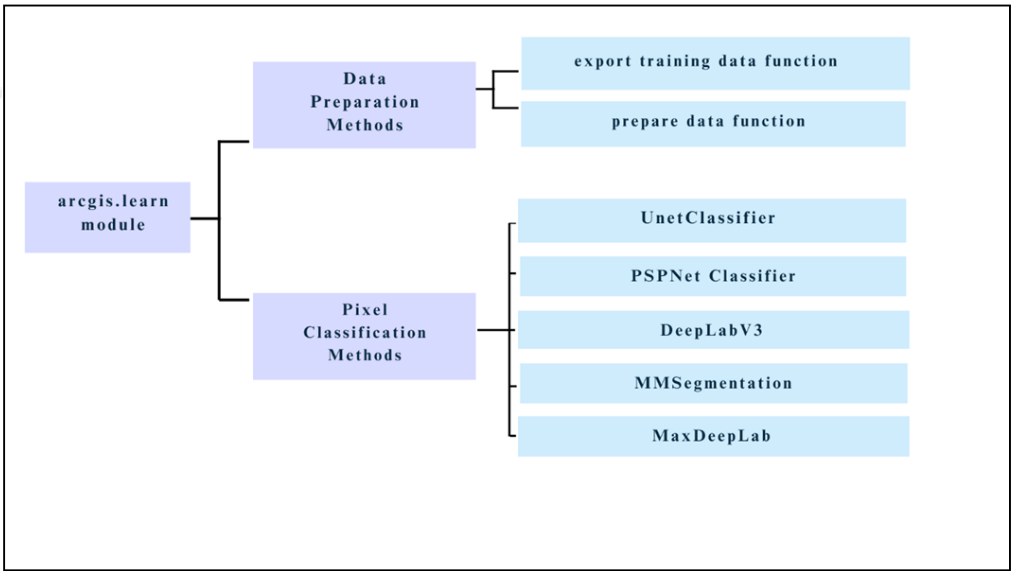


**Figure 3. 40.** arcgis.learn module methods and models.

The ArcGIS API for Python has the arcgis.learn module and its Data Preparation Methods, such as exporting training data and preparing data. The previously mentioned export training data can be utilized prior to training the dataset. If desired, adjustments can be made to the path of the pretrained model. This includes parameters like chip size, stride size, the percentage split between training and validation datasets, batch size, among others. Also, to make the dataset more balanced, we used the weighted random sampler function from PyTorch to weight the classes according to their numbers in the dataset and used various transformations via Fastai background. This way, low participation is encouraged, and the importance of the majority of the classes in the dataset is decreased in the model. For custom model and data preparations, using Jupyter Notebook in ArcGIS Pro was more beneficial to control the situation. Custom-made data preparation options we preferred are listed below (Table 3.3).

**Table 3. 2.** Outputs after using of the Train Deep Learming model Tool.

| Training outputs | Explanation |
|---|---|
| dlpk | Deep learning package available for ArcGIS after model training |
| emd | Esri model definition JSON file (.emd) |
| Loss graph | Train and validation loss graph |
| Optimum learning rate | Optimum learning rate for the model |
| Per class metrics | Output as table |
| Ground truth/ prediction image | As png images |

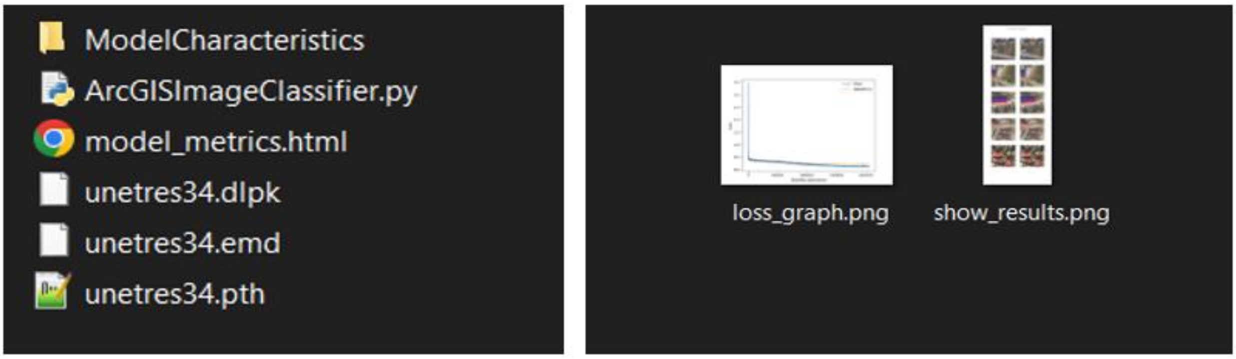


**Figure 3. 41**. Outputs of the Train Deep Learming model Tool.

**Table 3. 3.** Parameters we used in our custom model.

| Tool Parameters | Description |
|---|---|
| **Path** | Our data directory path |
| **class_mapping** | We used 4 damage classes |
| **chip_size** | Image size 256x256 and 128x128 in x and y direction |
| **stride_size** | 128x128 and 64x64 in x and y direction |
| **val_split_pct** | 20 % of the training dataset is validation |
| **batch_size** | 4,2 and 1 |
| **train transforms** | Rotate 30 degrees with 0.5 percentage,<br>Crop size 256<br>Brightness change in scale btw from 0.4 to 0.6,<br>Conrast change in scale btw from 1.0 to 1.5,<br>Random zoom change in scale btw from 1 to 1.2 |
| **validation transforms** | Crop size (256) |
| **dataset_type** | Classified Tiles |
| **Metadata** | Clasified Tiles. This option will output one classified image chip per input image chip in pixel based classification. |
| **cell size** | Same resolution with raster (31cm) |
| **learning rate** | The optimal learning rate for training the model is automatically determined. |
| **epochs** | 100 for PSPNet, 50 for others |
| **model_type** | UnetClassifier, PSPNetClassifier, DeepLabV3, MMSegmentation, |
| **backbone_model** | Resnet34, resnet50, resnext50,densenet 121, |
| **monitor** | Dice and focal loss besides train and validation loss |

# 4. RESULTS AND DISCUSSION

In this section, we delve into the implementation particulars of the experiments carried out within the context of the thesis. We elaborate on the data augmentation strategies employed, encompassing techniques like rotation, cropping with stride, brightness and contrast adjustments, and random zoom, all aimed at augmenting the dataset's diversity and scale for training machine learning models. Furthermore, we provide an outline of the training specifics, including batch sizes, data types, cell sizes, and image dimensions. The backbone models employed, namely ResNet34, ResNet50, ResNeXt50, and DenseNet121, are introduced, along with their respective training durations and the loss functions employed (dice and focal loss). Additionally, we address the automatic determination of the optimal learning rate for training. Lastly, we discuss the evaluation metrics employed to assess the experiments' performance, culminating in an overview of the experiment results.

## 4.1 Inference

To obtain the desired output, we can leverage the trained models to utilize ArcGIS Pro tools such as *Detect Objects Using Deep Learning, Classify Pixels Using Deep Learning*, or *Classify Objects Using Deep Learning.* These advanced technologies allow us to generate final raster image results and facilitate interpretation. In this experiment, our focus will be on pixel based classification. The objective is to create a classified raster in which each pixel is assigned to a specific class or category. To accomplish this, we will employ the *Classify Pixels Using Deep Learning Tool* available within the Image Analyst toolbox in ArcGIS Pro (“Classify Pixels Using Deep Learning”, n.d.).

For final interpretation, we used inference tools in ArcGIS Pro, and with 0.94 accuracy, the DeepLabV3 ResNet 34 model gave us pixelwise prediction results as an example in the Figure 3.42. Red pixels correspond to damaged classes, and orange pixels correspond to heavily damaged classes. As we can see in Figure 3.43. b., our inference shows that prediction matches the attained damage points with high accuracy.

**Figure 3. 42.** Results of Classify Pixels Using Deep Learning Tool in Antakya District.

In Figure 3.42., Hatay Province is seen as through ArcGIS Pro's inference capabilities, particularly utilizing the UNet-ResNet model for image segmentation, have played a crucial role in a comprehensive study focusing on damage assessment. For damage assessment in Hatay Province, UNet-ResNet 34 emerged as the primary model of choice. This model was utilized to segment and classify damaged structures and infrastructure in the aftermath of seismic events, providing valuable insights into post-disaster response and recovery efforts. This approach delivered accurate and actionable insights, contributing to the province's resilience and sustainable development in the face of its unique geospatial challenges.

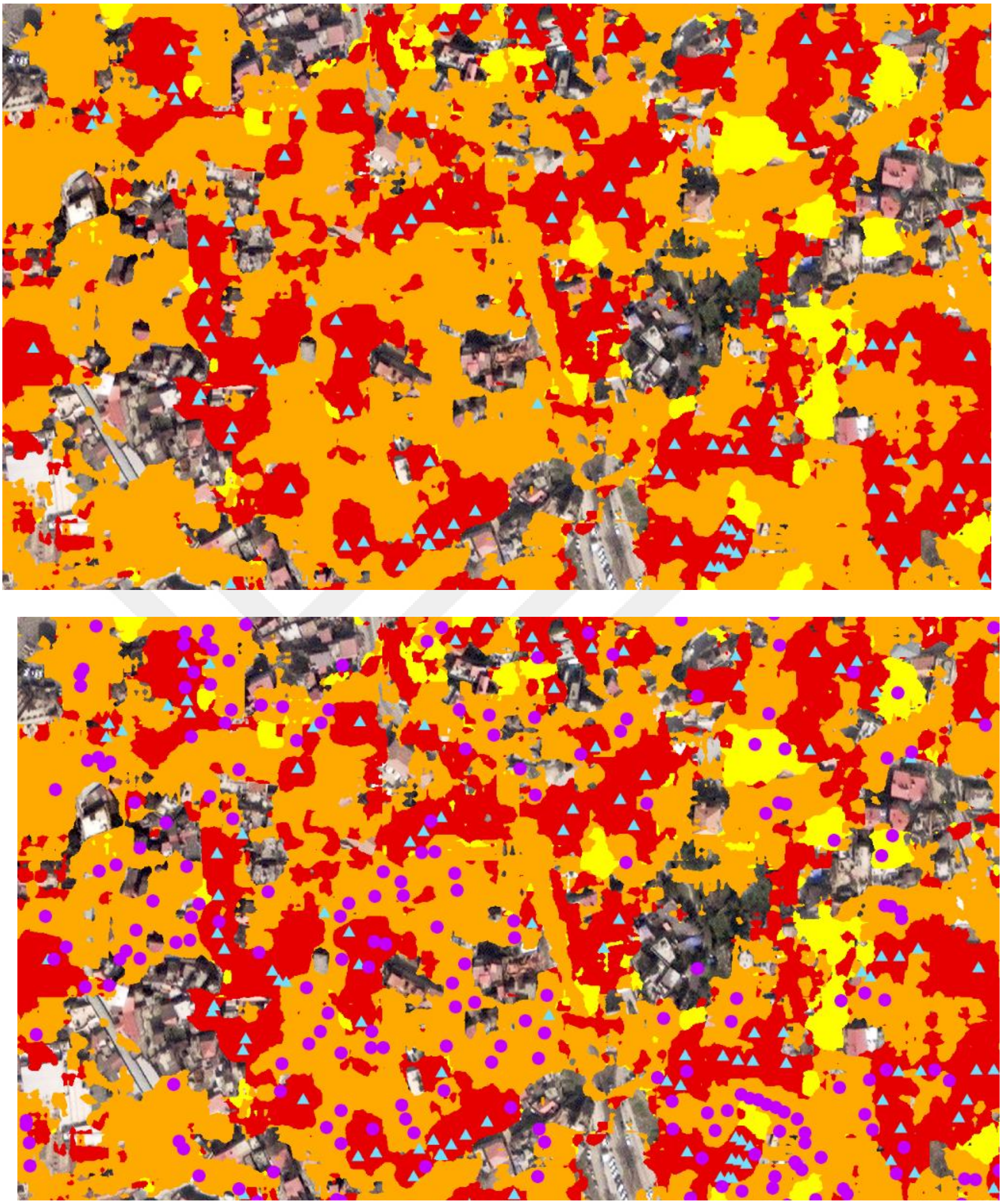

**Figure 3. 43. a)** Red areas: predicted damaged areas, orange: heavily damaged, yellow: slightly damaged areas.

**b)** Predicted pixel around damaged points (blue) and heavily damaged points (purple).

## 4.2 Implementation details

For training the models, we prepared customized training datasets from different earthquake-affected regions with different sizes to enrich our experiment results. The images are resized to 256x256 image chip sizes with 128 stride sizes and 128x128 chip sizes with 64 stride sizes, and the latter was found to be too small for training and decreased the model accuracy. Even though the model was trained for more than 30 hours, the results were very poor and hard to interpret, so we left this option behind (Figure 4.11-4.12). The batch sizes used during training are set to 4, 2, and 1, based on the GPU memory error encountered. The data type used for the model training is "Classified Tiles," with each tile having a cell size of 31 cm. The training is performed for 100 epochs for the PSPNet architecture models and 50 epochs for the Unet and DeepLabV3 models. The loss functions used are dice loss and focal loss, in addition to the standard train and validation losses. The backbone models used are ResNet34, ResNet50, ResNeXt50, and DenseNet121. The optimal learning rate for training the model is determined automatically thanks to the arcgis.learn module in the ArcGIS Pro Python API. The model is trained to classify the images into four damage classes: damaged, heavily damaged, needs demolished, and slightly damaged.

Data augmentation involves, in the Pytorch library, applying various transformations such as rotation (30 degrees with 0.5 probability), cropping size 256 with a stride size of 128x128 in both x and y directions, brightness adjustment (scale between 0.4 and 0.6), contrast adjustment (scale between 1.0 and 1.5), and random zoom (scale between 1 and 1.2) to increase the diversity and size of a dataset for training machine learning models. Additionally, 20% of the training dataset is reserved for validation.

## 4.3 Evaluation Metrics

Evaluation metrics play a vital role in the context of pixel based classsification in the deep learning. By assessing how well the model classifies individual pixels in an image, evaluation metrics offer valuable insights into its accuracy, precision, recall, and overall effectiveness. Pixel based classsification, which involves assigning class labels to each pixel in an image, is a fundamental task in semantic segmentation. The ability to accurately evaluate the performance of such models is crucial for determining its potential deployment in real-world applications, comparing and selecting the model, tuning hyperparameters such as learning rates, batch sizes, and layer configurations, and optimizing the model's performance. Commonly used evaluation metrics for pixel based classsification include Intersection over Union (IoU) or Jaccard Index, mIoU (mean Intersection over Union), Dice coefficient, accuracy, precision, recall, and F1-score. Each metric provides valuable information about different aspects of the model performance, allowing researchers to gain a comprehensive understanding of its strengths and weaknesses.

### 4.3.1 Precision and recall

Precision measures the proportion of true positive predictions (correctly classified positive pixels) out of all the positive predictions made by the model (both true positives and false positives). In other words, it represents the accuracy of the positive predictions. A high precision indicates that the model is making fewer false positive errors, which is essential in applications where misclassifying positive pixels can have significant consequences.

$$\text{Precision} = \text{True Positives} / (\text{True Positives} + \text{False Positives}) \tag{4.1}$$

Recall (also known as Sensitivity or True Positive Rate ) measures the proportion of true positive predictions made by the model out of all the actual positive pixels in the ground truth. In other words, it represents the model's ability to correctly identify positive pixels, regardless of how many false negatives (misclassifying actual positive pixels as negatives) are present. High recall is crucial in applications where it is essential to detect as many positive pixels as possible, even if it means tolerating some false positives.

$$\text{Recall} = \text{True Positives} / (\text{True Positives} + \text{False Negatives}) \tag{4.2}$$

### 4.3.2 F1 score

F1-score, is an evaluation metric used to assess the performance of classification models, particularly in binary classification tasks. It is a harmonic mean of precision and recall, providing a balanced measure of the model's performance, especially when dealing with imbalanced datasets.

$$\text{F1-score} = 2 * (\text{Precision} * \text{Recall}) / (\text{Precision} + \text{Recall}) \tag{4.3}$$

The F1-score is commonly used in scenarios where both false positives and false negatives are equally important, and there is a need to strike a balance between them. It is widely used in various applications, such as information retrieval, medical diagnosis, and sentiment analysis, where class imbalance and classification accuracy are critical considerations.

### 4.3.3 Mean Intersection over union

Mean Intersection over Union (mIoU) is a popular evaluation metric used in semantic segmentation tasks, including pixel based classsification in deep learning. It measures the accuracy of a model's pixel-level predictions by calculating the overlap between the predicted segmentation masks and the ground truth masks for each class and then taking the average across all classes.

To calculate mIoU, first, the Intersection over Union (IoU), also known as the Jaccard Index, is computed for each class as follows:

$$\text{IoU (Class)} = \text{(True Positives for the Class) / (True Positives + False Positives + False Negatives for the Class)} \quad (4.4)$$

Then, mIoU is obtained by averaging the IoU values over all the classes present in the dataset:

$$\text{mIoU} = \text{(IoU (Class1) + IoU (Class2) + ... + IoU (ClassN)) / N} \quad (4.5)$$

Where N is the total number of classes.

mIoU is particularly useful for tasks where class imbalance is present since it takes into account both false positives and false negatives, providing a more balanced measure of the model's performance. A higher mIoU value indicates that the model's predicted segmentation masks better align with the ground truth masks, suggesting better overall performance in pixel based classsification and semantic segmentation tasks.

## 4.4 Results

As it was mentioned earlier, we conducted many experiments for the sake of making the dataset more balanced, finding the optimum match between the data resources, or optimizing the model. This section covers the various experiments used to compare the models in this study.

### 4.4.1 Experiment-1: Unet architecture for Kahramanmaraş province

The first experiment focuses on evaluating the Unet architecture for image segmentation using the dataset from Kahramanmaraş province imagery because Unet is a widely-used encoder-decoder neural network designed for semantic segmentation tasks. The experiment involves

**Table 4. 1.** Experiment of Unet ResNet-34 Architecture for 256x256 sized image.

| **ResNet34** | **Background** | **Collapsed** | **Heavily Damaged** | **Demolished** | **Slightly Damaged** |
|---|---|---|---|---|---|
| **precision** | 0.960 | 0.775 | 0.754 | 0.751 | 0.764 |
| **recall** | 0.976 | 0.554 | 0.644 | 0.535 | 0.686 |
| **f1** | 0.968 | 0.646 | 0.695 | 0.625 | 0.723 |
| **miou** | 0.937 | 0.0672 | 0.292 | 0.062 | 0.535 |

training the Unet model on images of size 256x256 pixels from the Kahramanmaraş province dataset with a stride of 128, which controls the step size of convolutional filters during feature extraction and impacts the spatial dimensions of the output feature maps.

Analysis of the model per class metrics:

| **Model** | **Backbone** | **Learning Rate** | **Train loss** | **Valid loss** | **Accuracy** | **Dice loss** | **Total time** |
|---|---|---|---|---|---|---|---|
| UnetClassifier | ResNet34 | 1.096e-04 | 0.1098 | 0.1970 | 0.9421 | 0.6593 | 16 hours |

As seen in Table 4.1, background pixels always have a higher percentage in metrics because the unlabeled areas in the images outnumbered the labeled areas, even though we avoid this by only using areas of interest in our custom datasets.

**Table 4. 2.** Experiment of Unet ResNet-34 Architecture for 256x256 sized image.

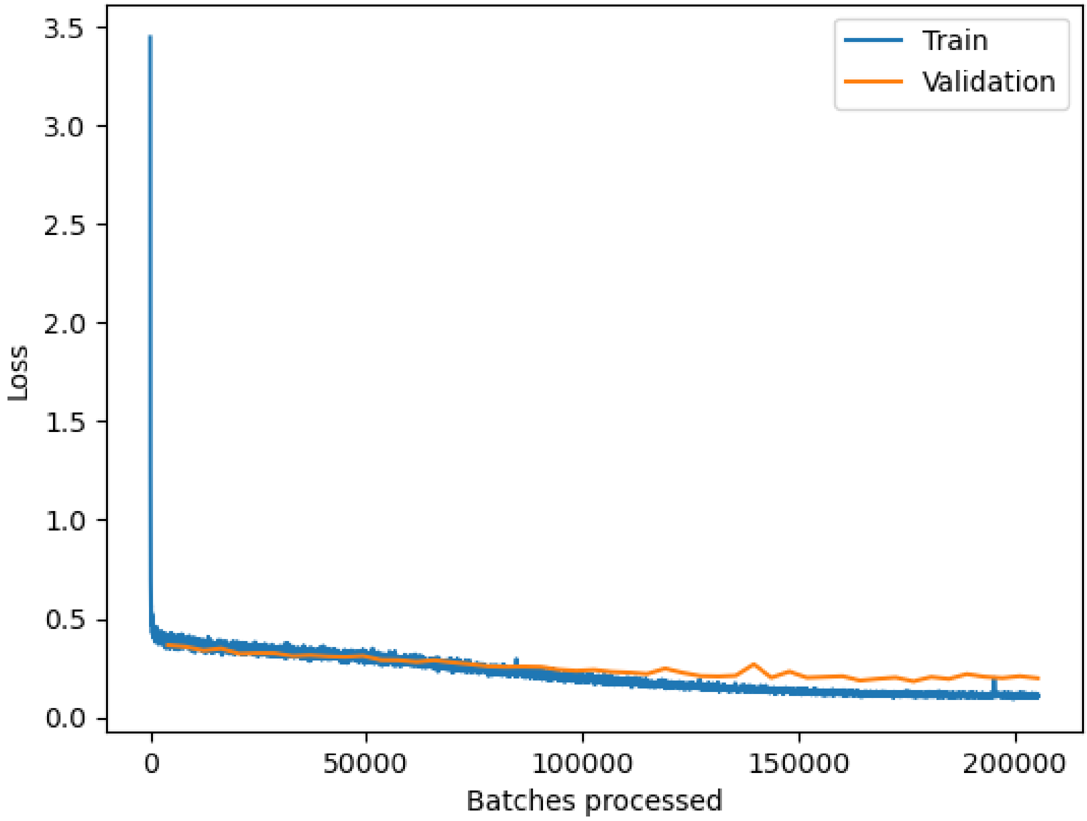


**Figure 4. 1.** Loss functions of the Unet ResNet-34 Architecture.

It is important to note that although we wanted to investigate additional encoders like ResNet-50, we were unable to do so due to GPU memory issues that we experienced when doing our tests. Despite these difficulties, UNet and ResNet-34 worked together to help us accomplish our study goals, demonstrating the potential of these models for better disaster management.

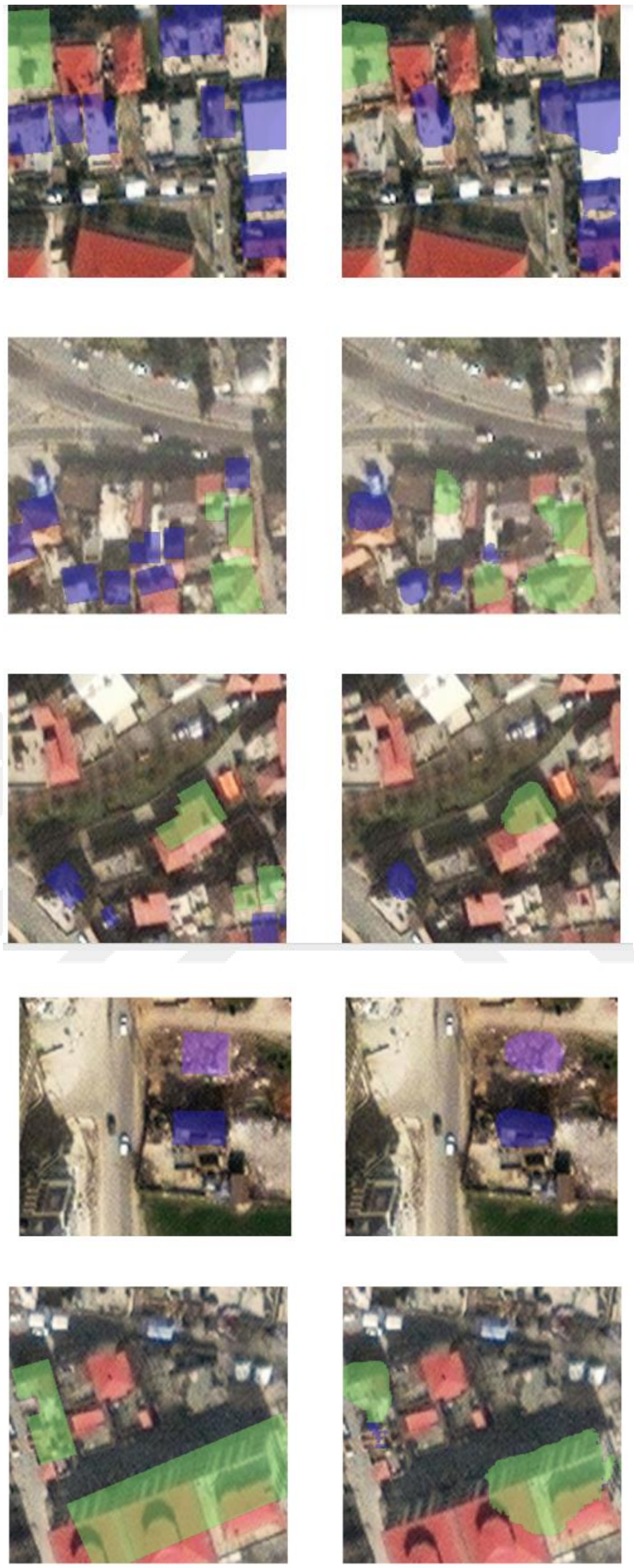

**Figure 4. 2.** Experiment of Unet ResNet-34 Architecture for Pixel based classsification

(Ground Truth and Predictions are portrayed).

### 4.4.2 Experiment-2: DeepLabV3 architecture for Kahramanmaraş province

As below, we demonstrated all the visual and numeric results with all the details by showing the DeepLabV3 model as an example.

**DeepLabV3 Model Metrics**

**Table 4. 3**. Metrics results for the DeepLabV3 architecture with ResNet34 encoder.

| ResNet34 | Background | Collapsed | Heavily Damaged | Demolished | Slightly Damaged |
|---|---|---|---|---|---|
| **precision** | 0.869 | 0.850 | 0.863 | 0.815 | 0.869 |
| **recall** | 0.639 | 0.711 | 0.678 | 0.770 | 0.639 |
| **f1** | 0.737 | 0.774 | 0.760 | 0.791 | 0.737 |
| **miou** | 0.083 | 0.347 | 0.084 | 0.623 | 0.083 |

**Table 4. 4.** Metrics results for the DeepLabV3 architecture with ResNet50 encoder.

| ResNet50 | Background | Collapsed | Heavily Damaged | Demolished | Slightly Damaged |
|---|---|---|---|---|---|
| **precision** | 0.9007 | 0.868 | 0.890 | 0.863 | 0.9007 |
| **recall** | 0.706 | 0.796 | 0.780 | 0.802 | 0.706 |
| **f1** | 0.792 | 0.830 | 0.831 | 0.831 | 0.792 |
| **f1** | 0.792 | 0.830 | 0.831 | 0.831 | 0.792 |
| **miou** | 0.098 | 0.400 | 0.102 | 0.686 | 0.098 |

**Table 4. 5.** Metrics results for the DeepLabV3 architecture with ResNext50 encoder.

| ResNext50 | Background | Collapsed | Heavily Damaged | Demolished | Slightly Damaged |
|---|---|---|---|---|---|
| **precision** | 0.861 | 0.853 | 0.862 | 0.826 | 0.861 |
| **recall** | 0.646 | 0.719 | 0.715 | 0.758 | 0.646 |
| **f1** | 0.738 | 0.780 | 0.782 | 0.791 | 0.738 |
| **miou** | 0.087 | 0.349 | 0.090 | 0.623 | 0.087 |

**Table 4. 6.** Metrics results for the DeepLabV3 architecture with DenseNet121 encoder.

| ResNet121 | Background | Collapsed | Heavily Damaged | Demolished | Slightly Damaged |
|---|---|---|---|---|---|
| **precision** | 0.673 | 0.561 | 0.524 | 0.604 | 0.673 |
| **recall** | 0.113 | 0.174 | 0.096 | 0.277 | 0.113 |
| **f1** | 0.194 | 0.265 | 0.162 | 0.380 | 0.194 |
| **miou** | 0.007 | 0.045 | 0.006 | 0.193 | 0.007 |

When training the Dense 121 encoder, we trained with fewer epochs because we accepted the early epoch as true and the metrics were poorer, while other DeepLabV3 encoders had 50 epochs, so we got better results.

**Table 4. 7.** Hyperparameters of the DeepLabV3 architecture.

| Model | Backbone | Learning Rate | Train loss | Valid loss | Accuracy | Dice loss | Total time | Model |
|---|---|---|---|---|---|---|---|---|
| DeepLabV3 | ResNet34 | 2.51e-03 | 0.163 | 0.133 | 0.954 | 0.747 | 15 hours | DeepLabV3 |
| DeepLabV3 | ResNet50 | 2.08e-03 | 0.142 | 0.132 | 0.954 | 0.746 | 25 hours | DeepLabV3 |
| DeepLabV3 | ResNext50 | 1.73e-03 | 0.129 | 0.113 | 0.964 | 0.808 | 25 hours | DeepLabV3 |
| DeepLabV3 | DenseNet121 | 1.44e-03 | 0.352 | 0.289 | 0.901 | 0.279 | 15 hours | DeepLabV3 |

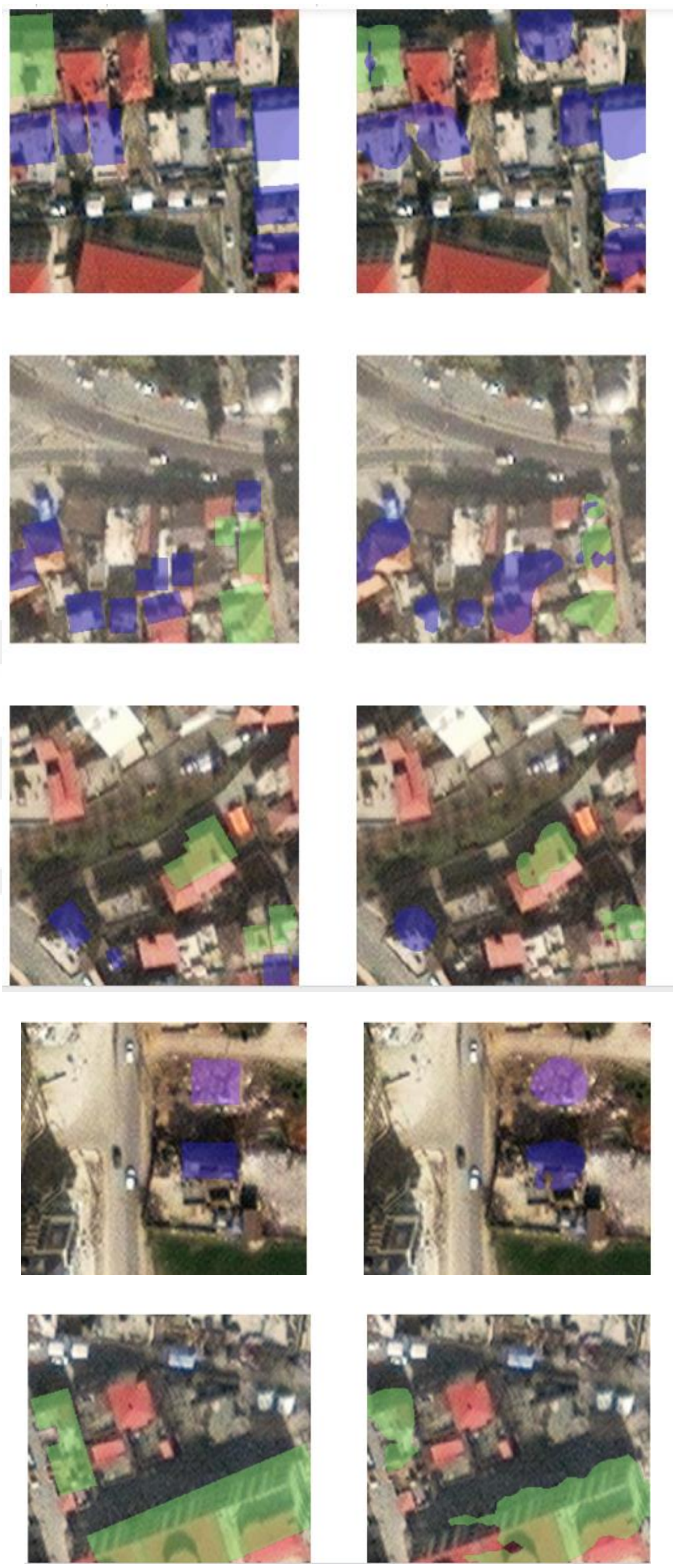

**Figure 4. 3.** Experiment of DeepLabV3 ResNet 34 Architecture for Pixel based classsification.

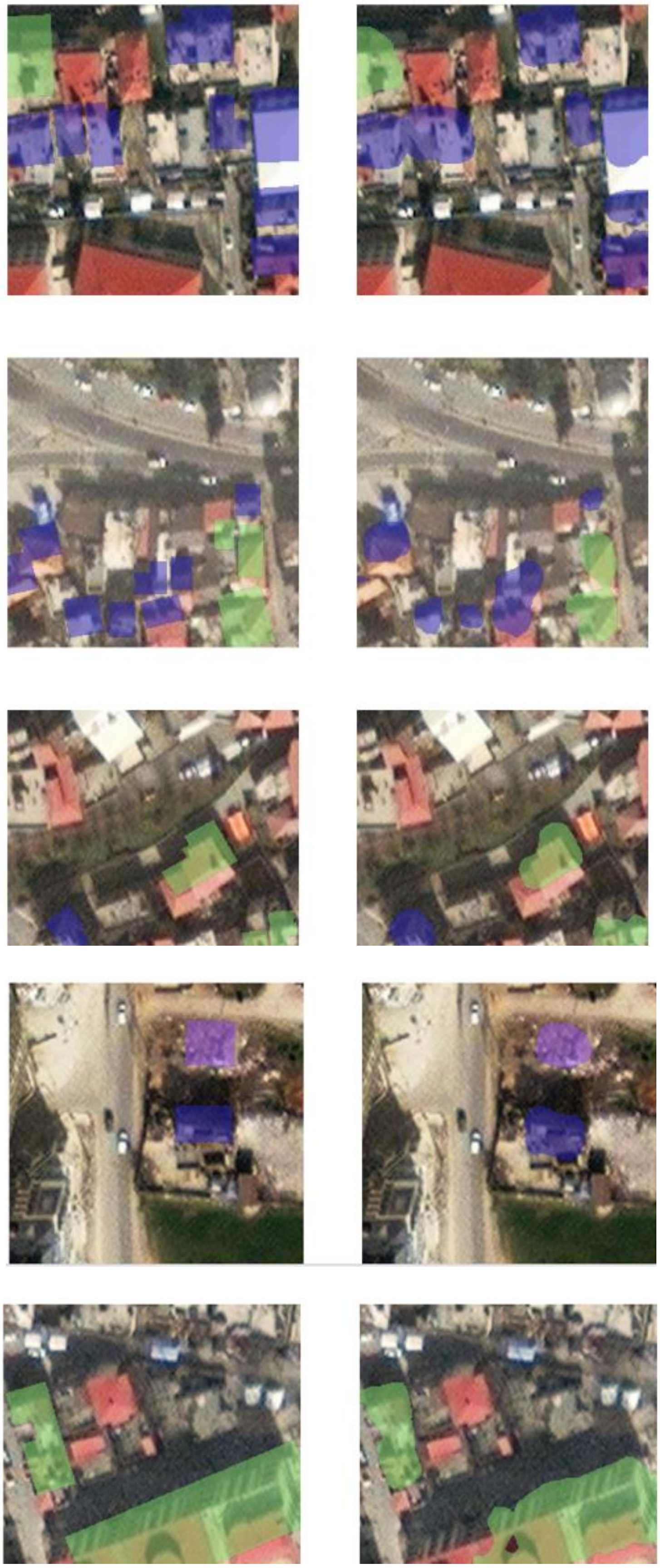

**Figure 4. 4.** Experiment of DeepLabV3 ResNet50 Architecture for Pixel based classsification.

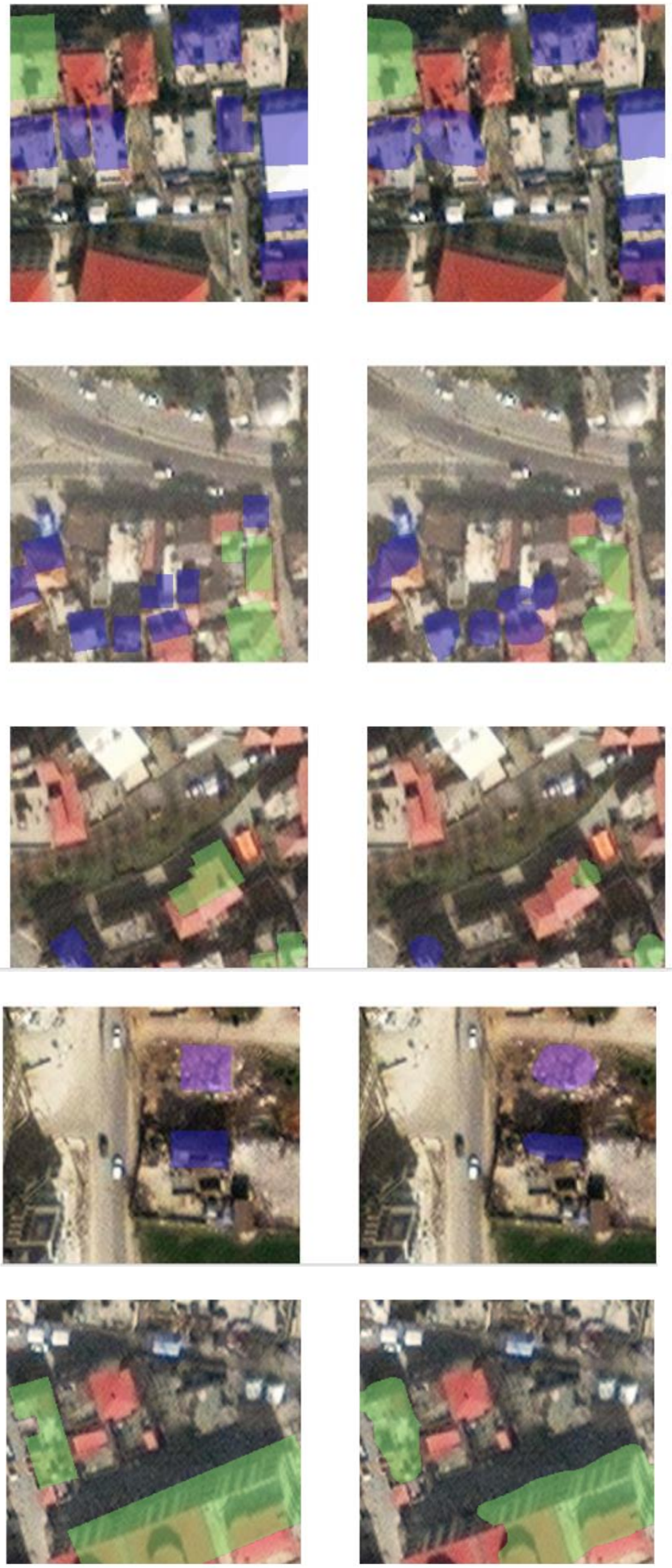

**Figure 4. 5.** Experiment of DeepLabV3 RexNet50 Architecture for Pixel based classsification.

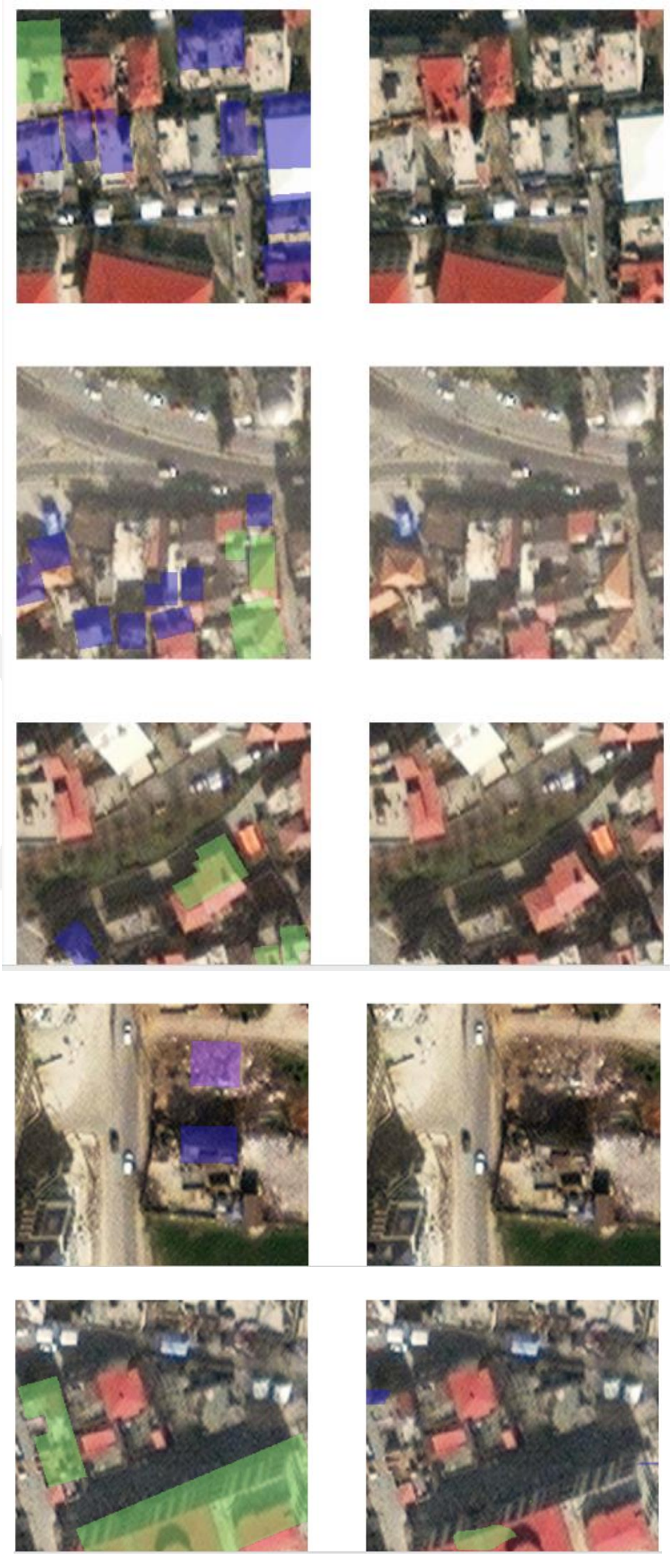

**Figure 4. 6.** Experiment of DeepLabV3 DenseNet121 Architecture for Pixel based classsification.

The key advantage of DeepLabV3 is its capacity for exact pixel-level segmentation through the use of arous convolution, which enables it to capture delicate picture information at various scales without noticeably raising computational complexity. In this study, this architecture excels in feature extraction when used in conjunction with the ResNet50 encoder, ensuring precise detection and delineation of damaged zones in satellite data following seismic events. In this thesis, the importance of choosing the right model for this crucial task is emphasized, and DeepLabV3's efficacy in this context is highlighted, especially in the context of the Kahramanmaraş earthquake research.

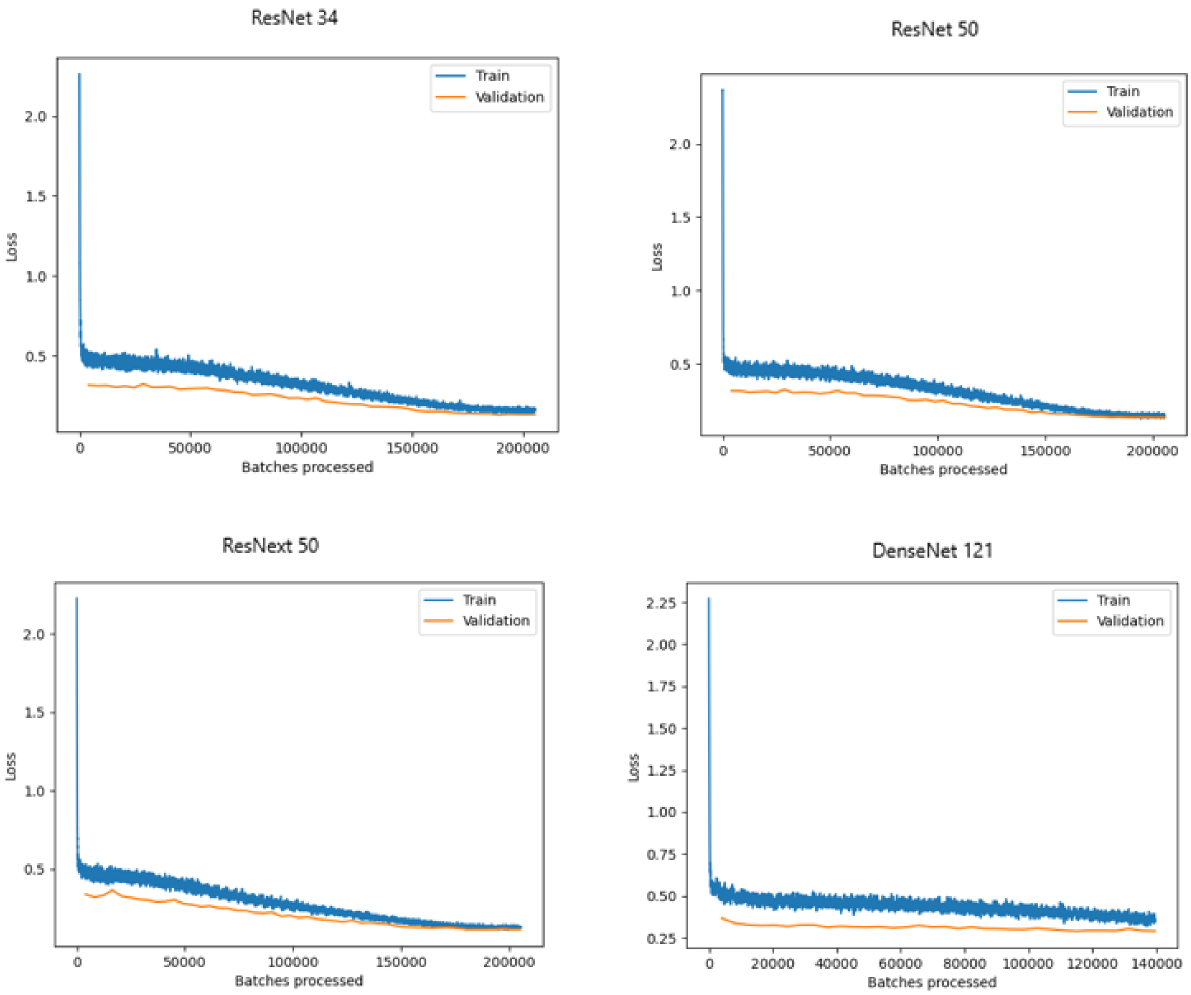


**Figure 4. 7.** Loss functions of the DeepLabV3.


**Figure 4. 8.** Experimental results of the DeepLabV3 architecture.

### 4.4.3 Experiment-3: PSPNet architecture for Kahramanmaraş province

The experiment involves using the PSPNet model with ResNet34 and ResNet50 backbones. The learning rate for the ResNet34 backbone is set to 1.000e-03, while for the ResNet50 backbone, it is set to 6.918e-04. The training dataset used is customized and derived from the Kahramanmaraş Province, with a chip size of 256x256 and a stride size of 128. During training, a batch size of 4 is used.

Analysis of the model per class metrics:

**Table 4. 8.** Metrics results for the PSPNet architecture with ResNet34 encoder.

| PSPNet ResNet34 | Collapsed | Heavily Damaged | Damaged | Slightly Damaged |
|---|---|---|---|---|
| **precision** | 0.710 | 0.716 | 0.769 | 0.716 |
| **recall** | 0.381 | 0.472 | 0.348 | 0.532 |
| **f1** | 0.496 | 0.569 | 0.479 | 0.611 |
| **miou** | 0.038 | 0.196 | 0.033 | 0.401 |

**Table 4. 9.** Metrics results for the PSPNet architecture with ResNet50 encoder.

| PSPNet ResNet50 | Collapsed | Heavily Damaged | Damaged | Slightly Damaged |
|---|---|---|---|---|
| **precision** | 0.865 | 0.807 | 0.825 | 0.797 |
| **recall** | 0.483 | 0.639 | 0.590 | 0.647 |
| **f1** | 0.620 | 0.713 | 0.688 | 0.714 |
| **miou** | 0.064 | 0.294 | 0.071 | 0.523 |

**Table 4. 10.** Hyperparameters of the PSPNet architecture.

| Model | Backbone | Train Loss | Valid Loss | Accuracy | Dice Loss | Total Time |
|---|---|---|---|---|---|---|
| PSPClassifier | ResNet34 | 0.6275 | 0.2330 | 0.9228 | 0.5289 | 25 hours |
| PSPClassifier | ResNet50 | 0.4989 | 0.2469 | 0.9427 | 0.6809 | 28 hours |

For precisely identifying damaged areas in satellite photos, PSPNet excels at capturing contextual data at various sizes. In our study, we used PSPNet along with several encoders, such as ResNet-34 and ResNet-50. Notably, our research showed that using ResNet-50 as the encoder consistently outperformed other setups, resulting in higher damage assessment accuracy.

This result demonstrates how crucial it is to choose the optimum encoder architecture in the context of disaster management. The most efficient combination, providing improved precision and granularity in damage assessment, was PSPNet with ResNet-50. Together with UNet and DeepLabv3, these models make it easier to automatically identify and classify affected regions, delivering priceless information to support decision-makers in responding to and managing natural disasters' after effects.

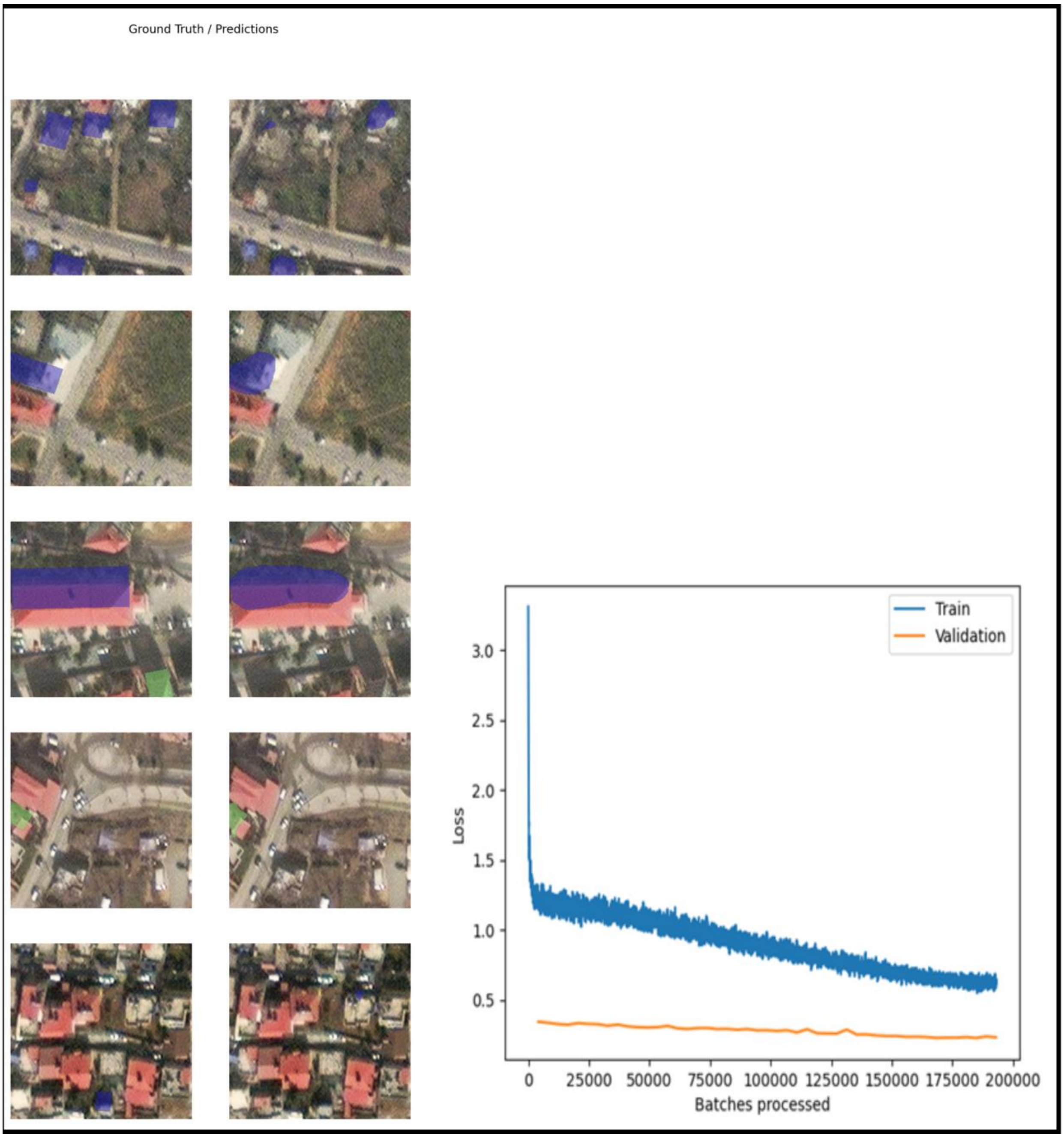


**Figure 4. 9.** Experiment of PSPNet ResNet34 Architecture for Pixel based classsification.

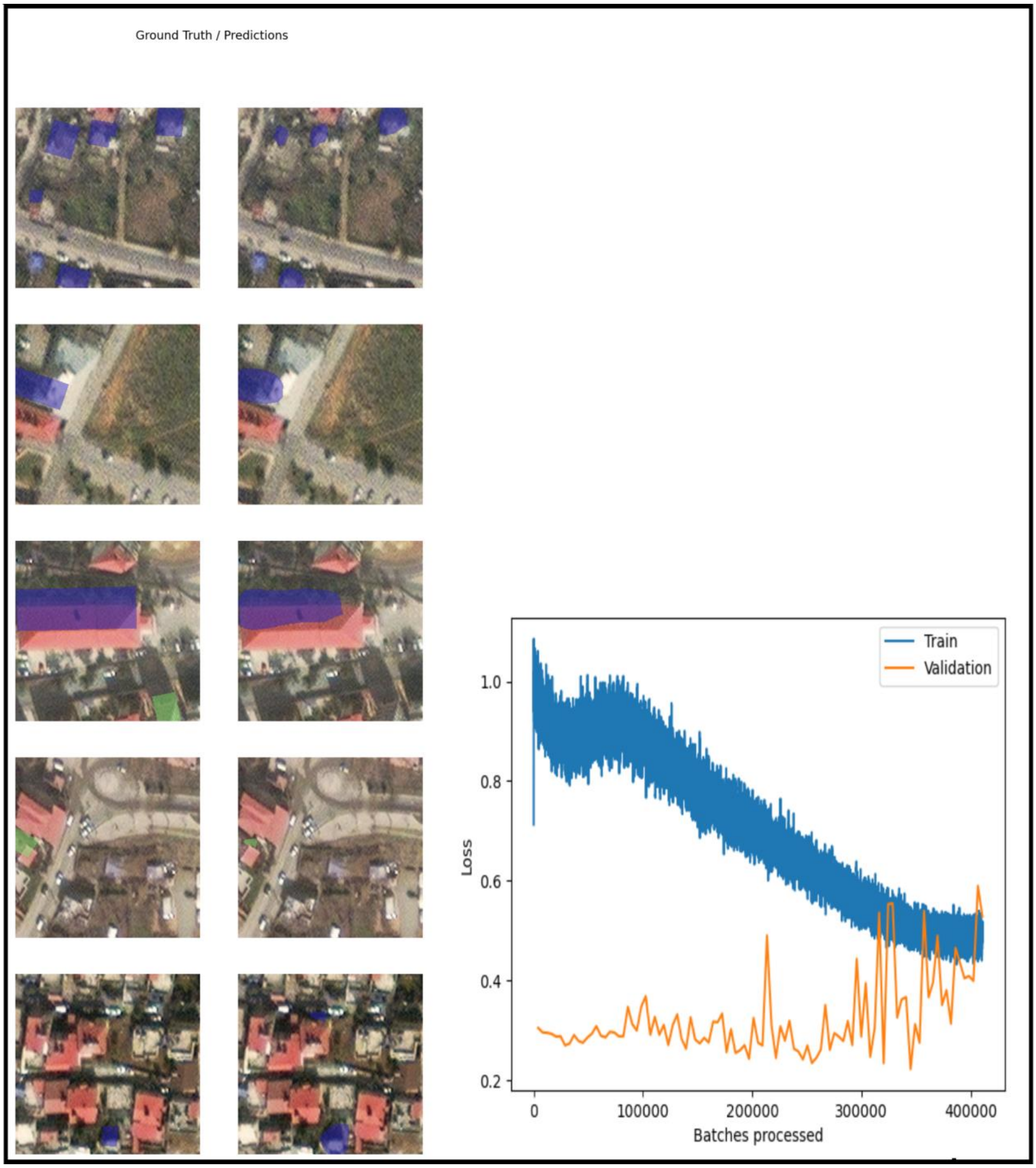


**Figure 4. 10.** Experiment of PSPNet ResNet50 Architecture for Pixel based classsification.

### 4.4.4 Experiment-4: Kahramanmaraş experiment for 128x128 chip size

As we mentioned earlier in the data preparataion part, some building footprints could not match very well. Even only this problem caused a very poor metric results.

```
images = 69825 *3*128*128

Class feature statistics:
features = 164773
features per image = [min = 1, mean = 2.36, max = 19]
classes = 4
```

| cls name | cls value | images | features |
|---|---|---|---|
| Col | 1 | 4551 | 7099 |
| HevDam | 2 | 20990 | 34543 |
| Dem | 3 | 4171 | 5718 |
| Slig | 4 | 55787 | 117413 |

**Figure 4. 11.** 128x128 image size with 64 stride image chips and statistics of the training dataset.

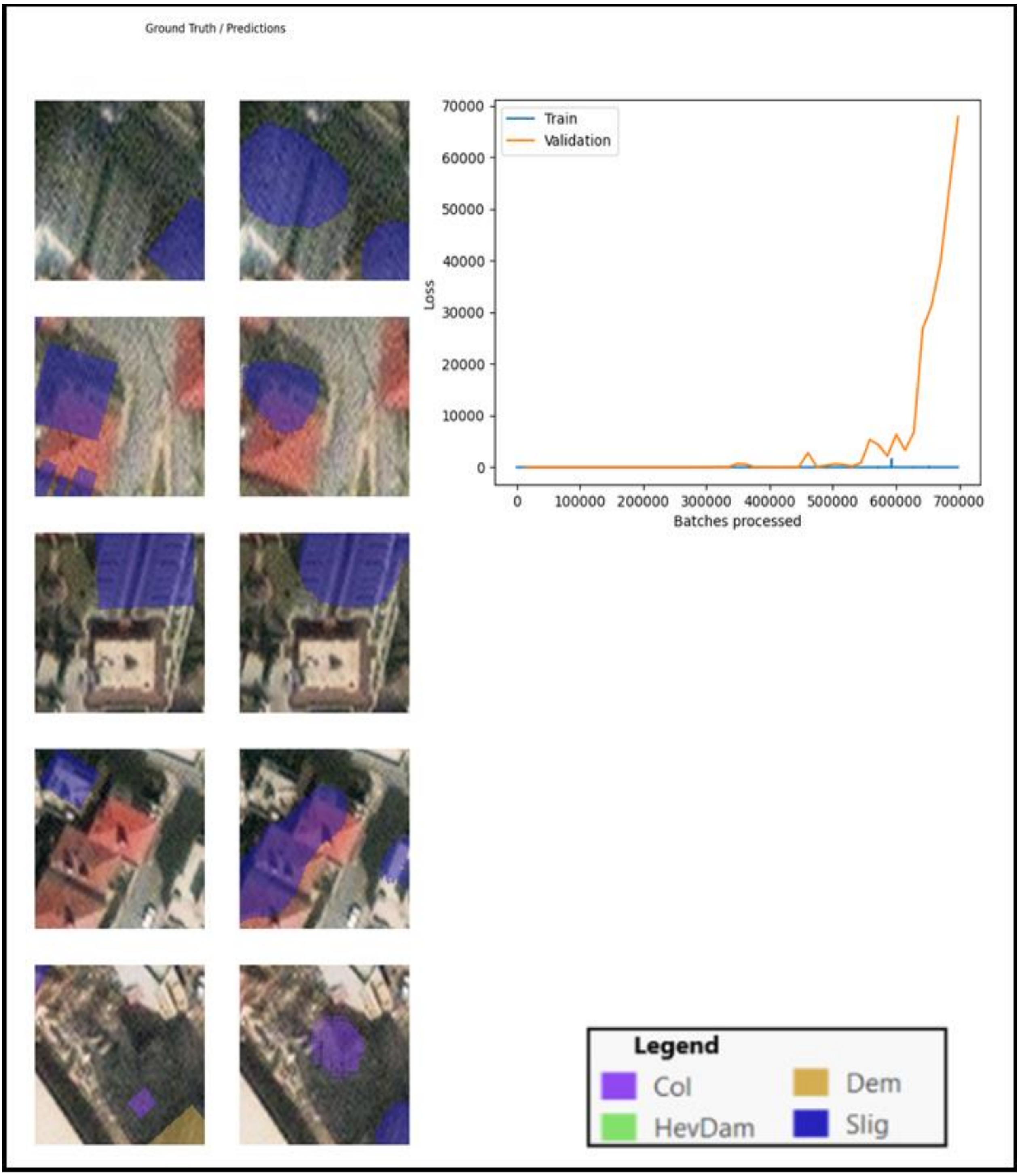


**Figure 4. 12.** Ground truth and predictions for Unet ResNet34 Architecture.

### 4.4.5 Experiment-5: Hatay experiment for 256x256 chip size

Hatay Province had the most unfavorable satellite images for our building footprints drawn by volunteer experts. As it is mentioned in Preparation of the Training Data section, many of our efforts were insufficient even though we tried to use the building footprint extraction deep learning models from living atlas website (ArcGIS Living Atlas of the World, n.d.).

```
images = 14489 *3*256*256

Class feature statistics:
features = 58963
features per image = [min = 1, mean = 4.07, max = 67]
classes = 4
cls name                            cls value    images   features
Col                                         1      3273       7640
HevDam                                      2      9508      29164
Dem                                         3      1532       2388
Slig                                        4      8573      19771
```

**Figure 4. 13.** Statistics of the Hatay dataset.

In this comprehensive study conducted in Hatay Province, advanced tools like ArcGIS Pro and its cutting-edge architectural model, such as UNet, were utilized. The primary objective was to delve into the intricate process of damage assessment, particularly in the context of earthquake-affected regions. Notably, Hatay Province posed distinct challenges, particularly concerning satellite imagery quality, arising from inconsistencies in building footprints drawn by volunteer experts. Despite persistent efforts, even basic models like Unet-Resnet 34 faced GPU memory errors after a month of optimization attempts for Hatay Province, emphasizing the complexity of the task. However, the persistent building footprint mismatch remained a substantial hurdle, highlighting the intricate nuances of real-world data challenges in damage assessment.

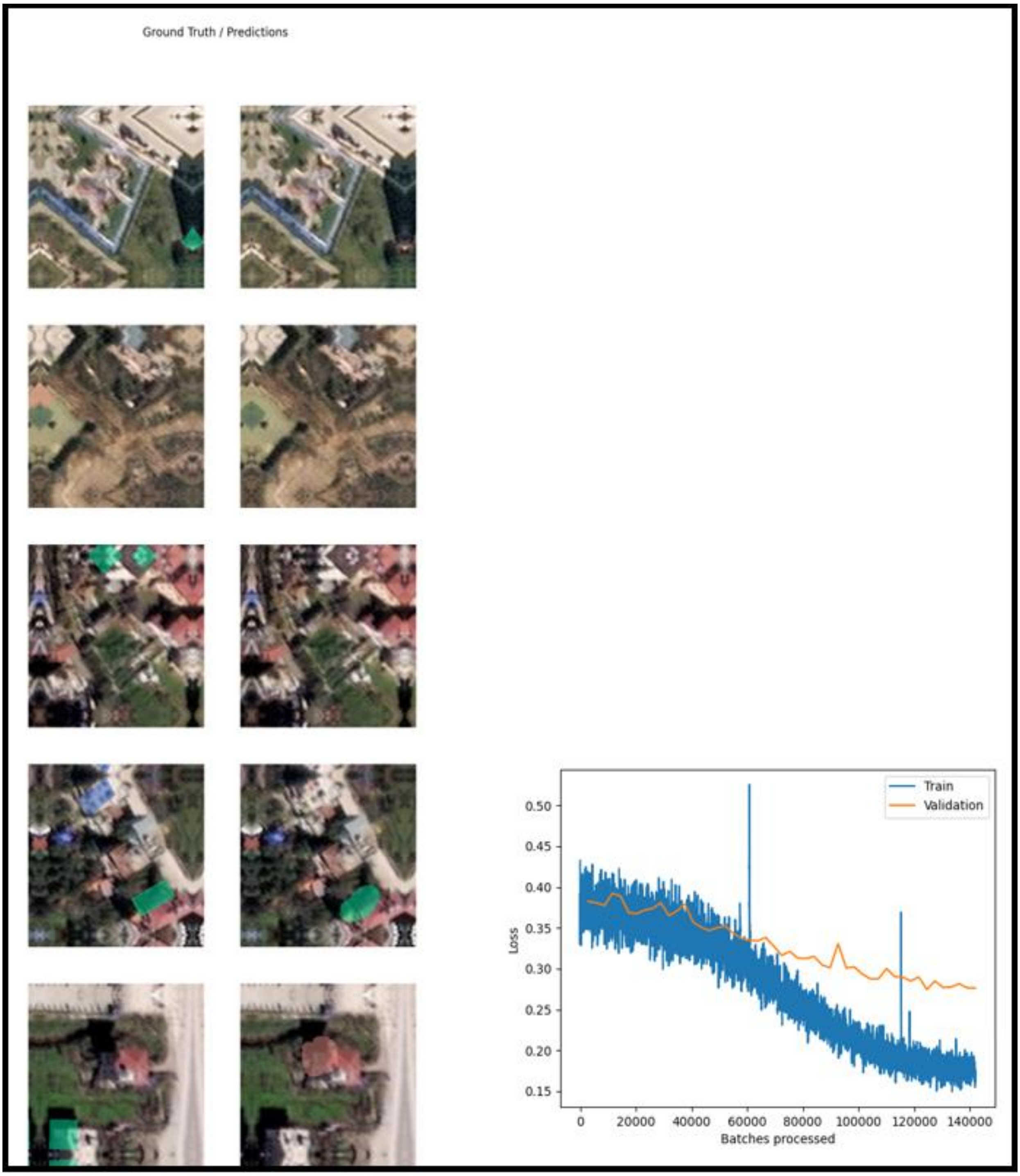


**Figure 4. 14.** Unet Resnet34 Architecture for Hatay dataset.

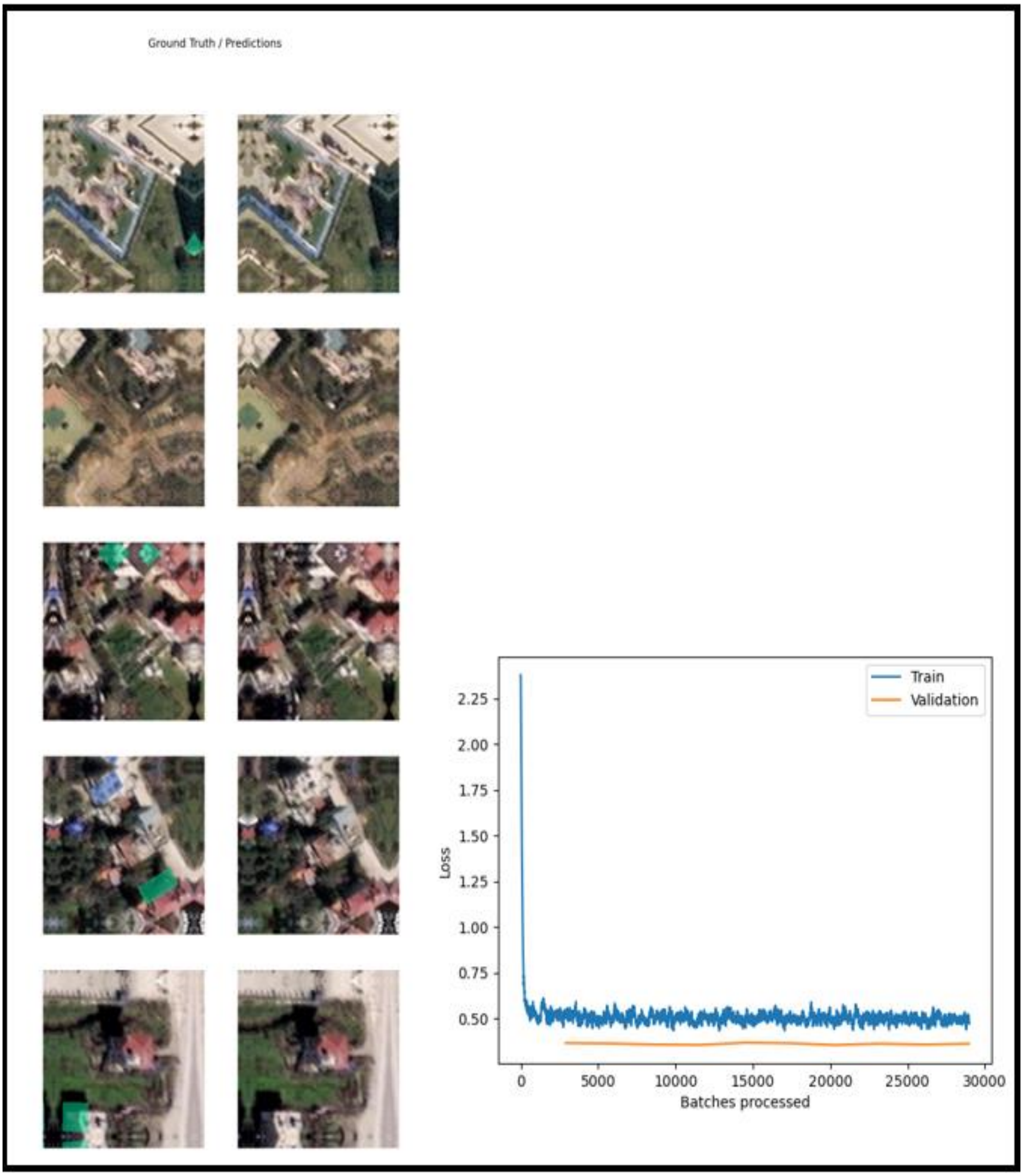


**Figure 4. 15.** DeepLabV3 ResNet34 Architecture for Hatay dataset.

### 4.5 Discussion

This thesis, carried out using ArcGIS Pro and multiple architectural models such as UNet, DeepLabV3, and PSPNet, yielded valuable insights into the process of damage assessment. As anticipated, DeepLabV3, employing various backbones, demonstrated the most favorable metrics and visual outcomes. By examining earthquake-affected cities, namely Kahramanmaraş, Hatay, and Gaziantep, this study sheds light on the challenges and possibilities associated with implementing such methodologies in diverse scenarios. The examination of the three cities, which were impacted by the Kahramanmaraş earthquake sequence, revealed the difficulties and opportunities in adopting these methodologies across various scenarios. While the results in Kahramanmaraş showed promise with well-matched building footprints and images, Hatay and Gaziantep presented certain limitations due to data distribution mismatches and imbalanced damage data. These findings underscore the importance of future research and methodological advancements to address the unique characteristics of each location. As mentioned earlier, Hatay Province had the most unfavorable satellite images because of the overlap between the building footprints drawn by volunteer experts.

As observed in the table, the metrics consistently show a higher percentage of the background pixels. This is primarily due to the larger number of unlabeled areas in the images compared to the labeled areas, despite our efforts to mitigate this issue by exclusively utilizing regions of interest in our custom datasets.

Also, after more than a month of trying to optimize the accuracy for Hatay province, our hardware system started giving GPU memory errors even for the simplest models, such as the Unet-Resnet 34 architecture. We simply tried to give the optimum results with the best imagery and the data we had. The imagery data source has been decided on as Kahramanmaraş, and we simply tried the most beneficial models with the best metric results. The DeepLabV3 architecture especially with the ResNet50 encoder gave us the best and the richest visual and numeric results. As we mentioned earlier, the mismatch of the recently adjusted building footprints made it impossible for the model to learn the classes. Because of this mismatch, the building footprint attains a pixel area that is heavily damaged, but in reality, these pixels represent a rail road and vice versa.

And based on these, tiling images as 128x128 with stride 64 gave quite poor results after training (as seen in Figure 4.10). We kept the 256x256 chip size and applied various models for the training. One of the best parts of the ArcGIS Pro Deep Learning tool is that we can see results for each class separately by default. IoU is the predicted segmentation's area of overlap divided by the predicted segmentation's area of union. For binary (two classes) or multi-class segmentation, the mean IoU of an image is obtained by averaging the IoU of each class. Most of the pixels are background due to the uneven representation of the damage classes in the mean intersection over union (mIoU), despite the fact that we eliminated this scenario by focusing on our custom Area of Interest (AoI). Also, the nadir angles that were used to draw the building from pre-disaster imagery created a shift in the post-disaster imagery. These setbacks might have caused false positives and low mIoU values for damage classes, unlike the background class, which always has more than 0.95 mIoU values (Table 3.4). Besides, PSPNet classifier models did not produce the successful outcomes. So we did not prefer to pursue other backbones and consume more time for this architecture.

Also, it is successfully developed a comprehensive dashboard as an outcome of this research conducted under the TÜBİTAK 2210-D scholarship, utilizing cutting-edge Esri technologies for this MSc thesis. This dashboard can be accessed via an intelligent URL, as seen in Url-24 and the QR code of the intelligent link is seen in Figure 4.16, which presents to users two distinct links leading to separate dashboards. These dashboards were generated to cater to both mobile devices and desktop users, ensuring a seamless and optimized user experience. The primary tool employed in the creation of these dashboards was ArcGIS Maps, Dashboards, and Experience Builder. This innovative platform offers a revolutionary approach to building web applications, featuring a user-friendly drag-and-drop interface that empowers users to effortlessly craft robust information products. Within this unified web experience, various elements are integrated, such as text, media, multiple maps, surveys, and diverse content types. What sets ArcGIS applications like Experience Builder apart is its adaptability and mobile friendliness, as it equips users with the tools necessary to fine-tune their applications for desktop, tablet, and mobile views.

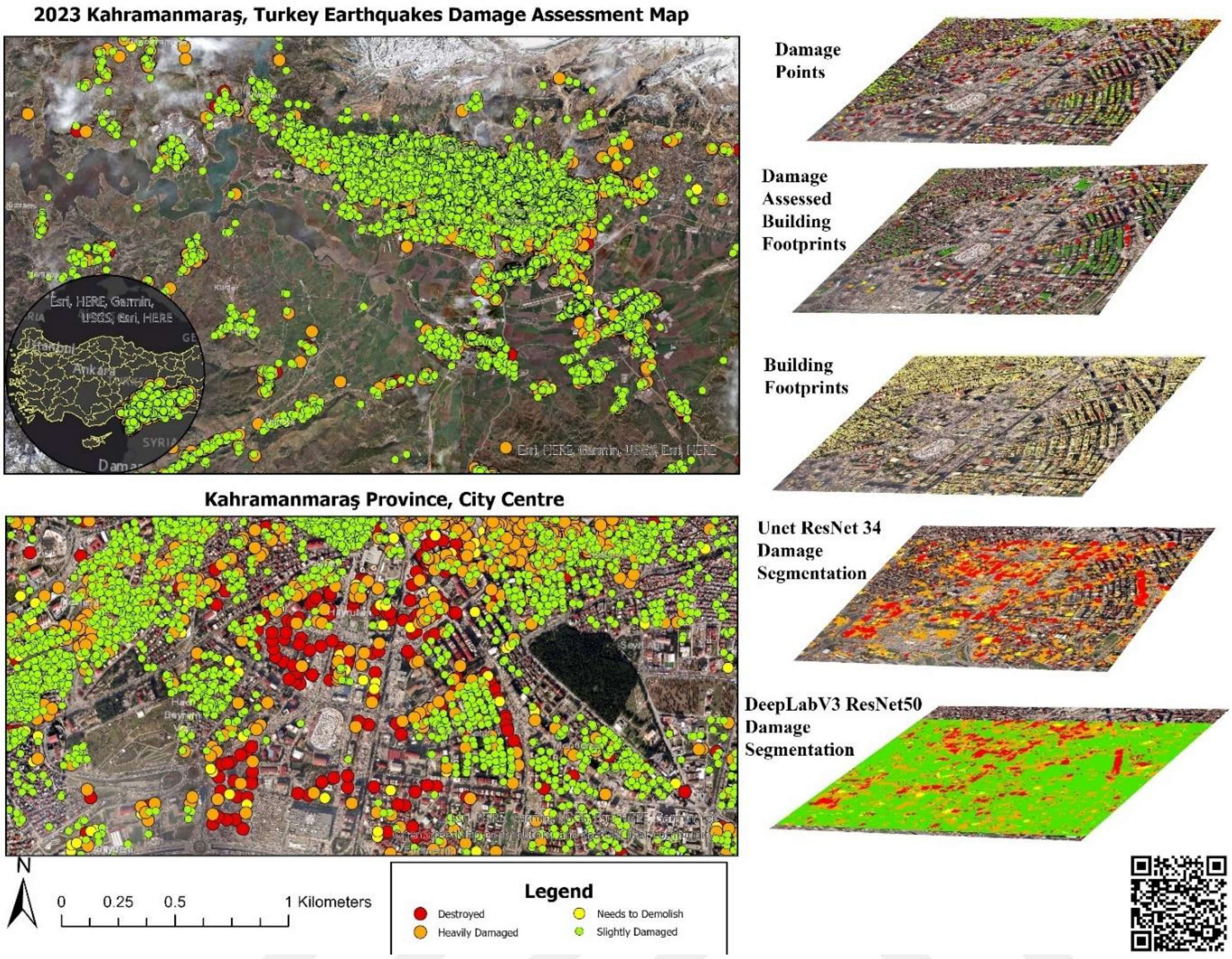


**Figure 4. 16.** Kahramanmaraş Earthquake Damage Assessment Map with QR of the multiple linked dashboard.

# 5. CONCLUSION

The aim of this thesis is to explore the applicability of diverse deep learning techniques, assess their precision in identifying structurally damaged buildings, and leverage satellite imagery alongside diverse open-source spatial data for enhancing earthquake studies. This master's thesis has successfully explored the integration of remote sensing, computer vision, and earth observation techniques for geophysics and earthquake studies, focusing on damage assessment in the aftermath of earthquakes. By leveraging satellite imagery and pixel-based classification methods, computer vision has demonstrated its potential for rapid and accurate disaster management.

The investigation, carried out using ArcGIS Pro and multiple architectural models such as UNet, DeepLabV3, and PSPNet, provided useful insights into the damage assessment process. As expected, DeepLabV3 with various backbones gave us the best metrics and visual results. Through the examination of earthquake-affected cities, including Kahramanmaraş, Hatay, and Gaziantep, the study shed light on the challenges and opportunities associated with implementing such procedures in various scenarios. The examination of three cities damaged by the Kahramanmaraş earthquakes, namely Kahramanmaraş, Hatay, and Gaziantep, has revealed the difficulties and opportunities of adopting such procedures in various scenarios. While results of the Kahramanmaraş Province with well-matched building footprints and images were promising, Hatay and Gaziantep revealed certain limitations due to mismatched data distributions and imbalanced damage data. These findings emphasize the significance of future study and methodological development to address the unique characteristics of each location.

Collaboration among researchers, disaster management agencies, and data providers such as Yer Çizenler NGO and Humanitarian OpenStreetMap can also improve the interchange of knowledge, data, and resources, resulting in more comprehensive and efficient disaster response activities, as we aimed in this thesis. Finally, this thesis serves as a step toward realizing the potential of remote sensing, computer vision, and earth observation in geophysics and earthquake research. It adds to the expanding body of knowledge in the field of disaster management by addressing the obstacles and highlighting the opportunities, and it sets the way for future improvements that will assist in limiting the impact of the earthquakes and enhancing response techniques. Through constant research and innovation, we may aim toward a safer and more resilient future in the face of the natural disasters.

ArcGIS Pro offers diverse visual representation options, particularly beneficial for remote sensing tasks. It provides advanced tools for visualizing and analyzing remote sensing data, including 2D and 3D images. Additionally, ArcGIS Pro supports the integration of visualizations, such as graphs and charts, into GIS workflows. By incorporating visual representations of data, users can effectively communicate complex information and trends, enabling better decision-making and collaboration. The ability to visualize remote sensing data in different dimensions can enhance the analysis and interpretation of deep learning results, facilitating insights and discoveries.

ArcGIS Pro integrates with GIS data, allowing the merging of geographical data with deep learning models. This integration enables spatially aware predictive modeling, taking advantage of the capabilities of deep learning algorithms for geospatial analysis and mapping applications. Furthermore, the API provides data preparation features, such as data augmentation and feature extraction, that are especially tuned for geographical data and might be useful for deep learning applications in the GIS domain.

However, while ArcGIS Pro supports deep learning, it is not primarily designed as a dedicated deep learning framework. As a result, several sophisticated capabilities and optimizations available in specialist deep learning frameworks such as PyTorch or TensorFlow may be missing. This constraint has the potential to restrict the flexibility and customization choices available for deep learning models, such as pre-trained models. It may not support the latest state-of-the-art deep learning architectures and techniques. Furthermore, it may not deliver optimal performance for computationally expensive deep learning applications, particularly those requiring high-speed computer resources like GPUs. This can result in slower training and inference times compared to specialist deep learning frameworks. Additionally, dependency on the ArcGIS ecosystem might be a disadvantage for developers who are not mainly focused on GIS-related jobs, as it may necessitate additional setup, dependencies, and expertise with ArcGIS tools and concepts. For example, some data types (JSON, etc.) are not directly supported in every tool in the ESRI software system, which can lead to additional data correction or preprocessing steps.

## REFERENCES

*06 Şubat 2023 Kahramanmaraş Pazarcık depremi*. (2023, February 21). ATAG: Aktif Tektonik Araştırma Grubu. https://atag.itu.edu.tr/v4/?p=1084

**Abd-Elrahman, A., Britt, K., & Liu, T.** (2021). Deep Learning Classification of High-Resolution drone images using the ArcGIS Pro software. EDIS, 2021(5). https://doi.org/10.32473/edis-fr444-2021

**Abdi, G. and Jabari, S.** (2021) 'A multi-feature fusion using deep transfer learning for earthquake building damage detection', *Canadian Journal of Remote Sensing*, 47(2), pp. 337–352. doi:10.1080/07038992.2021.1925530.

Airbus DS Intelligence. (2023). Image Gallery Details. Retrieved 2023, April 15 from https://www.intelligence-airbusds.com/en/5751-image-gallery-details?img=77502#.Y-OB02TMKko

*ALOS-2 observations of earthquakes in southeastern Turkey in 2023 (Updated on March 2) – JAXA Earth-graphy / Space Technology Directorate I*. (2023b, February 14). JAXA Earth-graphy / Space Technology Directorate I. https://earth.jaxa.jp/en/earthview/2023/02/14/7381/index.html

ArcGIS Living Atlas of the World. (n.d.). Living Atlas. Retrieved 2023, May 10, from https://livingatlas.arcgis.com/en/browse/#d=2&type=tool

*ArcGIS dashboards. (n.d.).* Retrieved 2023, May 10 from https://irides.maps.arcgis.com/apps/dashboards/ffb8ae5f27964ad8843c5e99556e0ff5

ArcGIS Developers. (n.d.). How DeepLabV3 Works. Retrieved from https://developers.arcgis.com/python/guide/how-deeplabv3-works/

ArcGIS Developers. (n.d.). How PSPNet Works. Retrieved from https://developers.arcgis.com/python/guide/how-pspnet-works/

ArcGIS Developers. (n.d.). How U-Net Works. Retrieved from https://developers.arcgis.com/python/guide/how-unet-works/

ArcGIS Developers. (n.d.). Overview of the ArcGIS API for Python. Retrieved from https://developers.arcgis.com/python/guide/overview-of-the-arcgis-api-for-python/

Atlas. (n.d.). Retrieved April 10, 2023, from https://basic.atlas.gov.tr/

**Bai Y, Hu J, Su J, Liu X, Liu H, He X, Meng S, Mas E, Koshimura S.** (2020).Pyramid Pooling Module-Based Semi-Siamese Network: A Benchmark Model for Assessing Building Damage from xBD Satellite Imagery Datasets. Remote Sensing. 2020; 12(24):4055. https://doi.org/10.3390/rs12244055

**Blackshark-Ai. (n.d.).** GitHub - blackshark-ai/Turkey-Earthquake-2023-Building-Change-Detection: Turkey Earthquake 2023 Building Change Detection. GitHub. https://github.com/blackshark-ai/Turkey-Earthquake-2023-Building-Change-Detection

**B.Ü. Kandilli Rasathanesi Ve Deprem Araştırma Enstitüsü (KRDAE) Bölgesel Deprem-Tsunami İzleme Ve Değerlendirme Merkezi (BDTİM).** (2023). 06 Şubat 2023 Sofalaca- Şehitkamil- Gaziantep; Ekinözükahramanmaraş Ve 20 Şubat 2023 Hatay Depremleri Ön Değerlendirme Raporu. Retrieved 2023, April 10 from http://www.koeri.boun.edu.tr/sismo/2/wp-content/uploads/2023/02/022023_Kahramanmaras-Gaziantep_Hatay_-BDTIM_On_degerlendirme_raporu.pdf

**de Carvalho, O.L. *et al.*** (2022) 'Panoptic segmentation meets Remote Sensing', *Remote Sensing*, 14(4), p. 965. doi:10.3390/rs14040965.

**Cooner, A., Shao, Y., & Campbell, J.** (2016). Detection of urban damage using remote sensing and Machine Learning Algorithms: Revisiting the 2010 Haiti earthquake. *Remote Sensing*, *8*(10), 868. doi:10.3390/rs8100868

**Çetin, Ilgaç, Can, & Çakır.** (2023, February). 6 February 2023 Kahramanmaraş-Pazarcık Mw=7.7 and Elbistan Mw=7.6 Earthquakes Preliminary Evaluation Report (METU/EERC 2023-01). *Middle East Technical University Earthquake Engineering Research Centre*. Retrieved from https://eerc.metu.edu.tr/tr/system/files/documents/DMAM_2023_Kahramanmaras-Pazarcik_ve_Elbistan_Depremleri_Raporu_TR_final.pdf

**Desk, N.N.** (2023) *Stadiums become shelters: Satellite Pics show Turkey earthquake damage*, *NDTV.com*. Available at: https://www.ndtv.com/world-news/stadiums-become-shelters-satellite-pics-show-turkey-earthquake-damage-3766704 (Accessed: 26 May 2023).

**Ding, H.Y., Zhou, Y.J., Ge, Z.X., Taymaz, T., Ghosh, A., Xu, H.Y., Irmak, T.S., Song, X.D.** (2023). High-Resolution Seismicity Imaging and Early Aftershock Migration of the 2023 Kahramanmaraş (SE Türkiye) Mw 7.9 & 7.8 Earthquake Doublet. Earthquake Science, Vol. 36(4), https://doi.org/10.1016/j.eqs.2023.06.002, Received March 2023, Revised May 2023, Accepted June 2023, Published Online July 2023

**Dong, L., & Shan, J.** (2013). A comprehensive review of earthquake-induced building damage detection with remote sensing techniques. ISPRS Journal of Photogrammetry and Remote Sensing, 84, 85–99. doi:10.1016/j.isprsjprs.2013.06.0

**Earthquake Damage in Türkiye.** (2023, January 9). *Nasa Earth Observation*. Retrieved 2023, April 10 from *https://earthobservatory.nasa.gov/images/150949/earthquake-damage-in-turkiye*

**Esri**. (n.d.). Add Coded Value to Domain. ArcGIS Pro Documentation. Retrieved 2023, April 10 from https://pro.arcgis.com/en/pro-app/latest/tool-reference/data-management/add-coded-value-to-domain.htm

**Esri.** (n.d.). An Overview of Attribute Domains. ArcGIS Pro Documentation. Retrieved 2023, April 10 from https://pro.arcgis.com/en/pro-app/latest/help/data/geodatabases/overview/an-overview-of-attribute-domains.htm

**Esri.** (n.d.). Classify Pixels Using Deep Learning (Image Analyst). ArcGIS Pro Documentation. Retrieved 2023, April 10 from https://pro.arcgis.com/en/pro-app/2.7/tool-reference/image-analyst/classify-pixels-using-deep-learning.htm

**Esri.** (n.d.). Export Training Data for Deep Learning. ArcGIS Pro Documentation. Retrieved 2023, April 10 from https://pro.arcgis.com/en/pro-app/latest/tool-reference/image-analyst/export-training-data-for-deep-learning.htm

**Esri.**(n.d.).Deep Learning in ArcGIS Pro. ArcGIS Pro Documentation. Retrieved 2023, April 10 from https://pro.arcgis.com/en/pro-app/3.0/help/analysis/deep-learning/deep-learning-in-arcgis-pro.htm

**Esri.** (n.d.). Label Objects for Deep Learning. ArcGIS Pro Documentation. Retrieved 2023, April 10 from https://pro.arcgis.com/en/pro-app/latest/help/analysis/image-analyst/label-objects-for-deep-learning.htm

**Esri.** (n.d.). Select Features Using Attributes. ArcGIS Pro Documentation. Retrieved 2023, April 10 from https://pro.arcgis.com/en/pro-app/latest/help/mapping/navigation/select-features-using-attributes.htm

**Esri.** (n.d.). Spatial Join (Analysis). ArcGIS Pro Documentation. Retrieved 2023, April 10 from https://pro.arcgis.com/en/pro-app/latest/tool-reference/analysis/spatial-join.htm

***Esri Turkiye DRP.*** (n.d.). https://drp-esriturkiye.hub.arcgis.com/

**European Space Agency (ESA).** (2023). Satellites Support Impact Assessment after Turkey-Syria Earthquakes. Retrieved 2023, April 10 from https://www.esa.int/Applications/Observing_the_Earth/Satellites_support_impact_assessment_after_Tuerkiye_Syria_earthquakes

**Goldberg, D.E., Taymaz, T., Reitman, N.G., Hatem, A.E., Yolsal-Çevikbilen, S., Barnhart, W.D., Irmak, T.S., Wald, D.J., Öcalan, T., Yeck, W.L., Özkan, B., Thompson-Jobe, J.A., Shelly, D.R., Thompson, E.M., DuRoss, C.B., Earle, P.S., Briggs, R.W., Benz, H., Erman, C., Doğan, A.H., Altuntaş, C.** (2023). Rapid Characterization of the February 2023 Kahramanmaraş, Türkiye, Earthquake Sequence. The Seismic Record Vol. 3(2), 156–167, https://doi.org/10.1785/0320230009, Received 2023, March 14, Published Online 23 May 2023.

**Goldberg, D.E., Taymaz, T., Yeck, W.L., Barnhart, W.D., Yolsal- Çevikbilen, S., Irmak, T.S., Öcalan, T., Özkan, B., Erman, C., Doğan, A.H., Altuntaş, C.** (2023). Supporting Data and Models for Characterizing the February 2023 Kahramanmaraş, Türkiye, Earthquake Sequence: U.S. Geological Survey Data Release, USGS–ScienceBase, https://doi.org/10.5066/P9R6DSVZ, Published Online 15 May 2023.

**Gupta, Mishra.** (2022). Post-Disaster Segmentation Using FloodNet. *http://cs231n.stanford.edu/reports/2022/pdfs/21.pdf*. Stanford University CS class CS231n: Deep Learning for Computer Vision. Retrieved from http://cs231n.stanford.edu/reports/2022/pdfs/21.pdf

**Gupta, R., Hosfelt, R., Sajeev, S., Patel, N., Goodman, B., Doshi, J., Heim, E., Choset, H., & Gaston, M.** (2019). XBD: A Dataset for Assessing Building Damage from Satellite Imagery. *ArXiv*. /abs/1911.09296

**H., Erman, C., Doğan, A.H., Altuntaş, C.** (2023). Rapid Characterization of the February 2023 Kahramanmaraş, Türkiye, Earthquake Sequence. The Seismic Record Vol. 3(2), 156–

167, https://doi.org/10.1785/0320230009, Received 2023, March 14, Published Online 23 May 2023.

**Heidler, K. *et al.*** (2022). ‘Hed-unet: Combined segmentation and edge detection for monitoring the Antarctic coastline’, *IEEE Transactions on Geoscience and Remote Sensing*, 60, pp. 1–14. doi:10.1109/tgrs.2021.3064606.

**HOT Export Tool. (n.d.).** Retrieved 2023, May 10, from https://export.hotosm.org/en/v3/

**HOT’s Response to the Turkey & Syria Earthquake.** (2023, February 22). *Humanitarian OpenStreetMap Team*. https://www.hotosm.org/projects/join-the-turkey-and-syria-earthquake-response

**ITU CSCRS.** (2023, February 8). Deprem Bölgesine Ait Yüksek Çözünürlüklü Uydu Görüntüleri Web Harita Servisi Olarak Yayınlandı. *ITU CSCRS*. Retrieved from https://web.cscrs.itu.edu.tr/ deprem-bolgesine-ait-yuksek-cozunurluklu-uydu-goruntuleri-web-harita-servisi-olarak-yayinlandi

**Joyce, K. E., Belliss, S. E., Samsonov, S. V., McNeill, S. J., & Glassey, P. J.** (2009). A review of the status of satellite remote sensing and image processing techniques for mapping natural hazards and disasters. Progress in Physical Geography: Earth and Environment, 33(2), 183–207. doi:10.1177/0309133309339563

**Kandilli Observatory and Earthquake Research Institute (KOERI).**(2023). Şehitkamil (Gaziantep) Depremi - 6 Şubat 2023, Mw=7.4. Boğaziçi Üniversitesi Kandilli Rasathanesi ve Deprem Araştırma Enstitüsü. http://www.koeri.boun.edu.tr/sismo/2/06-subat-2023-ml7-4-sofalaca-sehitkamil-gaziantep-depremi/

**Kim, D., Won, J., Lee, E., Park, K. R., Kim, J., Park, S., Yang, H., & Cha, M.** (2022). Disaster assessment using computer vision and satellite imagery: Applications in detecting water-related building damages. Frontiers in Environmental Science, 10. https://doi.org/10.3389/fenvs.2022.969758

**Kürçer, Elmacı, Özdemir, Güven, Avcu, & Özalp.** (2023, February). 06 Şubat 2023 Pazarcık (Kahramanmaraş) Depremi (Mw 7,7) Saha Gözlem Raporları Serisi 1- Amanos Segmenti (Report No: 14121). *Department of Geological Studies*. Turkey: General Directorate Of Mining Research And Exploration. Retrieved from https://www.mta.gov.tr/files/img/popup/06022023_pazarc%C4%B1k_depremi_saha_gozlem_raporu_1_amanos_segmenti.pdf

Living Atlas of the World. (n.d.). Esri Living Atlas of the World. Retrieved 2023, April 13 from https://livingatlas.arcgis.com/en/browse/#d=2&type=tool

**Melgar, D., Taymaz, T., Ganas, A., Crowell, B., Öcalan, T., Kahraman, M., Tsironi, V., Yolsal-Çevikbilen, S., Valkaniotis, S., Irmak, T. S., Eken, T., Erman, C., Özkan, B., Dogan, A. H., & Altuntaş, C.** (2023). Sub- and super-shear ruptures during the 2023 Mw 7.8 and Mw 7.6 earthquake doublet in SE Türkiye. Seismica, 2(3). https://doi.org/10.26443/seismica.v2i3.387

**Moradi, M. and Shah-Hosseini, R.** (2020). ‘Earthquake damage assessment based on Deep Learning method using VHR images’, *IECG 2020* [Preprint]. doi:10.3390/iecg2020-08545.

**NASA Earth Observatory.** (2023, February 24). Dark nights in Antakya. Retrieved from https://earthobservatory.nasa.gov/images/151029/dark-nights-in-antakya

**Okuwaki, R., Yagi, Y., Taymaz, T., Hicks, S.P.** (2023). Multi-Scale Rupture Growth with Alternating Directions in a Complex Fault Network During the 2023 South-Eastern Türkiye and Syria Earthquake Doublet. Geophysical Research Letters, Vol. 50(12), e2023GL103480, https://doi.org/10.1029/2023GL103480, Received 3 March 2023, Revised 6 May 2023, Accepted 1 June 2023, Published Online 21 June 2023.

**Paal, Stephanie & Brilakis, Ioannis & Desroches, Reginald.** (2014). Automated computer vision-based detection of exposed transverse reinforcement for post-earthquake safety assessments. Conference: World Conference of Structural Control and Monitoring, Barcelona, Spain, July 2014

**Presidency of The Republic of Turkey Presidency of Strategy and Budget.** (2023, March). 2023 Kahramanmaraş And Hatay Earthquakes Report. *Presidency of the Republic of Turkey Presidency of Strategy and Budget*. Turkey. Retrieved from https://www.sbb.gov.tr/wp-content/uploads/2023/03/2023-Kahramanmaras-ve-Hatay-Depremleri-Raporu.pdf

**Press Bulletin-36** about the Earthquake in Kahramanmaraş. (2023, March 1). Retrieved from https://en.afad.gov.tr/press-bulletin-36-about-the-earthquake-in-kahramanmaras

**Prime Ministry Disaster And Emergency Management Authority (AFAD)**.(2023). February 06, 2023 Pazarcık (Kahramanmaras) Mw 7.7 Elbistan (Kahramanmaraş) Mw 7.6 Earthquakes Prelimiınary Evaluatıon Report, 2023

**Qing, Y., Ming, D., Wen, Q., Weng, Q., Xu, L., Chen, Y., Zhang, Y., & Zeng, B.** (2022). Operational earthquake-induced building damage assessment using CNN-based direct remote sensing change detection on superpixel level. International Journal of Applied Earth Observation and Geoinformation, 112, 102899. ISSN 1569-8432. DOI: 10.1016/j.jag.2022.102899

**Rahnemoonfar, M. *et al.*** (2021) 'FloodNet: A high resolution aerial imagery dataset for post flood scene understanding', *IEEE Access*, 9, pp. 89644–89654. doi:10.1109/access.2021.3090981.

**Rao, A., Jung, J., Silva, V., Molinario, G., & Yun, S.-H.** (2023). Earthquake building damage detection based on synthetic-aperture-radar imagery and machine learning. Natural Hazards and Earth System Sciences, 23(2), 789–807. doi:10.5194/nhess-23-789-2023

**Rathje, Ellen & Franke, Kevin.** (2016). Remote sensing for geotechnical earthquake reconnaissance. Soil Dynamics and Earthquake Engineering. 91. 10.1016/j.soildyn.2016.09.016**.**

**Rodkin, M.V., Irmak, T.S., Taymaz, T.** (2023). Doublet of Turkish Earthquakes on February 6, 2023: Questions and Lessons (Дуплет турецких землетрясений 6 февраля 2023 года: вопросы и уроки), PRIRODA (природа) (Nature), Vol. 1293(5), 13-21, in Russian, https://doi.org/10.7868/S0032874X23050022, The Russian Academy of Sciences (RAS)-ИССЛЕДОВАНИЯ, ОБЗОРЫ: ГЕОФИЗИКА, Published Online 28 May 2023**.**

**Šarić, J., Oršić, M. and Šegvić, S**. (2023) 'Panoptic SWIFTNET: Pyramidal fusion for real-time panoptic segmentation', *Remote Sensing*, 15(8), p. 1968. doi:10.3390/rs15081968.

**Singh, R.** (2021, December 10). Building footprint extraction and damage classification. Medium. https://medium.com/geoai/building-footprint-extraction-and-damage-classification-8a5458759332

*Stadiums become shelters: Satellite pics show Turkey earthquake damage*. (2023). NDTV.com. Retrieved 2023, April 10 from https://www.ndtv.com/world-news/stadiums-become-shelters-satellite-pics-show-turkey-earthquake-damage-3766704

**Takhtkeshha, N., Mohammadzadeh, A., & Salehi, B.** (2022). A rapid self-supervised deep-learning-based method for post-earthquake damage detection using UAV data (case study: Sarpol-e zahab, Iran). *Remote Sensing*, *15*(1), 123. doi:10.3390/rs15010123

**Tanırcan, G., Kaya Eken, T.** (2023). (rep.). 6 Şubat 2023 Mw7.7 Gaziantep 6 Şubat 2023 Mw.7.6 Kahramanmaraş 20 Şubat 2023 Mw6.4 Hatay Depremleri Ön Değerlendirme Raporu. Kandilli Observatory and Earthquake Research Institute. Retrieved from http://www.koeri.boun.edu.tr/new/tr/duyuru/06-%C5%9Fubat-2023-gaziantep-kahramanmara%C5%9F-ve-20-%C5%9Fubat-2023-hatay-depremleri-%C3%B6n-de%C4%9Ferlendirme

**Tozer, B., D. T. Sandwell, W. H. Smith, C. Olson, J. R. Beale, and P. Wessel** (2019). Global bathymetry and topography at 15 arc sec: SRTM15+, Earth Space Sci. 6, no. 10, 1847–1864, doi: 10.1029/ 2019EA000658.

**Turkey and Syria Earthquake 2023.** (2023, February 8). Retrieved May 15, 2023, from https://www.maxar.com/open-data/turkey-earthquake-2023

**Turunçtur, B., Eken, T., Chen, Y., Taymaz, T., Houseman, G.A., Saygin, E.** (2023). Crustal Velocity Images of Northwestern Türkiye Along the North Anatolian Fault Zone from Transdimensional Bayesian Ambient Seismic Noise Tomography. Geophysical Journal International, Vol. 234(1), 636–649, https://doi.org/10.1093/gji/ggad082, Received 08 February 2023, Accepted 19 February 2023, Published Online 21 February 2023.

**Wang, Z., Zhang, W., Taymaz, T., He, Z., Xu, T., Zhang, Z.** (2023). Dynamic Rupture Process of the 2023 Mw 7.8 Kahramanmaraş Earthquake (SE Türkiye): Variable Rupture Speed and Implications for Seismic Hazard. Geophysical Research Letters, Vol. 50(15), e2023GL104787. https://doi.org/10.1029/2023GL104787, Received 1 June 2023, Revised 17 July 2023, Accepted 24 July 2023, Published Online 3 August 2023.

**Wen, H., Zhou, X., Zhang, C., Liao, M., & Xiao, J.** (2023). Different-classification-scheme-based Machine Learning Model of Building Seismic Resilience Assessment in a mountainous region. Remote Sensing, 15(9), 2226. doi:10.3390/rs15092226

**Wu, F., Xie, J.J,, An, Z., Lyu, C.H., Taymaz, T., Irmak, T.S., Li, X.J., Wen, Z.P., Zhou, B.F.** (2023). Pulse-Like Ground Motion Observed During the 6 February 2023 Mw 7.8 Pazarcık Earthquake (Kahramanmaraş, SE Türkiye). Earthquake Science, Vol. 36(4), 328-339, https://doi.org/10.1016/j.eqs.2023.05.005, Received 20 March 2023, Revised 3 April 2023, Accepted 7 April 2023, Published Online 5 July 2023.

**Xu, C., Zhang, Y., Hua, S., Zhang, X., Xu, L., Chen, Y., Taymaz, T.** (2023). Rapid Source Inversions of the 2023 SE Türkiye Earthquakes with Teleseismic and Strong-Motion Data, Earthquake Science Vol. 36(4), 316–327, https://doi.org/10.1016/j.eqs.2023.05.004, Received 14 March 2023, Revised 5 April 2023, Accepted 9 April 2023, Published Online 5 July 2023.

**Yaşar, Arzuman, Kalkan Ertan, Yavuz, Mehmetoğlu, Duran, & Tut.** (2023, February). *Gaziantep And Kahramanmaraş Earthquakes*. Turkey: Istanbul Metropolitan Municipality Department Of Earthquake Risk Management and Urban Improvement Earthquake And Soil Investigation Branch Directorate Seismological Group. Retrieved from https://8luvomezzzsk.merlincdn.net/wp-content/uploads/2023/02/ibb_gaziantep-kahramanmaras_deprem_10022023-1600.pdf

**Youngjun Choe, Valentina Staneva, Tessa Schneider, Andrew Escay, Christopher Haberland, Sean Chen.** (2018). Benchmark Dataset for Automatic Damaged Building Detection from Post-Hurricane Remotely Sensed Imagery. IEEE Dataport. https://dx.doi.org/10.21227/1s3n-f891

**Yürür.** (2023). *6 Şubat 2023 Gaziantep depremi hakkında bilgiler*. Turkey: Hacettepe University, Department of Geological Engineering. Retrieved 2023, April 10 from https://jeomuh.hacettepe.edu.tr/2023%20duyuru/6%20%C5%9Eubat%202023%20depremi%20bilgi%20notu_MT%20Y%C3%BCr%C3%BCr.pdf

**Url-1** < *http://cs231n.stanford.edu/reports/2022/pdfs/21.pdf* >, date retrieved 20.05.2023.

**Url-2** < *http://www.koeri.boun.edu.tr/scripts/lst9.asp* >, date retrieved 20.05.2023.

**Url3** <*https://deprem.afad.gov.tr/earthquake-reports* >, date retrieved 20.05.2023.

**Url-4** < *https://www.mta.gov.tr/v3.0/sayfalar/bilgi-merkezi/deprem/pdf/Deprem_Bilgi_Notu_2023-02-06_Pazarcik-Kahramanmaras_2.pdf* >, date retrieved 20.05.2023.

**Url-5** < *https://basic.atlas.gov.tr/?_appToken=&metadataId* >, date retrieved 20.05.2023.

**Url-6**< *https://www.eorc.jaxa.jp/ALOS/jp/library/disaster/dis_pal2_turkey_earthquake_20230209_j.htm*>, date retrieved 20.05.2023.

**Url-7**< *https://www.capellaspace.com/gallery/2023-islahiye-turkey-earthquake/*>, date retrieved 20.05.2023.

**Url-8**< *https://sentinel-asia.org/EO/2023/article20230206TR.html*>, date retrieved 20.05.2023.

**Url-9**< *https://aria-share.jpl.nasa.gov/20230206_Turkey_EQ/*>, date retrieved 20.05.2023.

**Url-10**< *https://maps.disasters.nasa.gov/arcgis/apps/MinimalGallery/index.html?appid=cb116456d682456abc38b90d96a72713* >, date retrieved 20.05.2023.

**Url-11**< *https://www.tusaga-aktif.gov.tr/Web/DepremVerileri.aspx* >, date retrieved 20.05.2023.

**Url-12**< *https://tasks.hotosm.org/projects/14235* >, date retrieved 20.05.2023.

**Url-13**< *http://www.koeri.boun.edu.tr/scripts/lst9.asp* >, date retrieved 20.05.2023.

**Url-14**< *https://deprem.afad.gov.tr/map* >, date retrieved 20.05.2023.

**Url-15**< *https://earthquake.usgs.gov/earthquakes/map/?extent=33.30299,23.73047&extent=43.90581,48.33984* >, date retrieved 20.05.2023.

**Url-16** < *https://geomatik.beun.edu.tr/deprem-calismalarimiz.html* >, date retrieved 20.05.2023.

**Url-17**< *https://www.gsi.go.jp/cais/topic20230206-e_Turkey.html* >, date retrieved 20.05.2023.

**Url-18**< *https://drive.google.com/drive/folders/1Qyp5V_CzG5kSgeAaQQ0VqwkEVntPB0NK* >, date retrieved 20.05.2023.

**Url-19**< *https://atlas.harita.gov.tr/#5/39/35*>, date retrieved 20.05.2023.

**Url-20**< *https://openaerialmap.org/*>, date retrieved 20.05.2023.

**Url-21** < *https://spacenet.ai/*>, date retrieved 20.05.2023.

**Url-22** < *https://tadas.afad.gov.tr/*>, date retrieved 20.05.2023.

**Url-23** < *https://www.openstreetmap.org/#map=7/39.031/35.252/*>, date retrieved 20.05.2023.

**Url-24** < *https://experience.arcgis.com/experience/47802940cc7b42b5b800baf979bcaffb/*> ,date retrieved 10.08.2023

**Url-25**< *https://hasar.6subatdepremi.org/*>, date retrieved 10.08.2023

# APPENDIX

## APPENDIX A: ArcGIS Pro Deep Learning Tutorial

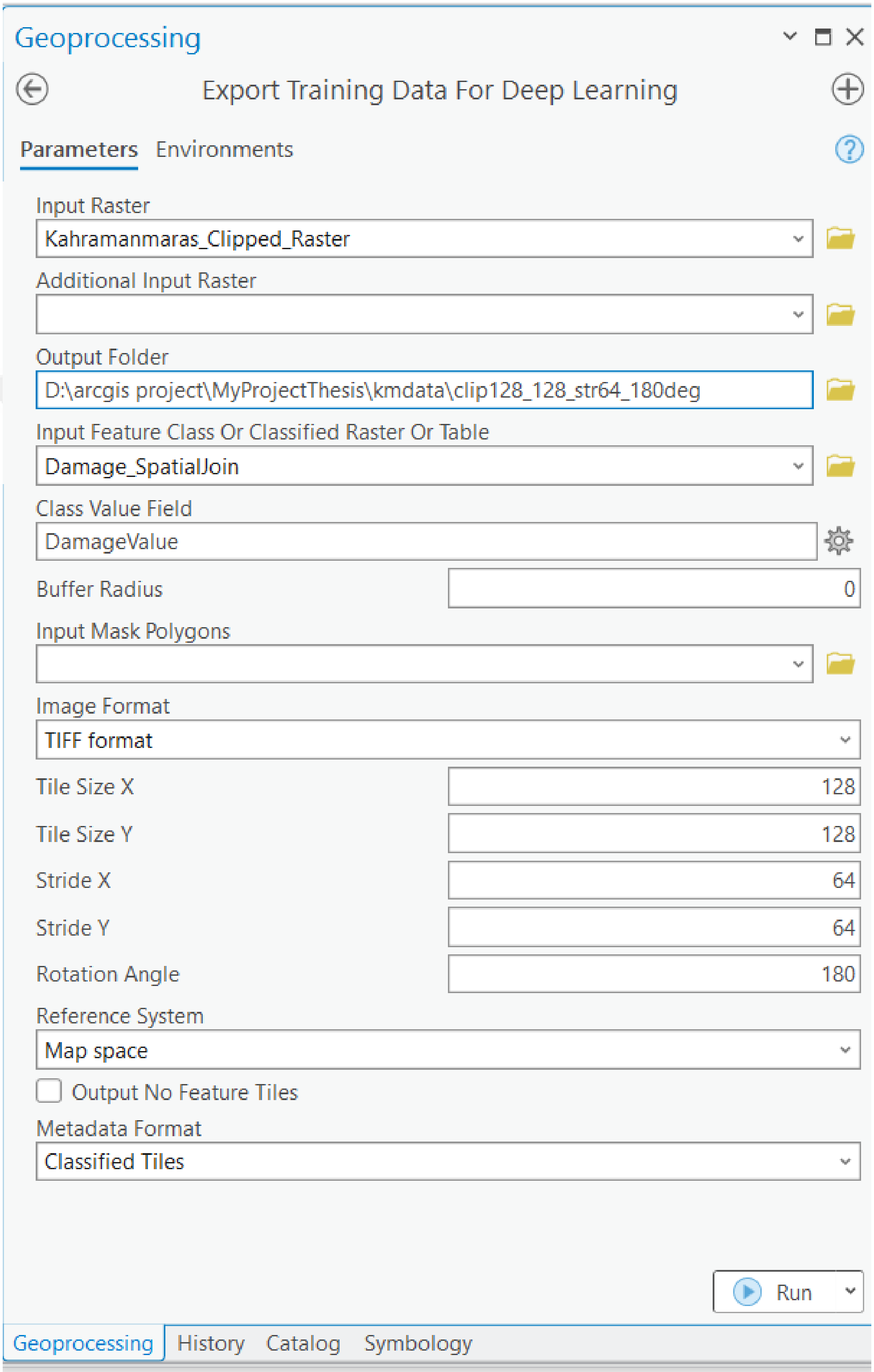

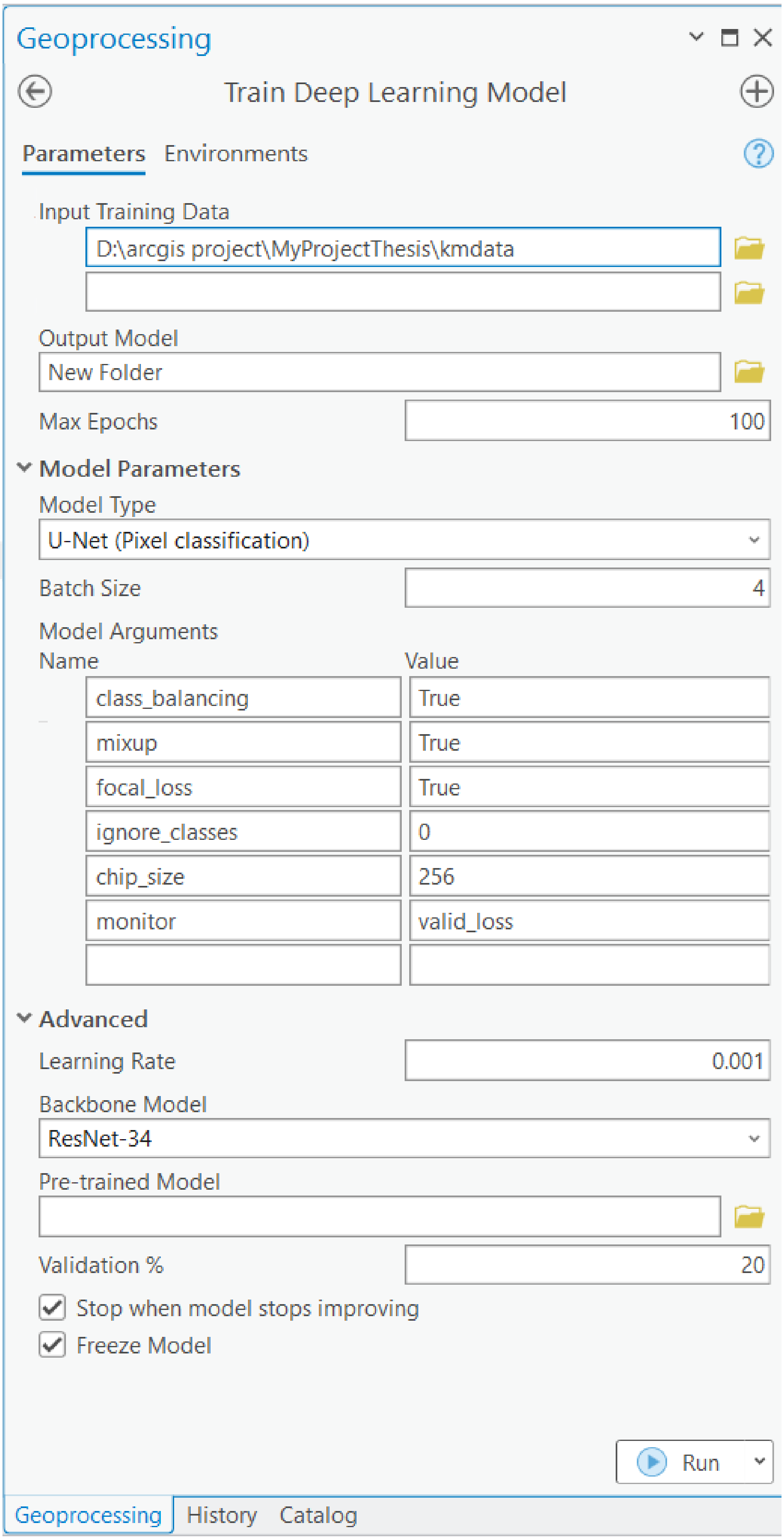
Geoprocessing
Train Deep Learning Model
Parameters
Environments
Input Training Data
D:\arcgis project\MyProjectThesis\kmdata
Output Model
New Folder
Max Epochs
100
Model Parameters
Model Type
U-Net (Pixel classification)
Batch Size
4
Model Arguments
Name
Value
class_balancing
True
mixup
True
focal_loss
True
ignore_classes
0
chip_size
256
monitor
valid_loss
Advanced
Learning Rate
0.001
Backbone Model
ResNet-34
Pre-trained Model
Validation %
20
Stop when model stops improving
Freeze Model
Run
Geoprocessing
History
Catalog

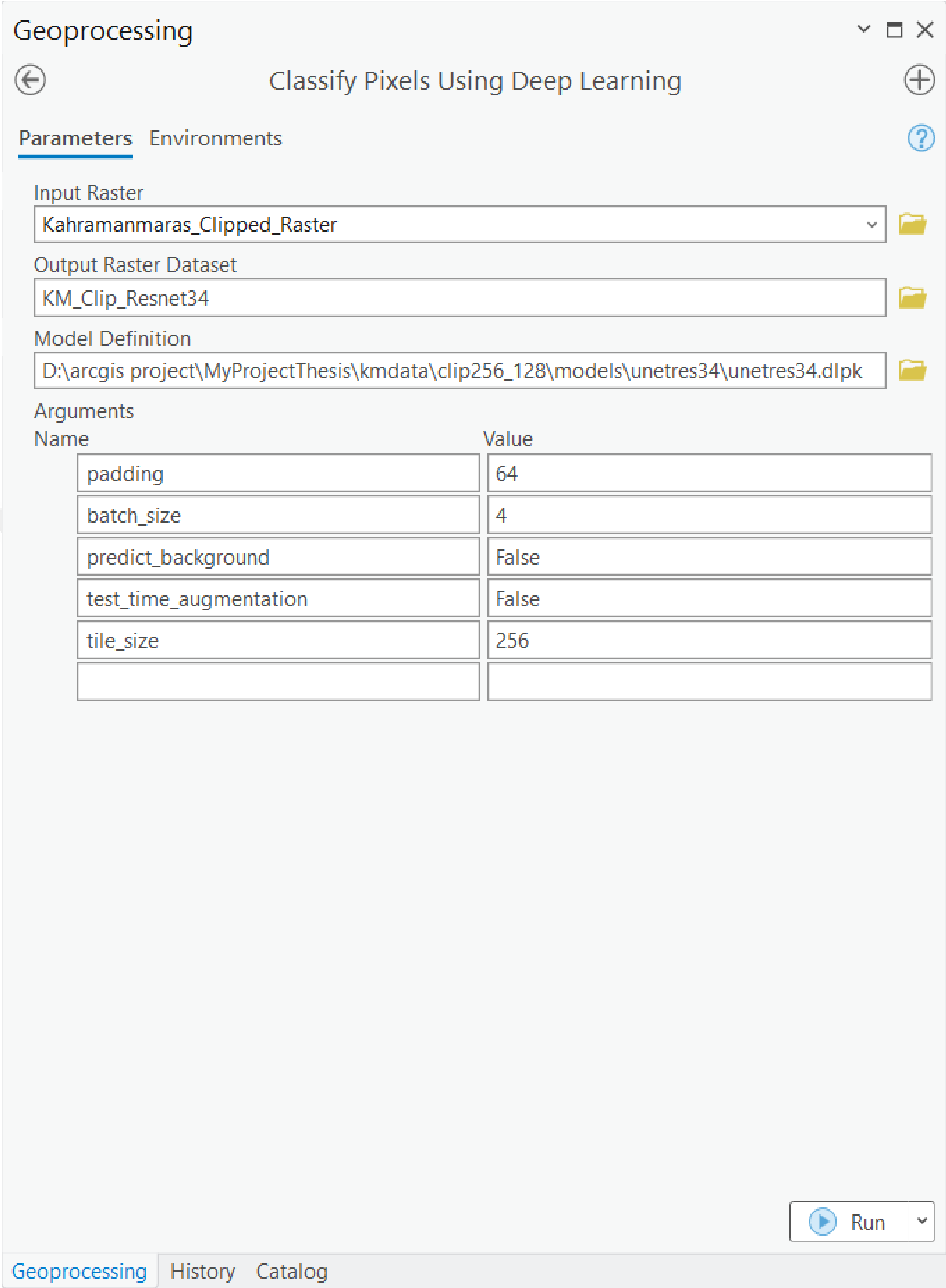
Geoprocessing
Classify Pixels Using Deep Learning
Parameters
Environments
Input Raster
Kahramanmaras_Clipped_Raster
Output Raster Dataset
KM_Clip_Resnet34
Model Definition
D:\arcgis project\MyProjectThesis\kmdata\clip256_128\models\unetres34\unetres34.dlpk
Arguments
Name
Value
padding
64
batch_size
4
predict_background
False
test_time_augmentation
False
tile_size
256
Run
Geoprocessing
History
Catalog

## APPENDIX B: ArcGIS Pro Train Deep Learning Model (Image Analyst) Outputs

**UnetClassifier**

**Backbone:** resnet34

**Learning Rate:** 1.0965e-04

**Training and Validation loss**

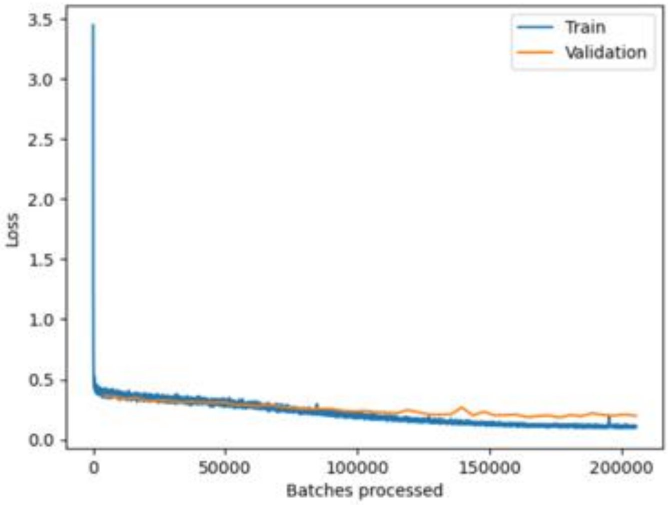


**Analysis of the model**

**Per class metrics:**

| | NoData | Col | HevDam | Dem | Slig |
|---|---|---|---|---|---|
| **precision** | 0.960956 | 0.775086 | 0.754261 | 0.751958 | 0.764346 |
| **recall** | 0.976303 | 0.554103 | 0.644462 | 0.535034 | 0.686786 |
| **f1** | 0.968569 | 0.646225 | 0.695052 | 0.625214 | 0.723493 |

Ground Truth / Predictions

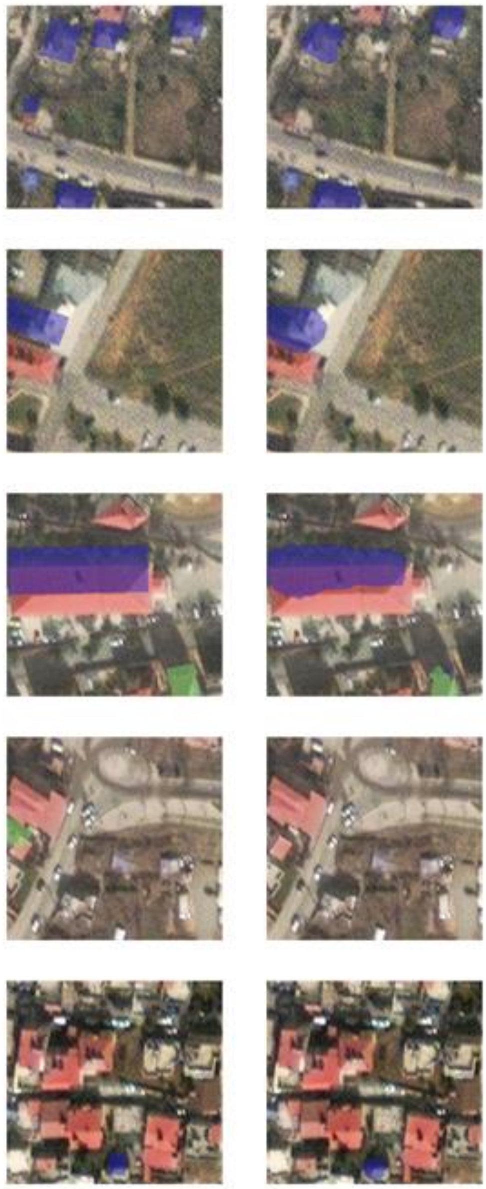

**DeepLab**

**Backbone:** resnet34

**Learning Rate:** 2.5119e-03

**Training and Validation loss**

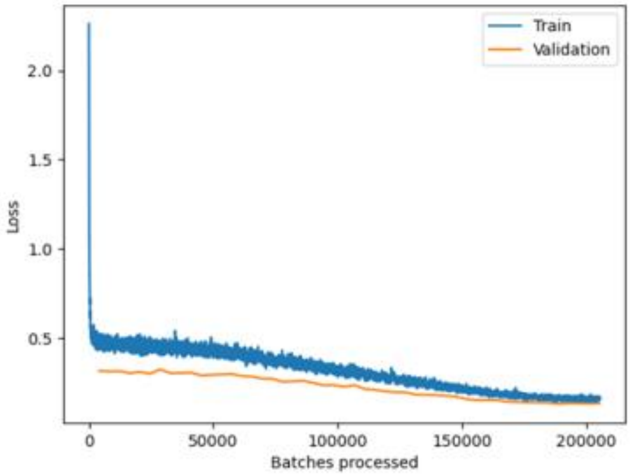


**Analysis of the model**

**Per class metrics:**

| | NoData | Col | HevDam | Dem | Slig |
|---|---|---|---|---|---|
| **precision** | 0.969282 | 0.869145 | 0.850190 | 0.863835 | 0.815068 |
| **recall** | 0.980647 | 0.639911 | 0.711707 | 0.678655 | 0.770059 |
| **f1** | 0.974932 | 0.737117 | 0.774810 | 0.760129 | 0.791925 |

Ground Truth / Predictions

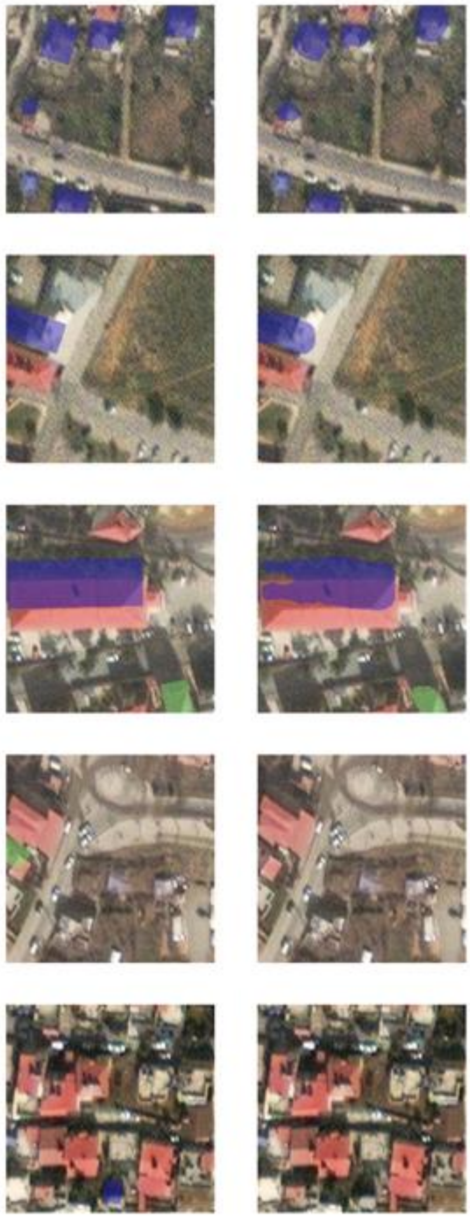

**DeepLab**

**Backbone:** timm:gluon_resnext50_32x4d

**Learning Rate:** 1.7378e-03

**Training and Validation loss**

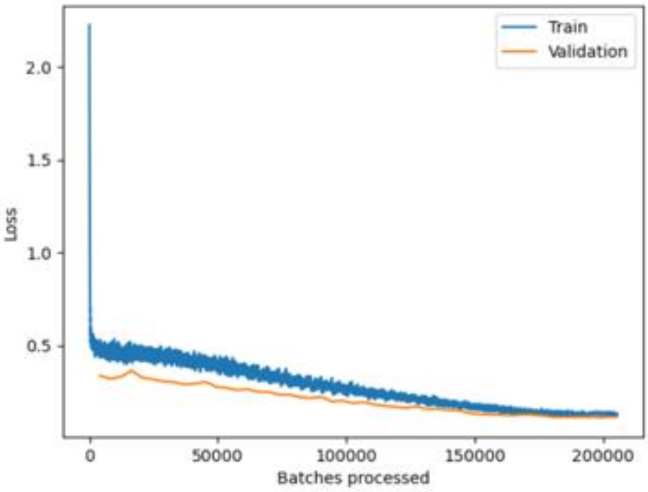


**Analysis of the model**

**Per class metrics:**

| | NoData | Col | HevDam | Dem | Slig |
|---|---|---|---|---|---|
| **precision** | 0.974668 | 0.900797 | 0.868658 | 0.890884 | 0.863037 |
| **recall** | 0.984745 | 0.706823 | 0.796001 | 0.780220 | 0.802756 |
| **f1** | 0.979681 | 0.792108 | 0.830744 | 0.831888 | 0.831806 |

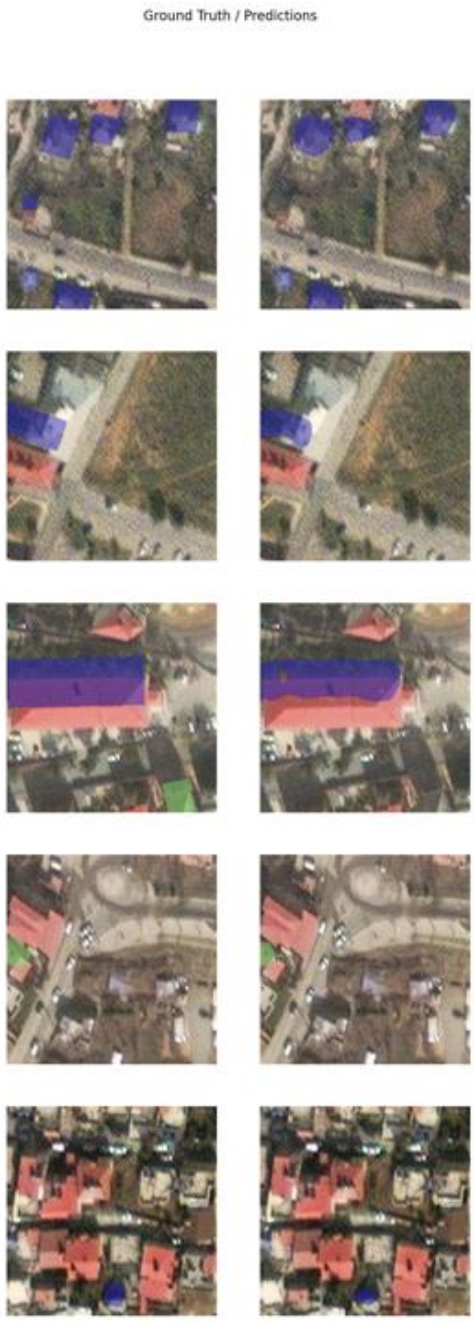

**DeepLab**

**Backbone:** resnet50

**Learning Rate:** 2.0893e-03

**Training and Validation loss**

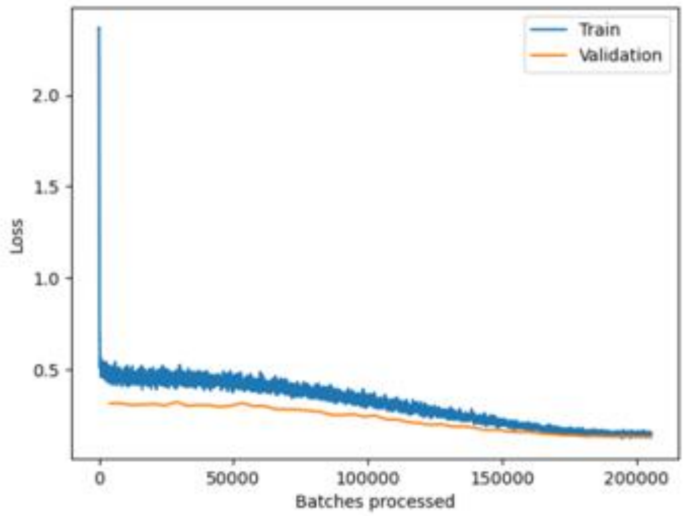


**Analysis of the model**

**Per class metrics:**

| | NoData | Col | HevDam | Dem | Slig |
|---|---|---|---|---|---|
| **precision** | 0.968606 | 0.861367 | 0.853891 | 0.862770 | 0.826567 |
| **recall** | 0.981993 | 0.646865 | 0.719189 | 0.715695 | 0.758489 |
| **f1** | 0.975254 | 0.738863 | 0.780773 | 0.782381 | 0.791066 |

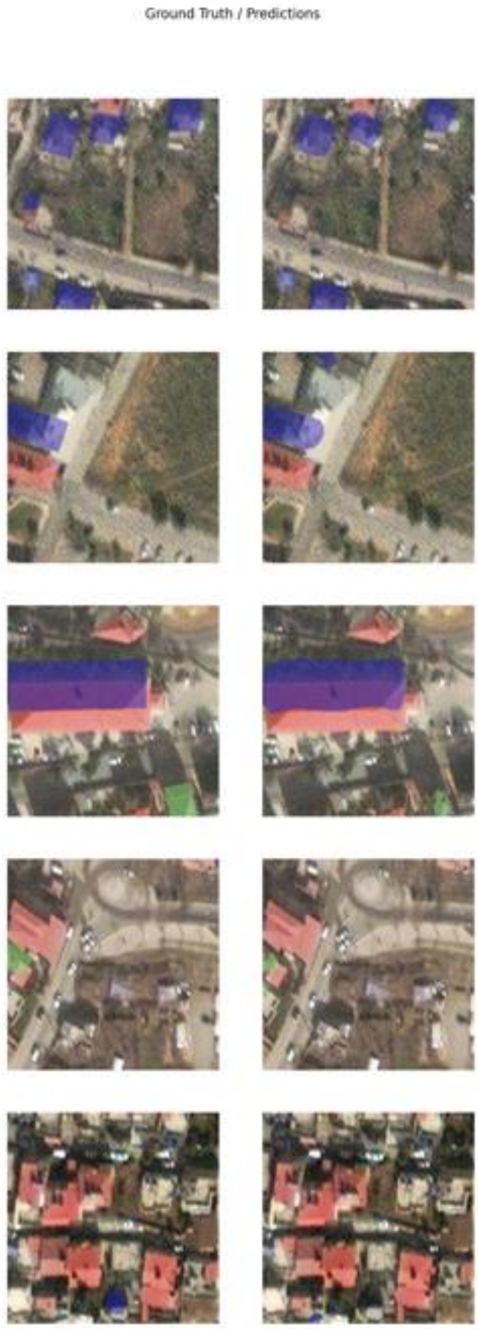

**DeepLab**

**Backbone:** densenet121

**Learning Rate:** 1.4454e-03

**Training and Validation loss**

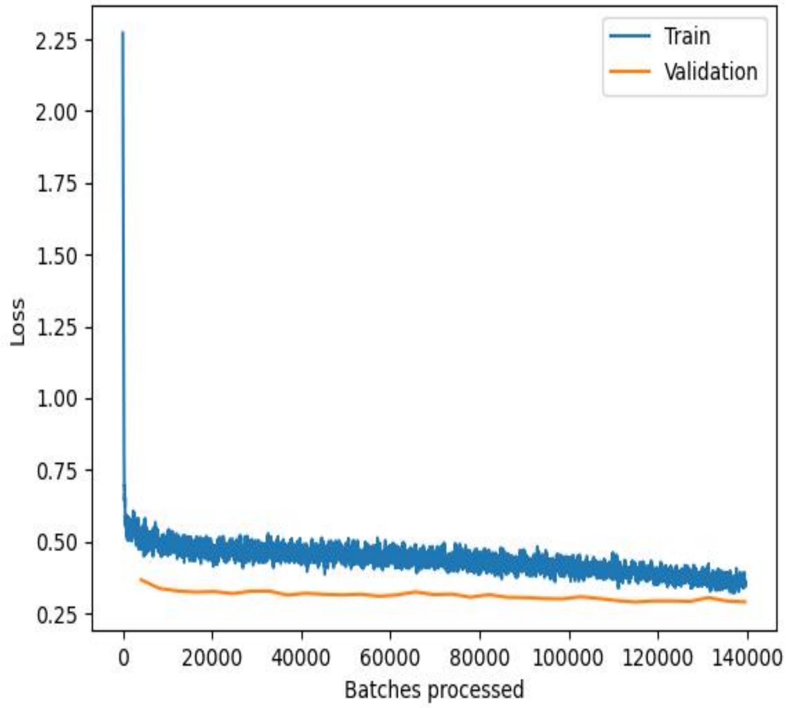


**Analysis of the model**

**Per class metrics:**

| | NoData | Col | HevDam | Dem | Slig |
|---|---|---|---|---|---|
| **precision** | 0.912974 | 0.673794 | 0.561782 | 0.524802 | 0.604091 |
| **recall** | 0.982298 | 0.113609 | 0.174174 | 0.096316 | 0.277877 |
| **f1** | 0.946368 | 0.194434 | 0.265907 | 0.162761 | 0.380656 |

**PSPNetClassifier**

**Backbone:** resnet34

**Learning Rate:** 1.0000e-03

**Training and Validation loss**

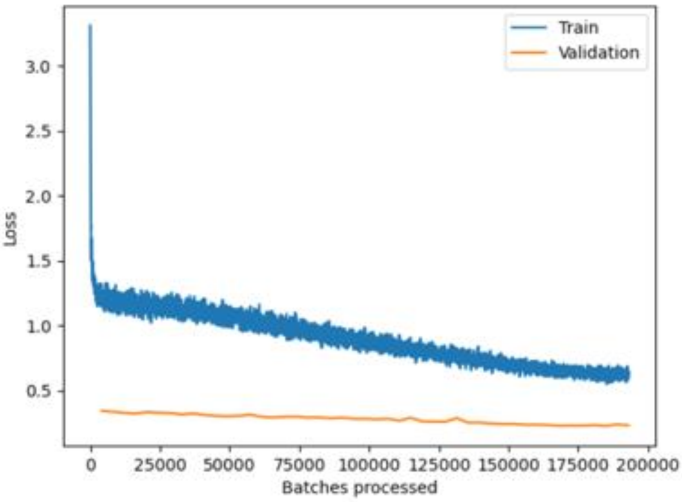


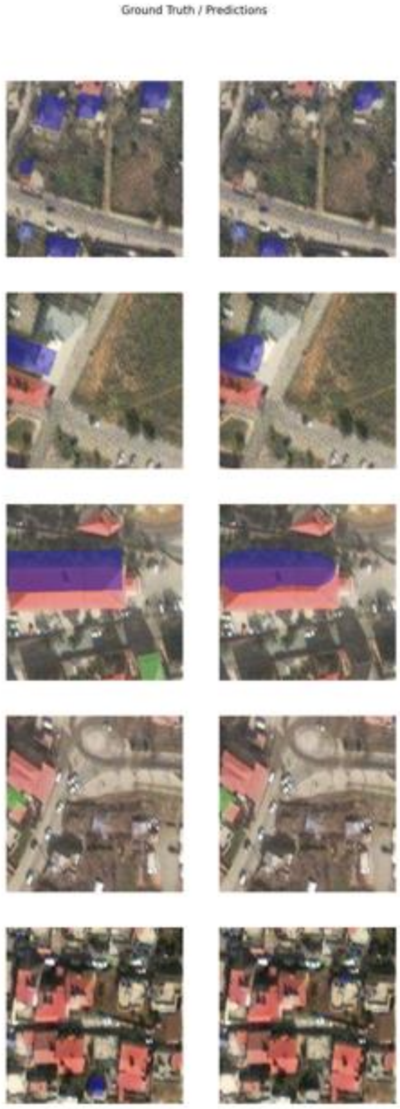


**Analysis of the model**

**Per class metrics:**

| | NoData | Col | HevDam | Dem | Slig |
|---|---|---|---|---|---|
| **precision** | 0.941975 | 0.710384 | 0.716778 | 0.769645 | 0.716280 |
| **recall** | 0.977214 | 0.381793 | 0.472978 | 0.348349 | 0.532885 |
| **f1** | 0.959271 | 0.496659 | 0.569899 | 0.479618 | 0.611120 |

**PSPNetClassifier**

**Backbone:** resnet50

**Learning Rate:** 6.9183e-04

**Training and Validation loss**

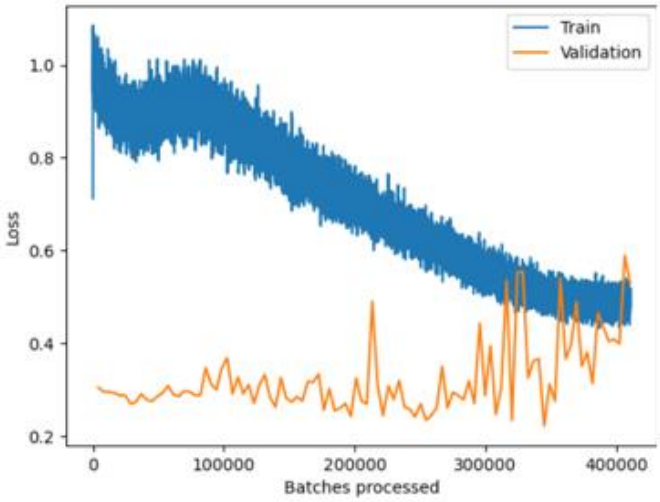


**Analysis of the model**

**Per class metrics:**

| | NoData | Col | HevDam | Dem | Slig |
|---|---|---|---|---|---|
| **precision** | 0.955750 | 0.865830 | 0.807281 | 0.825818 | 0.797121 |
| **recall** | 0.981034 | 0.483041 | 0.639030 | 0.590651 | 0.647038 |
| **f1** | 0.968227 | 0.620121 | 0.713369 | 0.688713 | 0.714281 |

Ground Truth / Predictions

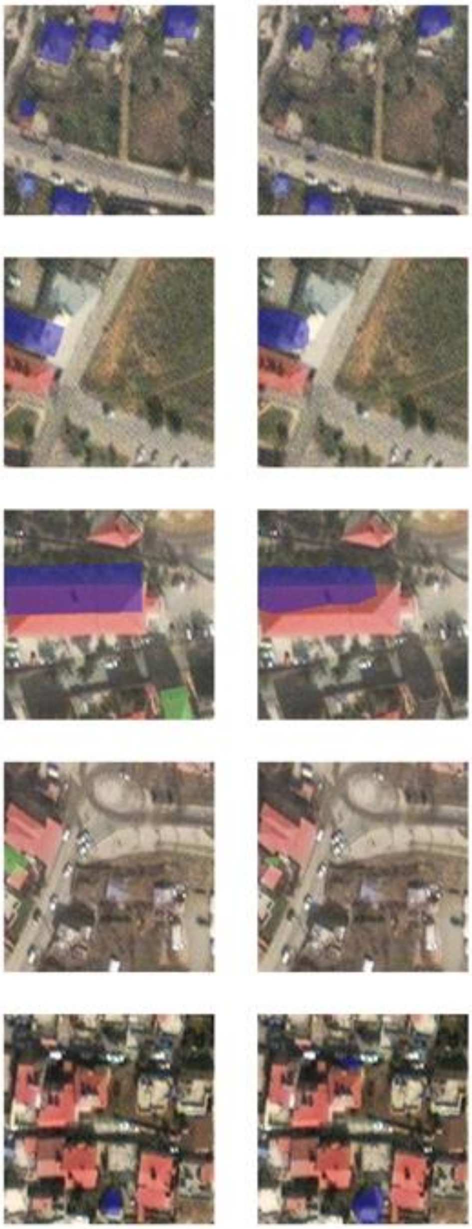

## APPENDIX C: Inference Results- Kahramanmaraş Disctrict Example Imageries


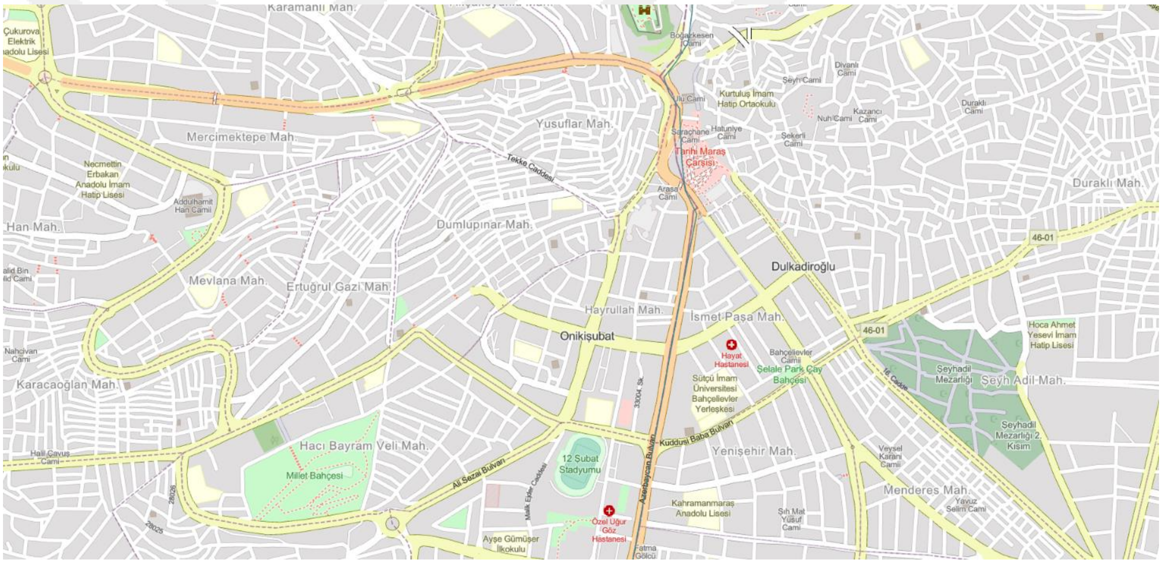


## Damage Assessed Building Footprints

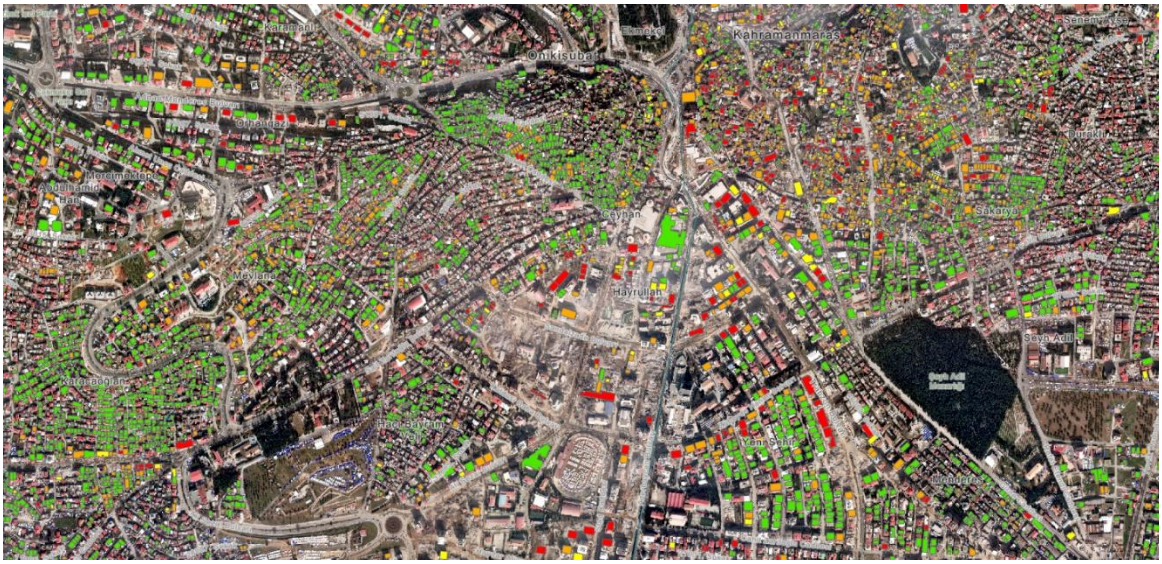

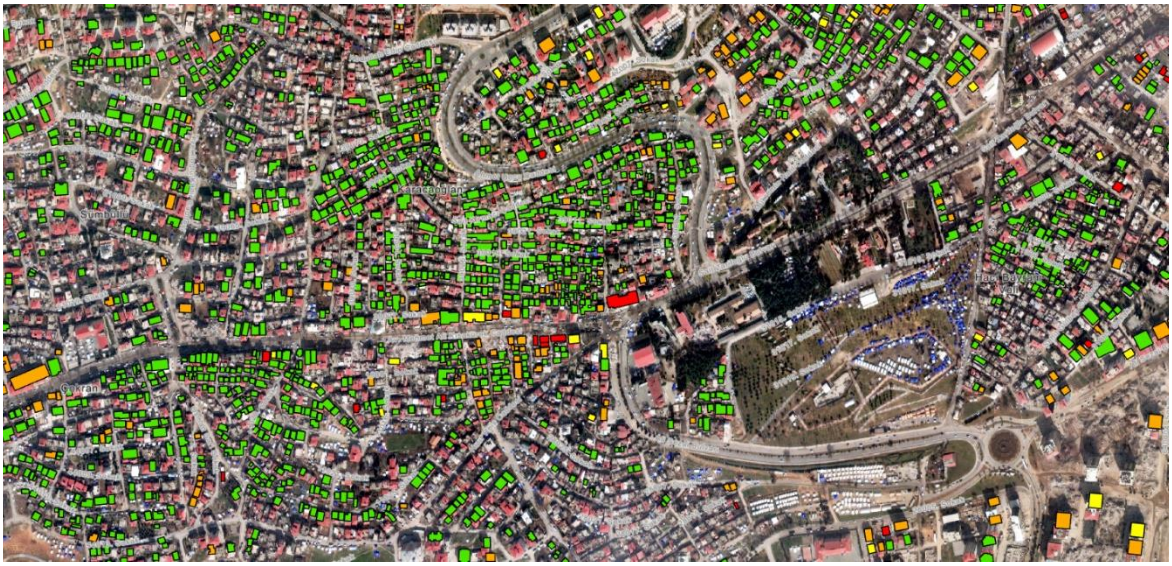

The results of overlapping the model inferences with the damage labelled footprints are:

Unet ResNet34

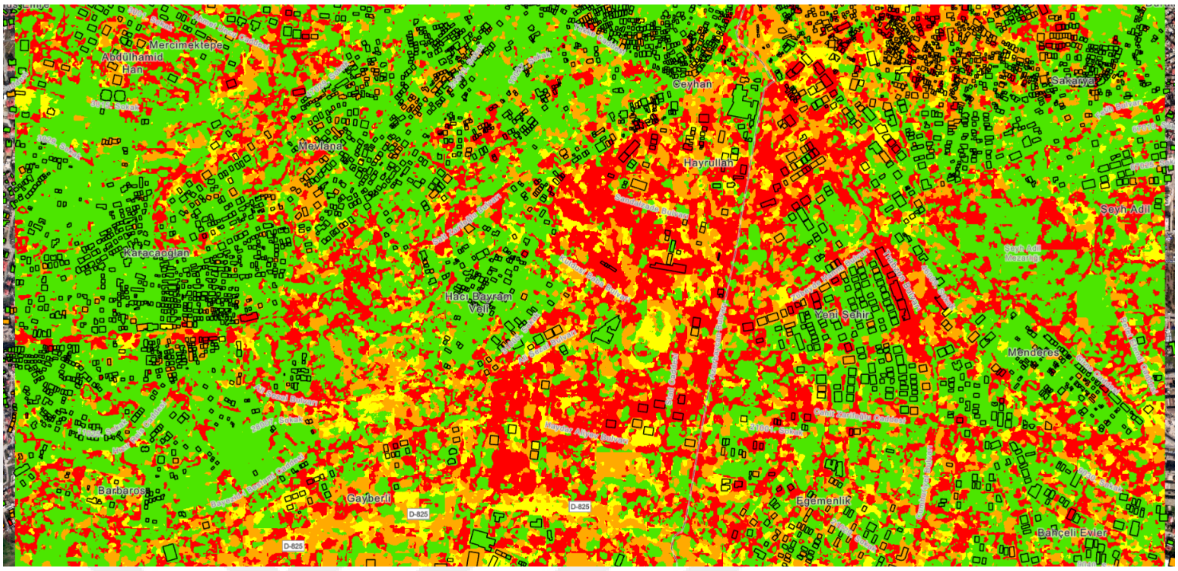

DeepLabV3 ResNet34

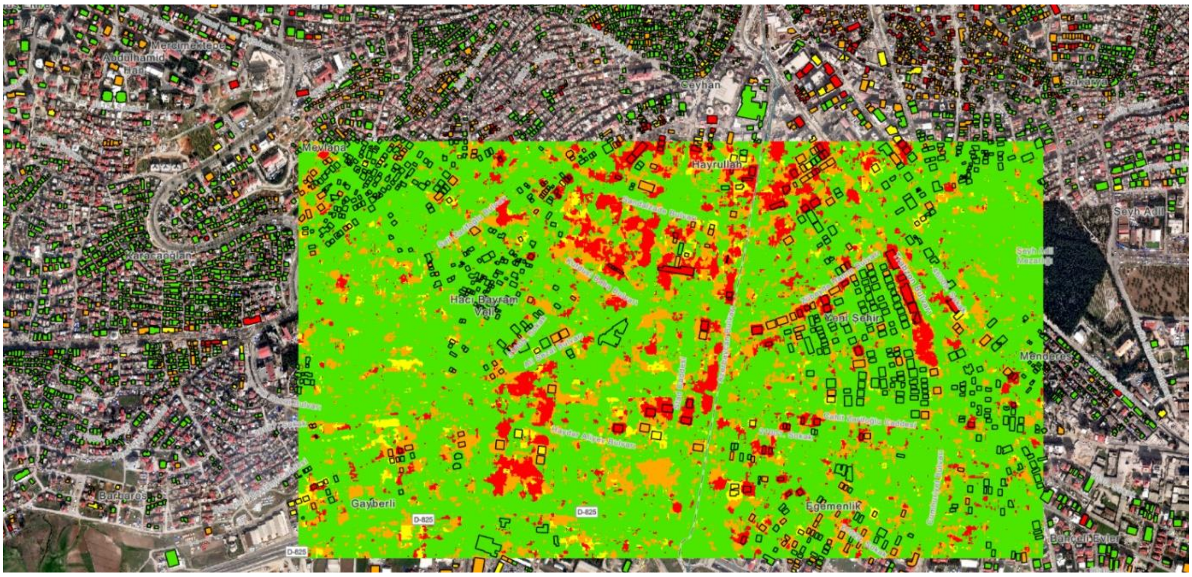

DeepLabV3 ResNet50

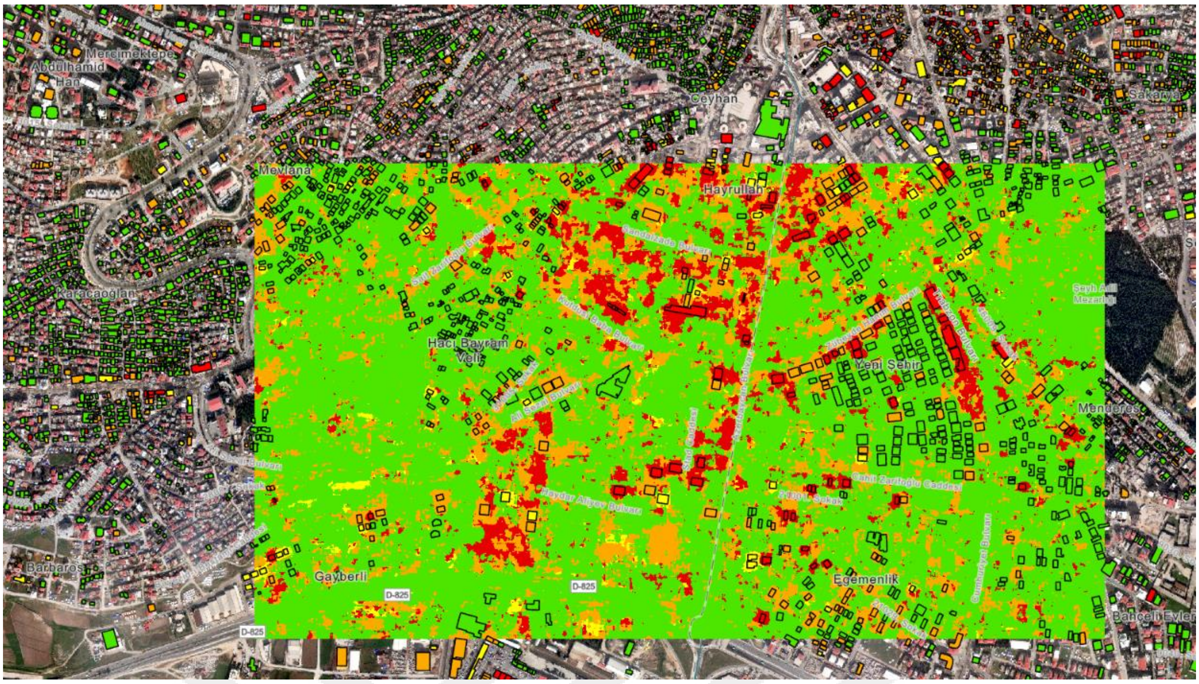


DeepLabV3 ResNext50

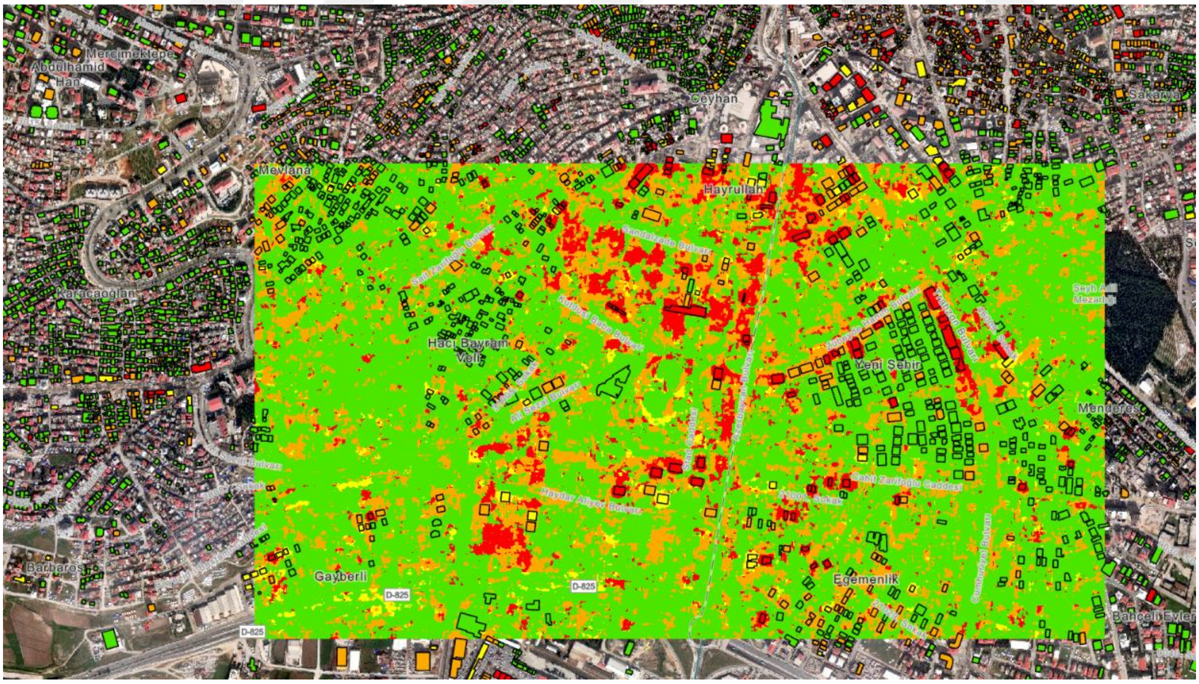


DeepLabV3 DenseNet 121

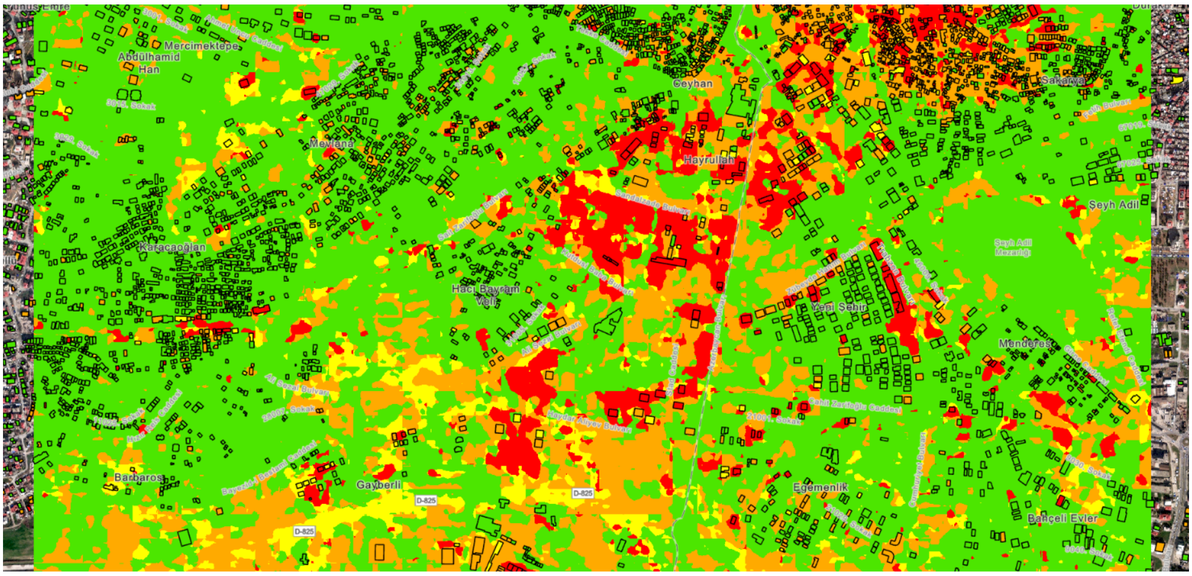


PSPNet ResNet 34

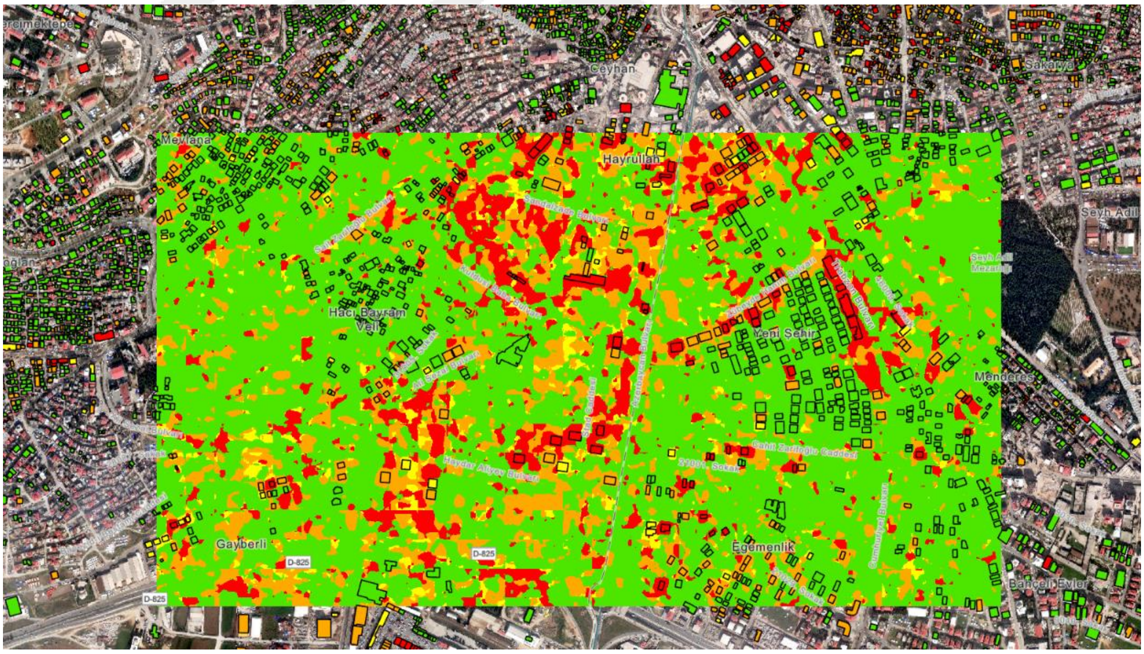


## APPENDIX C: Final Part of the Damage Assessment: Monitoring via ArcGIS Dashboard

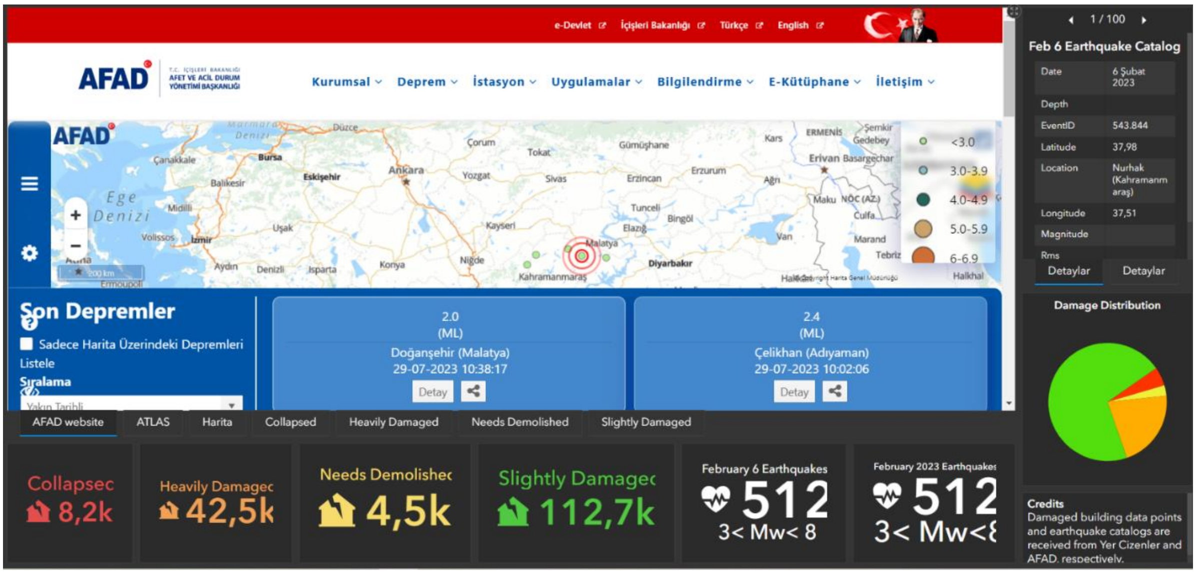



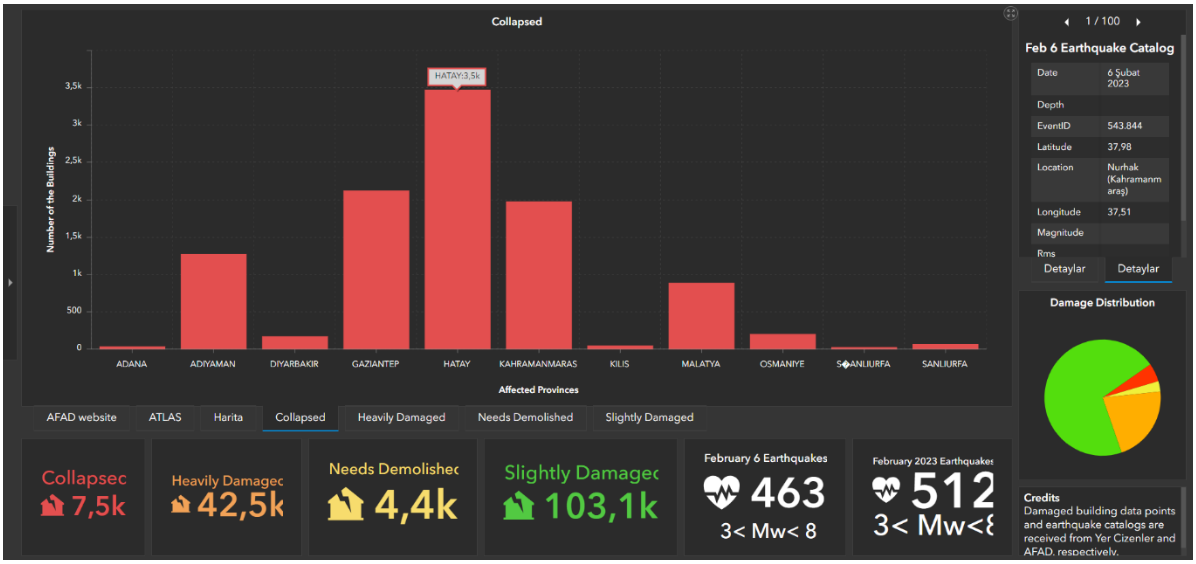


**Emercency Management in Kahramanmaraş Region**

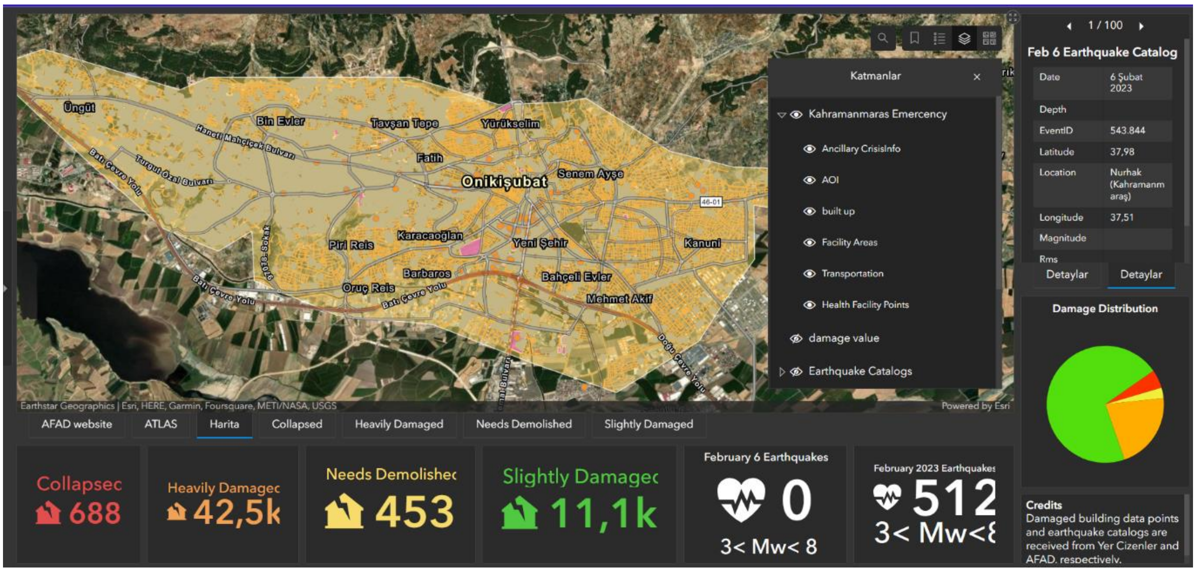
Katmanlar
Kahramanmaras Emercency
Ancillary CrisisInfo
AOI
built up
Facility Areas
Transportation
Health Facility Points
damage value
Earthquake Catalogs
1 / 100
Feb 6 Earthquake Catalog
Date
6 Şubat 2023
Depth
EventID
543.844
Latitude
37,98
Location
Nurhak (Kahramanmaraş)
Longitude
37,51
Magnitude
Rms
Detaylar
Detaylar
Damage Distribution
AFAD website
ATLAS
Harita
Collapsed
Heavily Damaged
Needs Demolished
Slightly Damaged
Collapsec
688
Heavily Damagec
42,5k
Needs Demolishec
453
Slightly Damagec
11,1k
February 6 Earthquakes
0
3< Mw< 8
February 2023 Earthquakes
512
3< Mw<{
Credits
Damaged building data points and earthquake catalogs are received from Yer Cizenler and AFAD, respectively.


Katmanlar
Kahramanmaras Emercency
Ancillary CrisisInfo
AOI
built up
Facility Areas
Transportation
Health Facility Points
damage value
Earthquake Catalogs
1 / 100
Feb 6 Earthquake Catalog
Date
6 Şubat 2023
Depth
EventID
543.844
Latitude
37,98
Location
Nurhak (Kahramanmaraş)
Longitude
37,51
Magnitude
Rms
Detaylar
Detaylar
Damage Distribution
AFAD website
ATLAS
Harita
Collapsed
Heavily Damaged
Needs Demolished
Slightly Damaged
Collapsec
88
Heavily Damagec
42,5k
Needs Demolishec
21
Slightly Damagec
363
February 6 Earthquakes
0
3< Mw< 8
February 2023 Earthquakes
512
3< Mw<{
Credits
Damaged building data points and earthquake catalogs are received from Yer Cizenler and AFAD, respectively.

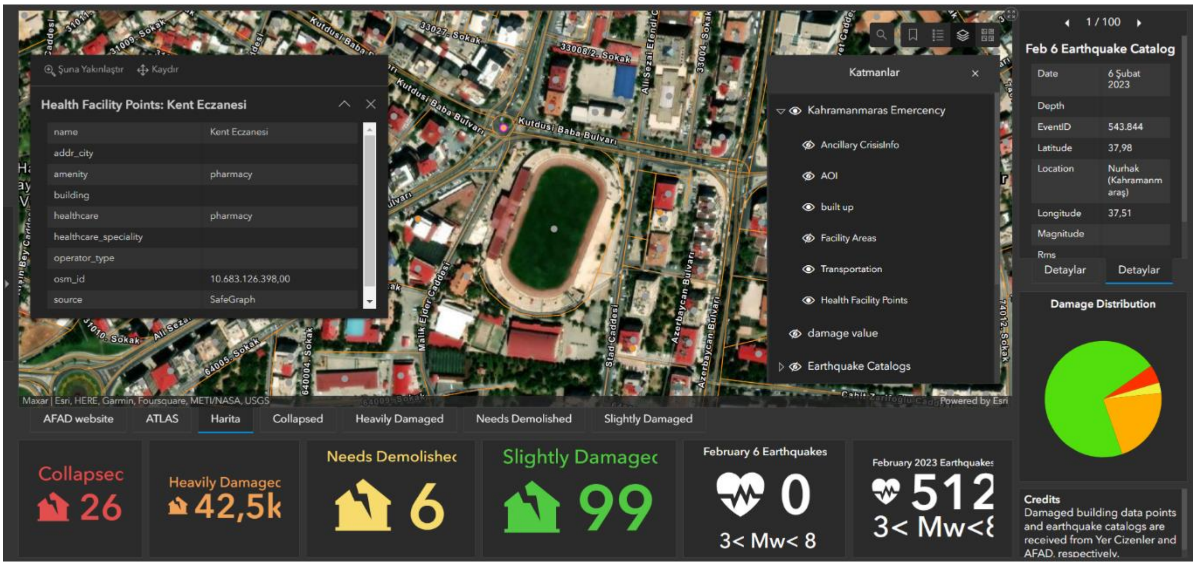
Şuna Yakınlaştır
Kaydır
Health Facility Points: Kent Eczanesi
name
Kent Eczanesi
addr_city
amenity
pharmacy
building
healthcare
pharmacy
healthcare_speciality
operator_type
osm_id
10.683.126.398,00
source
SafeGraph
Katmanlar
Kahramanmaras Emercency
Ancillary CrisisInfo
AOI
built up
Facility Areas
Transportation
Health Facility Points
damage value
Earthquake Catalogs
1 / 100
Feb 6 Earthquake Catalog
Date
6 Şubat 2023
Depth
EventID
543.844
Latitude
37,98
Location
Nurhak (Kahramanmaraş)
Longitude
37,51
Magnitude
Rms
Detaylar
Detaylar
Damage Distribution
AFAD website
ATLAS
Harita
Collapsed
Heavily Damaged
Needs Demolished
Slightly Damaged
Collapsec
26
Heavily Damagec
42,5k
Needs Demolishec
6
Slightly Damagec
99
February 6 Earthquakes
0
3< Mw< 8
February 2023 Earthquakes
512
3< Mw<{
Credits
Damaged building data points and earthquake catalogs are received from Yer Cizenler and AFAD, respectively.

## CURRICULUM VITAE

**Name Surname:** Fatma Elik

**EDUCATION:**

**B.Sc. :** 2019 - Istanbul Technical University University, Geophysical Engineering

**M.Sc. :** 2023 - Istanbul Technical University, Satellite Communication and Remote Sensing Program

**PROFESSIONAL EXPERIENCE AND REWARDS:**

- The Scientific and Technological Research Council of Turkey (TUBITAK) under the 2210-D National Industrial MSc/MA Scholarship Program.
- 2021 - Istanbul Metropolitan Municipality

**PUBLICATIONS, PRESENTATIONS AND PATENTS ON THE THESIS:**

- **Elik, F.,** 2023. Detection of Earthquake Damages With Satellıte Imagery And Deep Learning Approaches. *IV. International Science and Innovation Congress, 27-30 July 2023, TURKEY* -Accepted as an oral presentation.
-